



UNIVERSITÄT
BAYREUTH



UNIVERSITY OF BAYREUTH – MICROMETEOROLOGY

Master Thesis

Urban climate – just warm streets and cool parks?

**Investigating the variabilities of heat
at street-canyon and city-wide scale in Bayreuth**



Isabel Spies

July 2019

supervised by
Prof. Dr. Christoph Thomas
Dr. habil. Johannes Lüers

Abstract

Due to urban development, settlement areas are characterized by modified atmospheric conditions in comparison to the rural surroundings. As a result of different thermal mechanisms, urban areas are often warmer than rural ones. This phenomenon is called *Urban Heat Island* (UHI). High temperatures, especially at night, can cause serious health problems for vulnerable people. This health risk is increased by the additional heat stress in cities. However, the heat load is spatially not evenly distributed within an urban area. Urban parks for example are often associated with lower temperatures: they form a *Park Cool Island* (PCI) in a warmer urban surrounding. The objective of this thesis was to determine the magnitude of those thermal differences within a medium-sized city and to identify their causes. It was hypothesised that urban parks show similar thermal conditions as the rural surroundings of the city. The largest city-internal thermal variabilities were expected to occur under calm, anticyclonic conditions. It was additionally expected that hot spots form at highly sealed sites, while lower temperatures develop at vegetated ones. These hypotheses were tested with meteorological measurements conducted in the city of Bayreuth. In a first approach, mobile measurements were made in and around an urban park in the city centre to investigate the thermal differences on a street-canyon scale. For a second approach, a city-wide network of eleven weather stations was set up at structurally different urban sites. The results showed an average UHI between 0.5 K during the day and 2 K at nighttime. The parks within the city were on temporal average 0.8 K (day) to 2 K (night) cooler than the urban surrounding. Under calm, anticyclonic conditions, even larger nocturnal differences occurred (UHI: 4.8 K; PCI: -4.2 K). The UHI in Bayreuth ranged within the magnitudes of heating in larger European cities, while the PCI was even more pronounced than reported in literature. A comparison of the diurnal courses of the UHI and PCI revealed that the magnitude of the UHI was in the first half of the night larger than the magnitude of the PCI. Between midnight and sunrise, the magnitudes were equal, while during daytime the PCI exceeded the UHI. The city-wide measurements revealed additionally that the core of the UHI changed its location with the time of day. Also the PCI changed its location between forested parks during daytime and meadows at night. For the site-specific heat load, different elements of urban design were relevant: large cover ratios of pavement and buildings had a significant contribution to increased air temperatures at a site. A negative correlation with the site-specific temperature, however, was shown for the amount of vegetation as well as for the separation distance to the city-centre. The latter correlation is interpreted to be the result of effective ventilation with cool, rural air, which reduces the heat load in the city. As ventilation and vegetation had a significant influence on the site-specific urban heating in Bayreuth, it was concluded that a medium city-size and building density provide the possibility for an effective integration of heat mitigation strategies. With a sustainable, adapted urban planning, the city can increase the quality of live for the inhabitants.

Zusammenfassung

Städte weisen im Vergleich zum ruralen Umland veränderte atmosphärische Bedingungen auf. Aufgrund verschiedener thermisch-wirksamer Mechanismen sind urbane Gebiete häufig wärmer als rurale. Dieses Phänomen wird als *Urbane Wärmeinsel* (UHI) bezeichnet. Hitzeperioden stellen für geschwächte Menschen allgemein ein Gesundheitsrisiko dar, welches durch den zusätzlichen Hitzestress in Städten verstärkt wird. Die Hitzebelastung ist jedoch nicht überall im urbanen Gebiet gleich groß. In urbanen Parks ist es beispielsweise häufig kühler als in ihrem bebauten Umfeld. Es bildet sich eine *Park-Kälteinsel* (PCI).

Ziel dieser Arbeit war es, diese Temperaturunterschiede in einer mittelgroßen Stadt zu quantifizieren und ihre Ursachen zu bestimmen. Es wurde die Hypothese aufgestellt, dass urbane Parks ähnliche thermische Bedingungen aufweisen wie das rurale Umland der Stadt. Zudem wurde vermutet, dass die größten Temperaturunterschiede innerhalb der Stadt unter windstillen, antizyklonalen Wetterbedingungen auftreten. Es wurde erwartet, dass sich die höchsten Temperaturen an hoch versiegelten Standorten entwickeln, während Grünflächen die niedrigsten Temperaturen aufweisen.

Die Hypothesen wurden mit Hilfe meteorologischer Messungen in Bayreuth überprüft. Zunächst wurden mobile Messungen in und um einen Park im Stadtzentrum durchgeführt, um die thermischen Unterschiede auf einer räumlichen Skala von ca. 400 m zu untersuchen. Für einen zweiten Messansatz wurde ein stadtweites meteorologisches Messnetzwerk aufgebaut.

Die Messungen ergaben eine UHI von 0.5 K am Tag und 2 K in der Nacht. Die urbanen Parks waren im Mittel 0.8 K (Tag) bzw. 2 K (Nacht) kälter als ihr bebautes Umfeld. Unter windstillen, antizyklonalen Wetterbedingungen waren die nächtlichen Unterschiede deutlich größer (UHI: 4.8 K; PCI: -4.2 K). Die urbane Erwärmung in Bayreuth ist somit ähnlich ausgeprägt wie in größeren europäischen Städten, während die gemessene PCI größer war als in Referenzpublikationen. Durch einen Vergleich der mittleren Tagesgänge der UHI und PCI konnte gezeigt werden, dass die urbanen Parks in der ersten Nachthälfte wärmer waren als das rurale Umland. Zwischen Mitternacht und Sonnenaufgang waren die beiden Inseleffekte gleich stark ausgeprägt. Tagsüber waren einzelne urbane Grünflächen sogar kälter als die rurale Fläche. Die stadtweiten Messungen ergaben zusätzlich, dass im Laufe eines Tages verschiedene Standorte die maximale Erhitzung erfahren. Auch die maximale PCI wechselte zwischen bewaldeten Parks am Tag und Wiesenflächen in der Nacht. Wie stark sich ein Standort aufheizt hängt von verschiedenen Parametern der Stadtgestaltung ab: ein hoher Versiegelungsgrad und eine hohe Gebäudedichte hatten einen signifikanten Anteil an erhöhten Lufttemperaturen. Negative, signifikante Korrelationen mit der Temperatur eines Standortes zeigten hingegen der Vegetationsanteil sowie der Abstand des Standortes zum Stadtzentrum. Letzteres wurde als Folge effektiver Ventilation mit kühlerer, ruraler Luft interpretiert, welche die Hitzebelastung in der Stadt reduziert. Mit dieser Arbeit konnte gezeigt werden, dass eine mittelgroße Stadt wie Bayreuth genauso stark

von urbaner Erwärmung betroffen ist wie größere Städte. Dennoch wird aufgrund der großen innerstädtischen Temperaturunterschiede darauf geschlossen, dass die Stadt das Potential hat, mit Hilfe angepasster, nachhaltiger Stadtplanung, die urbaner Erwärmung abzumildern und somit die Lebensqualität in der Stadt zu verbessern.

Contents

Abstract	I
Zusammenfassung	III
1. Introduction	1
1.1. Motivation	1
1.2. Theoretical background	2
1.3. Objective	6
2. Methods	7
2.1. Street-canyon scale approach	8
2.1.1. Instruments	8
2.1.2. Study area	9
2.1.3. Spatially continuous measurements (transects)	9
2.1.4. Point measurements	11
2.1.5. Sampling routine	12
2.1.6. Quality assessment	13
2.2. City-wide approach	16
2.2.1. Instruments	16
2.2.2. Measuring sites	17
2.2.3. Multiresolution Decomposition	18
3. Results	19
3.1. Street-canyon scale approach	19
3.1.1. Spatially continuous measurements (transects)	19
3.1.2. Point measurements	22
3.2. City-wide approach	26
3.2.1. Overview of the rural weather conditions during the measuring period	26
3.2.2. Daily mean thermal differences	27
3.2.3. Diurnal course of the thermal differences	32
3.2.4. Multiresolution Decomposition	38
4. Discussion	43
4.1. Quantification of the thermal differences	43
4.1.1. Urban Heat Island	43
4.1.2. Park Cool Island	44
4.1.3. Comparison UHI vs. PCI	45

4.2. Explanation of the thermal differences	46
4.2.1. Influence of external forcings	46
4.2.2. Influence of the urban design	47
4.2.3. Impact on heating and cooling mechanisms	49
5. Conclusions	53
Acknowledgements	55
Bibliography	57
A. Site descriptions (city-wide measurements)	63
B. Additional tables and figures	69

List of Figures

1.1. Schematic of the parameters and mechanisms that are relevant for the urban heating. External forcings that influence the general potential for urban heating are presented in the upper part. The lower part shows city-internal, spatially variable factors that are important for the site-specific heating. These are mainly given by the urban design.	5
2.1. Map of the location and surrounding of Bayreuth. The Ecological Botanical Garden (EBG) was used as rural reference for the urban meteorological measurements. The case study was performed in the urban park “Hofgarten” in the city centre (map: LDBV)	7
2.2. Response time of the mobile air temperature sensor (Pt100) with and without radiation shield and ventilation (3 m s^{-1}); time constant = time to detect 63 % of the temperature difference	9
2.3. Map and schematic of the urban surroundings of the three transects and the measuring points A to G; The colours and symbols represent the different types of urban surroundings (housing area, street, wooded park, meadow, mixed area) (map: OpenStreetMap)	10
2.4. a) Scheme of the dynamic error occurring during the determination of an oscillating signal with a sensor with a certain time constant. b) Example for the dynamic error occurring during the air temperature measurements along the transects (example: crossing the Cosima-Wagner-Str. along T3). The maximum air temperature at the street was underestimated by 0.16 K.	15
2.5. Locations of the permanent meteorological measurements in Bayreuth. Highly sealed sites (orange): 1 Markt, 2 Kämmererei, 3 St. Georgen, 6 Spinnerei, and 11 Karstadt; Vegetated sites (green): 7 Mistel, 8 Hofgarten, 9 Wilhelminenaue, and 10 Röhrensee; Housing areas (blue): 4 Altstadt and 5 Birken; Rural reference site: 12 EBG (map: OpenStreetMap)	17
3.1. Daily mean air temperature $\overline{T_{air}}$ along the three transects T1 (a), T2 (b), and T3 (c). (data: temporal mean of 15 transect measurements per transect, spatial resolution: 1 m)	20
3.2. Comparison of the spatial perturbation of the air temperature $\widehat{T_{air}}$ along the transects T1 (a) and T2 (b) during the different times of day (data: temporal mean of 4 transect measurements per time of day, or, respectively 3 measurements for the midday round)	21
3.3. Comparison of the daily mean air temperature $\overline{T_{air}}$ along the transects T1 (a) and T2 (b) during the two analysed measuring days (temporal mean of 7 (28.08.2018) or 8 (19.09.2018) transect measurements per day)	21

3.4.	Overview of the determined parameters air temperature (a), surface temperature (b), absolute humidity (c), wind speed (d), and perceived temperature (e) at all measuring points in the evening of all three measuring days. The perceived temperature was estimated with the UTCI (chapter 2.1.4). Each grey data point is the temporal mean over 20 s of 1 Hz measurements at one measuring point. The blue data points are the temporal mean over all measuring days. All parameters are plotted as spatial perturbation.	23
3.5.	Comparison of the air temperatures in the city and in the rural reference area (EBG) in the morning (a) and evening (b). Red dots represent the measuring points in housing areas (A and E). Point E was used for the quantification of the ΔT_{UHI_air}	24
3.6.	a) Temporal mean of the temperature differences $\overline{\Delta T}_{PCI}$ between the park (C and G) and the street (E) in the morning and evening (mean values of 3 days); b) Direct comparison of the evening temperatures at the street point E (T_{street}) and the mean temperature at the park points C and G (T_{park})	25
3.7.	Time series of the air temperature at the rural site in the EBG at 2 m height during the measuring period of the city-wide measurements (data: 10 min resolution, $N = 30.528$)	26
3.8.	Wind roses for daytime (10 am to 4 pm) and nighttime (10 pm to 4 am) for the rural site in the EBG at 17 m height (data: 10 min resolution, $N = 30.528$)	26
3.9.	Time series of the daily median and interquartile range of the city-internal air temperature difference ΔT_{PCI_air} during the whole sampling period (211 days, each day from 10 am to 10 am). The blue and orange lines indicate the 1. and 3. quartile of all air temperature differences; i. e. 50% of all days showed mean differences between these lines, 25% had larger (orange dots) or smaller differences (blue dots)	28
3.10.	Relation between the city-internal air temperature difference and the wind speed, both on daily average. The variables show a significant rank correlation of $r = -0.60$ ($p - value \ll 0.1$)	28
3.11.	Weather types during the sampling period. Blue: number of days with a certain weather type which showed small city-internal air temperature differences (in total 53 d); orange: number of days with a certain weather type which showed large city-internal air temperature differences (in total 53 d; <i>extreme days</i>)	29
3.12.	Scatterplots of the temporal mean of the spatial perturbation of the air temperature $\overline{\widehat{T}}_{air}$ vs. the percentile of the 20 m perimeter, which is covered by pavement, buildings, vegetation, or trees or, respectively, vs. the distance to the city centre. <i>Vegetation</i> relates in this context to the ground covered by vegetation, while the <i>tree cover</i> quantifies the sky view covered by tree crowns. The value r represents the Spearman's rank correlation coefficient, while the p-value is an indication for the significance of the correlation.	31
3.13.	Ensemble-averaged diurnal courses of the spatial perturbation of the air temperature $\overline{\widehat{T}}_{air}$ at all stations regarding a) <i>all days</i> from September 2018 to March 2019, b) only <i>extreme days</i> with large differences (53 d; $\Delta T_{PCI_air} > 75\% - quantile$), or c) only days with small differences (53 d; $\Delta T_{PCI_air} < 25\% - quantile$), respectively. Temporal resolution: 5 min	33

3.14. Direct comparison of the mean diurnal course of the air temperature at the Markt with four other stations for showing the influence of the following elements of the urban design: a) building density (Kämmerei), b) height of the measurements above ground (Karstadt), c) vegetation with trees (Hofgarten), and d) large distance from the city centre (Spinnerei); The ensemble average was calculated using only days with large city-internal differences ($\geq 75\%$ quantile; 53 d); The dotted blue lines indicate the difference between potential temperatures at the Markt and the other station. (temporal resolution: 5 min)	35
3.15. Direct comparison of the mean diurnal course of the air temperature at the Markt with the coolest urban station (Mistel) and the rural reference station (EBG); The ensemble average was calculated using only days with high city-internal differences ($\geq 75\%$ quantile; 53 d); The blue lines indicate the difference between potential temperatures at the Markt and the other two stations (temporal resolution: 5 min)	36
3.16. Wind roses for the three sites Altstadt (a), Mistel (b), Röhrensee (c), and Spinnerei (d) parted for daytime (10 am to 4 pm) and nighttime (10 pm to 4 am). Data: 211 d, temporal resolution: 5 min. Wind roses for all other sites are shown in the appendix (Fig. B.9)	37
3.17. Spatial two point correlation coefficient R_T of the air temperature at the Markt in comparison to all other stations in dependency of the separation distance between the Markt and the comparison stations. The various time scales are represented by graphs in different colours. R_T was determined for a) all data of all days (211 d; 10 am to 10 am), b) only daytime of all days (211 d; 10 am to 4 pm), c) only nighttime of all days (211 d; 10 pm to 4 am), and d) only nighttime of <i>extreme days</i> (53 d; 10 pm to 4 am) .	40
3.18. Spatial two point correlation coefficient R_T of the air temperature at six selected stations in comparison to all other stations for the time scale of 6 h. These R_T were determined using all available data (211 d; 10 am to 10 am). This selection highlights similar or distinct correlation coefficients of the T_{air} at the selected sites.	41
3.19. Spatial two point correlation coefficient R_T of the air temperature at six selected stations in comparison to all other stations for the time scale of 6 h. These R_T were determined using only nighttime data of <i>all days</i> (211 d; 10 pm to 4 am). This selection highlights similar or distinct correlation coefficients of the T_{air} at the selected sites.	41
4.1. Qualitative comparison of mean diurnal courses of the UHI (solid, orange graph) and the PCI (dashed, blue graph). As the PCI in this study is defined as a negative value, for comparability both temperature differences were plotted as magnitude. The vertical black lines indicate the time of day when the relation of the two island effects changed. As scale for the y-axis, the temperature differences on <i>extreme days</i> was chosen as an example.	46
4.2. Adapted schematic of the parameters and mechanisms that influence the urban heating. The external forcings that influence the general potential for urban heating are presented in the upper part. The lower part shows the factors that are important for the site-specific heating. The schematic was supplemented with the results of this thesis (bold arrows and text boxes).	51

A.1. Description of the sites Markt and Kämmerei. (map: OpenStreetMap)	63
A.2. Description of the sites St. Georgen and Altstadt. (map: OpenStreetMap) . . .	64
A.3. Description of the sites Birken and Spinnerei. (map: OpenStreetMap)	65
A.4. Description of the sites Mistel and Hofgarten. (map: OpenStreetMap)	66
A.5. Description of the sites Wilhelminenaue and Röhrensee. (map: OpenStreetMap)	67
A.6. Description of the sites Karstadt and EBG. (map: OpenStreetMap)	68
B.1. Influence of direct solar radiation on air temperature measurements	69
B.2. Comparison of the transect and point measurements in the evening. (data: mean of 4 transects or 2 point measurements, respectively)	69
B.3. Spatial perturbation of the air temperature at the measuring points during the four times of day. The different symbols represent the three measuring days; the colour marking indicates whether the measurements were made in the sun or shade.	70
B.4. Set-up of the instrument comparison conducted in July 2018 at the Campus of the University of Bayreuth.	72
B.5. Comparison of the measurements of air temperature of all weather stations (data: 17 d with 5 min resolution $\rightarrow N = 4837$)	72
B.6. Comparison of the wind measurements of the micro weather stations; (data: 17 days with 5 min resolution $\rightarrow N = 4837$)	73
B.7. Instrument comparison of the micro weather stations regarding the air temperature T_{air} . Each station was compared to the mean value of all 12 stations $\langle T_{air} \rangle$. (data: 17 d with 5 min resolution $\rightarrow N = 4837$)	74
B.8. Instrument comparison of the micro weather stations regarding the wind speed u . Each station was compared to the mean value of all 12 stations $\langle u \rangle$. (data: 17 d with 5 min resolution $\rightarrow N = 4837$)	75
B.9. Comparison of the wind regime at the sites Markt (a), Karstadt (b), Kämmerei (c), St. Georgen (d); (data: 211 days with 5 min resolution)	77
B.10. Comparison of the wind regime at the sites Birken (e), Hofgarten (f), and Wilhelmine- naue (g); (data: 211 days with 5 min resolution)	78

List of Tables

2.1.	Technical information of the instruments used in the case study according to the manufacturer specifications	8
2.2.	Mean rural weather conditions during the measuring days (data from EBG using the daytime condition $K \downarrow > 10 \text{ W m}^{-2}$; measuring heights: radiation and temperature at 2 m, wind at 17 m; weather type classification by DWD (2019): SWZ = South-West cyclonic; WA = West anticyclonic; SWA = South-West anticyclonic)	13
2.3.	Technical information for the micro weather station ATMOS41 according to the manufacturer specifications	16
2.4.	Summary of the four variations, the two-point correlation coefficients were determined.	18
3.1.	Air temperature difference $\Delta T_{UHI,air}$ between the urban street measuring point E and the rural EBG	24
3.2.	Temperature differences between the park (C and G) and the street (E) in the evening	25
3.3.	Classification of the measuring sites, which were used for the correlation analysis. The temporal mean of the spatial perturbation of the air temperature $\overline{\widehat{T}_{air}}$ was determined using the whole dataset of 211 days and for the 53 days, which showed extremely large differences. The percentiles of the 20 m perimeter, which were covered by pavement, buildings, vegetation, or trees were estimated using aerial photos of the sites (appendix A)	30
3.4.	Quantification of the UHI and PCI for daytime and nighttime using the city-wide measurements. The determination was made for the whole measuring period (<i>all days</i>) and only for days showing extremely large differences (<i>extreme days</i>).	32
B.1.	Summary of the measurements made in the Hofgarten	71
B.2.	Maximal heating and cooling rates of each site during the mean diurnal course of <i>extreme days</i>	76

List of Abbreviations and Symbols

EBG	Ecological Botanical Garden
ET	Evapotranspiration
IR	Infra-red
MRD	Multiresolution Decomposition
PCI	Park Cool Island
UHI	Urban Heat Island
UTCI	Universal Thermal Climate Index

a	Absolute humidity	(g m^{-3})
e	Vapor pressure	(hPa)
$I \uparrow$	Outgoing longwave radiation	(W m^{-2})
$K \downarrow$	Incoming shortwave radiation	(W m^{-2})
p	Atmospheric pressure	(hPa)
r	Spearman's correlation coefficient	(-)
rH	Relative humidity	(%)
R_T	Spatial two-point correlation coefficients (air temperature)	(-)
T_{air}	Air temperature	($^{\circ}\text{C}$)
T_{felt}	Perceived temperature	($^{\circ}\text{C}$)
$T_{surface}$	Surface temperature	($^{\circ}\text{C}$)
u	Wind speed	(m s^{-1})
ΔT	Temperature difference	(K)
Θ	Potential temperature	($^{\circ}\text{C}$)
φ	Wind direction	($^{\circ}$)

Weather type classification (Hess and Brezowsky, 1969):

BM	Anticyclonic ridge, Central Europe	NWZ	North-West, cyclonic
HB	High pressure British Isles	NZ	North, cyclonic
HFA	High pressure Fennoscandia, anticyclonic	SA	South, anticyclonic
HM	High pressure Central Europe	SEA	South-East, anticyclonic
HNFZ	High pressure Norwegian Sea / Fennoscandia, cyclonic	SWA	South-West, anticyclonic
HNZ	High pressure Norwegian Sea, cyclonic	SWZ	South-West, cyclonic
NEA	North-East, anticyclonic	TB	Low pressure British Isles
NWA	North-West, anticyclonic	TRM	Trough, Central Europe
		TRW	Trough, Western Europe
		WA	West, anticyclonic
		WW	West, angular
		WZ	West, cyclonic

1. Introduction

1.1. Motivation

Settlement and urban development are always associated with modifications of the settlement area: artificial materials and heat release are part of urbanization as well as structural changes of soil and urban geometry and a modified energy and water budget. An increase of air temperature in an urban area was first documented in 1833 in the city of London (Howard, 1833). Subsequent studies have found that other meteorological parameters like humidity and the wind regime were affected in addition to the air temperature. The term *urban climate* has been established for atmospheric conditions that are modified by urban structures (Oke, 1969; Taha, 1997). Especially since the 1950s, a large research interest has evolved on this topic (Stewart, 2011), as cities are the centre of human activity and human comfort and health highly depend on the atmospheric conditions in the city. The temperature sensation of humans is influenced by the energy balance at the human skin. Cooling by evapotranspiration is an important mechanism that depends on the humidity, the wind velocity, and the human activity. The air temperature is also relevant as well as the mean radiative temperature, which depends on the emission of longwave radiation of the surrounding surfaces. Taking all these parameters into account, the determination of a so-called perceived temperature is useful for indicating how the environmental conditions affect people (Fanger, 1970).

Humans are vulnerable to extreme temperatures as thermal stress has to be compensated by the body. As cities are often warmer than rural areas, especially heat stress is a risk for the urban population. During heat waves, especially the nocturnal minimum temperature is relevant for human health in addition to the daily maximum (Kalkstein and Davis, 1989). High nocturnal temperatures can cause reduced recreation at night, as the required thermo-regulating mechanisms reduce the sleep effectiveness (Tsuzuki et al., 2004). At night, there are few possibilities to increase the thermal comfort. During daytime, however, people can adapt to heat by modifying clothings or by moving to places of higher thermal comfort (Thorsson et al., 2004). Zacharias et al. (2001) found that people tend to search for shadow when the air temperature exceeds 20 °C. Heat stress is a health risk especially for people with respiratory or cardiovascular diseases. Particularly elderly people are affected (Tobias et al., 2012; Wong et al., 2013). Each 1 K increase of the ambient temperature doubles the risk of death for elderly people (≥ 65 years) (Buchin et al., 2015). Additionally, there is an increased risk of pre-term birth during heat waves (Kloog, 2019).

The health effect caused by urban heat will be more relevant in future as the fraction of people living in cities will increase and the risk group generally grows with demographic change. Additionally, extremely high temperatures will occur more often due to climate change: An annual increase of + 0.2 heat days has been found (Gaffen and Ross, 1998; Stone et al., 2010).

A heat day in this context was defined as a day, on which the apparent temperature at a site exceeds the site-specific 85 %-percentile of the temperature during the base period from 1961 to 1990.

The intensity of urban heating is proportional to the population of an urban area (Oke, 1973). Most scientific quantifications are made in mega-cities, although smaller cities are also affected by urban heating. However, smaller cities have a more realistic possibility to improve their urban climate. Because of a less dense urban structure, policies for heat mitigation can be implemented more easily. The strategies of an sustainable urban planning are therefore more effective.

This concept is the main idea, on which the project named *MiSKOR* (Mitigation of urban climate and ozone risks) is based. This thesis is part of the project. MiSKOR aims to provide a scientific foundation for the development of sustainable urban planning strategies for medium-sized cities in Bavaria, Germany. The methods for determining the urban heating and ozone concentrations include data analysis, measurements in an urban area, and process-based modelling. This thesis is integrated in the part of MiSKOR that investigates the urban heating by doing meteorological measurements in a medium-sized urban area.

1.2. Theoretical background

Urban areas are, in comparison to rural ones, often characterized by higher temperatures due to modifications of the surface and the atmosphere. The term *Urban Heat Island* (UHI) has been established for this phenomenon, as cities are like warm islands in a sea of cooler rural surrounding (Oke, 1969). It can be found in all climatic regions and it might be one of the best documented examples of anthropogenic modification of the climate (Arnfield, 2003). The intensity of the UHI is generally defined as urban-rural temperature difference ΔT_{UHI} :

$$\Delta T_{UHI} = T_{urban} - T_{rural} \quad (1.1)$$

Depending on the research question, the urban temperature T_{urban} should be the highest temperature within the urban area for determining extrema. For the determination of the average heat load in the city, however, T_{urban} has to be a spatial mean value. The distance to the rural site should be 10^2 m to 10^4 m (Stewart, 2011). As the rural site acts as reference for the urban measurements, it has to be representative for the unaffected surroundings of the city. It could be chosen, for example, with regards to the population density around the site (Peterson and Owen, 2005).

The definition of the UHI is formulated in a general manner as different heat islands can be determined depending on the research question and the methods (Oke, 1995). Initially, the choice of temperature is relevant. The UHI is most commonly measured with the air, surface, or perceived temperature. While satellite images provide information about the surface temperatures of horizontal surfaces, stationary or mobile measurements are used to determine differences between air temperatures at different sites. However, the determined $\Delta T_{UHI,air}$ varies between different methods (Runnalls and Oke, 2000). Also the measuring height is of

relevance: The air temperature in the Urban Canopy Layer that is below roof level, is the result of the immediate site character, while above roof level, in the Urban Boundary Layer, the air temperature is influenced by a larger area (Oke, 1976, 1995). The average intensity of the UHI depends generally on the building density, the size of the city, and therewith on the population (Oke, 1973).

The UHI describes differences between urban and rural areas. Additionally, there are thermal differences within urban areas. Many studies have found that areas of lower temperature in a warmer urban surrounding are often located within urban parks; they form a so-called *Park Cool Island* (PCI) (Spronken-Smith and Oke, 1998). A PCI is generally defined as the temperature difference ΔT_{PCI} between an urban green space and a sealed site without vegetation such as streets or housing areas:

$$\Delta T_{PCI} = T_{park} - T_{street} \quad (1.2)$$

Although a PCI is always associated with a park, it can extend beyond the park boundary and cool nearby urban districts (Ca et al., 1998). This effect is limited to a maximum distance of one park width (Spronken-Smith and Oke, 1998).

Urban planning should strive to increase the quality of life for the inhabitants of a city. To increase the thermal comfort, negative effects of urban structures have to be mitigated. The relevant factors and mechanisms have to be found. The occurrence of large temperature differences, and the formation of an UHI or PCI, relates to external influences, but also to internal characteristics of the city (Oke, 1982). In this thesis, temporally variable forcings, whose origins are located outside the city, are referred to as *external forcings*. *Internal factors*, however, describe factors, which are part of the urban design and located within the city.

Substantial research has been made on evaluating the relevant factors, the most important results were summarized in figure 1.1.

External forcings like the weather and season can not be influenced by urban planning. Nevertheless, their influence is investigated in many studies as they provide the boundary conditions for potential heating or cooling mechanisms.

It was shown by Ivajnsič and Žiberna (2019) that UHI intensities are significantly higher under anticyclonic weather conditions. The smallest intensities, however, occur under turbulent, windy conditions, as rural and urban air masses get mixed. The most relevant meteorological parameters are clouds and advection. High wind speeds can diminish air temperature differences completely (Oke, 1976). It is irrelevant whether the air movement is induced by synoptic forcing or by large spatial temperature differences (Haeger-Eugensson and Holmer, 1999). Within a city, advection influences the horizontal extent of PCIs by transporting the cool park air (Spronken-Smith et al., 2000). While the PCI intensity is thereby decreased, districts in the lee of the park are cooled. Clouds also influence the urban heating. During daytime, they reduce the fraction of direct shortwave radiation, and with that the available energy. Additionally, nocturnal surface cooling by outgoing longwave emission is inhibited by the presence of clouds, as longwave radiation is absorbed and reemitted by the clouds. In addition to the cloud cover the cloud type has a significant influence (Runnalls and Oke, 2000).

Some studies connected the influences of clouds and advection on urban heating to a general *weather factor* (Runnalls and Oke, 2000; Morris et al., 2001).

In many cities the intensity of the UHI changes seasonally. However, the exact temporal behaviour of the UHI across a year differs between cities (Morris et al., 2001; Gedzelman et al., 2003). The reasons for the seasonality are various: Urban areas are heated by season-dependent, anthropogenic heat release e.g. by traffic or industry. This additional heat is especially relevant for the nocturnal heating (Ryu and Baik, 2012). However, the effect on the UHI intensity is not significant for every city (Runnalls and Oke, 2000). A second reason are seasonally varying cooling rates at the rural sites. These are caused by changes of the heat capacity and thermal conductivity of the rural ground depending on the soil moisture (Runnalls and Oke, 2000). The temporally variable water availability is also relevant for the formation of the PCI within the city (Spronken-Smith and Oke, 1998). Cooling by evapotranspiration (ET) is most effective in irrigated parks, as enough water and energy are available there (Spronken-Smith et al., 2000).

When the external conditions provide the potential for the formation of large temperature differences, the actual urban heating depends on city-internal parameters. The urban design is spatially variable and therefore the main reason for city-internal temperature differences.

Vegetation in cities has the potential to create cool spots within a warmer sealed surrounding. The shape and height of the vegetation are as relevant for the PCI intensity as the park size (Park et al., 2017; Yang et al., 2017). In regards to radiation, a dense tree cover has a similar effect on the site-specific heating and cooling as a large building density. It can be summarized as the effect of a reduced *sky view*: during daytime, trees and buildings provide shadow and at night, they inhibit outgoing longwave emissions (Oke, 1981; Wang and Akbari, 2016). Taken together, these two elements of urban design have a cooling effect during daytime and a warming effect at night (Ryu and Baik, 2012).

In addition to the influence of the building density on the sky view of a site, the three-dimensional urban geometry also has other impacts on the local climate: Due to the large amount of vertical structures, urban areas have a large surface, mostly made of artificial materials. In comparison to natural materials, these artificial ones are often characterized by a low albedo and different thermal material properties, which result in increased absorption of shortwave and longwave radiation and storage of the available energy. The additional absorption, heat storage, and reemission of longwave radiation has a large impact on the urban energy balance (Coutts et al., 2007). For the transport of heat, the wind near buildings is of importance. The wind regime, however, is also modified by the urban geometry: wind speeds may be reduced due to an increased surface roughness, which in turn reduces the mixing of air masses of different temperatures. In street canyons the wind speed may even exceed the average, as characteristic flow pattern evolve depending on the canyon geometry (DePaul and Sheih, 1986; Nunez and Oke, 1977; Eliasson et al., 2006).

In addition to the differences between urban and rural sensible heat fluxes, the latent heat flux are also affected: The water availability is limited in urban areas as there are more impervious surfaces and less vegetation. Water can not be stored in the soil and there is less ET. Sealed surfaces contribute to urban heating especially during daytime (Ryu and Baik, 2012). Urban water bodies provide the possibility for evaporative cooling (Hathway and Sharples, 2012).

However, there can be nocturnal heating effects similar to those of buildings, as water bodies also store heat.

All these external and internal forcings influence the urban climate on a city-wide scale or only locally at one specific urban site. The temperature at a site is therefore always the result of the mentioned heating and cooling mechanisms.

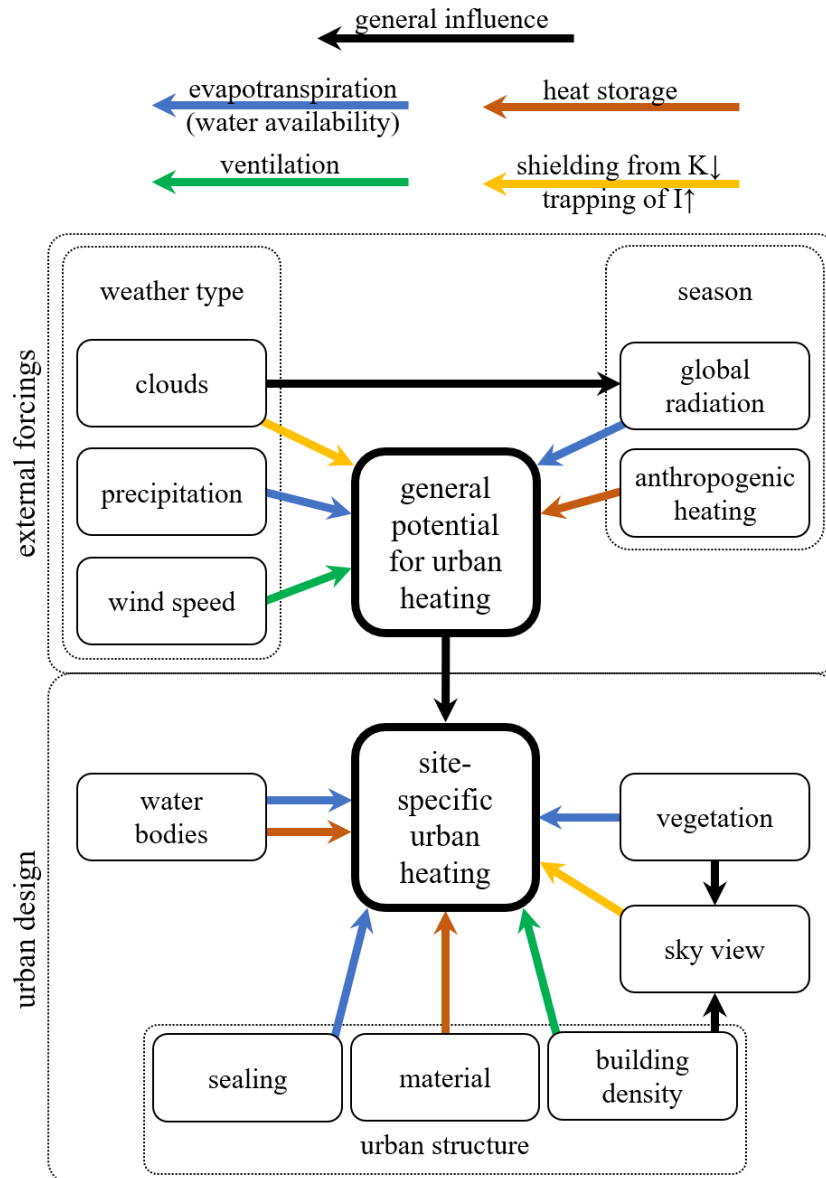


Figure 1.1.: Schematic of the parameters and mechanisms that are relevant for the urban heating. External forcings that influence the general potential for urban heating are presented in the upper part. The lower part shows city-internal, spatially variable factors that are important for the site-specific heating. These are mainly given by the urban design.

1.3. Objective

The objective of this thesis is to quantify and explain thermal differences within this medium-sized urban area. However, the focus lay on the air temperature, comprehensive meteorological measurements were made to detect the underlying processes and forcings inducing the thermal differences. The meteorological conditions in the city were determined at two different spatial scales: A city-wide network of micro weather stations and mobile measurements at the scale of a street canyon were used.

This data basis was used to investigate the following two research questions:

- I. What is the magnitude of the temperature differences of a medium-sized urban area?
Differences of air, surface, and perceived temperature are investigated on various temporal and spatial scales, city-internally (Park Cool Island) and in comparison to rural surroundings (Urban Heat Island).
- II. Which are the main external forcings and city-internal elements of urban design that induce or influence those thermal differences?

Based on the priorly presented current state of knowledge, hypotheses were formulated for the research questions:

- i. *Urban parks in a medium-sized city show similar thermal conditions as the rural surroundings of the city ($\rightarrow |UHI| = |PCI|$).*
This hypothesis is based on the expectation that the investigated urban area is so small that the arising urban heating can be compensated in urban parks by effective cooling mechanisms such as evapotranspiration or shading that are induced by the vegetation.
- ii. *The largest city-internal temperature differences occur under anticyclonic weather conditions with small advective forcing. The site-specific heating intensity is increasing with an increasing grade of sealing and a decreasing amount of vegetation.*

It is expected, that the PCI evolves similar to the UHI especially under clear and calm conditions. Due to high absorption, warm spots evolve at sites sealed with artificial materials, while cool spots are formed at unsealed, vegetated sites such as parks and urban river banks by evaporative cooling or shading. The large city-internal thermal differences occur as the urban air masses of different temperatures are not mixed by advection.

2. Methods

The measurements for this study were performed in the urban area of the city of Bayreuth, Germany (49° 56' 44.3" N, 11° 34' 16.8" E) (Fig. 2.1). This city is with nearly 75,000 inhabitants and an area of 67 km² a medium-sized town (LfStat, 2018). Like many towns in this region, the city of Bayreuth is located in a wide valley, surrounded by several hills. The elevation difference within the city is about 100 m.

As rural reference, the meteorological station in the Ecological Botanical Garden (EBG) of the University of Bayreuth was used. Although the garden is part of the municipal area of Bayreuth, its temperature measurements are independent of urban structures. The air temperature is measured there at 2 m height with a platinum resistance thermometer (Pt100, class 1/10B, Electrotherm, Germany) with an actively ventilated radiation shield (MetOne, USA).

For quantifying the urban temperature and its spatial differences, two measurement approaches were performed at different spatial scales: First, a three day case study with mobile measurements was made in an urban park to evaluate inner-urban temperature differences on a street-canyon scale of about 400 m. This approach comprised spatially continuous measurements along transects as well as point measurements. Secondly, permanent meteorological measurements were made for seven months at eleven urban sites to quantify city-wide heat differences.

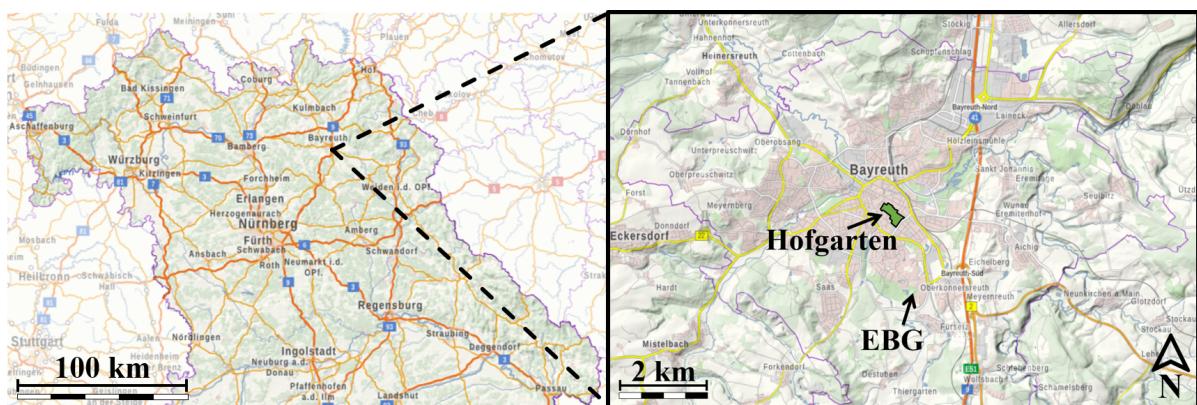


Figure 2.1.: Map of the location and surrounding of Bayreuth. The Ecological Botanical Garden (EBG) was used as rural reference for the urban meteorological measurements. The case study was performed in the urban park “Hofgarten” in the city centre (map: LDBV)

2.1. Street-canyon scale approach

The objective of the first approach was to quantify temperature differences that are perceivable for humans. The measurements were made around an urban park on a spatial scale of about 400 m to determine the thermal differences that pedestrians are exposed to when they are crossing the park.

2.1.1. Instruments

The human wellbeing depends on the air temperature as well as on the radiative temperature, relative humidity, and wind speed (Fanger, 1970). Based on measurements of these parameters, the quantification of thermal differences could be made for the air, radiative, and perceived temperature.

The data collection was made by mobile, bicycle-based measurements. The radiative temperature was estimated by measurements of the surface temperature of the surrounding of the measuring point. The 360° surface temperature was determined with an infra-red (IR) camera (PI 640, Optris GmbH, Germany). The IR camera was mounted on a tripod at a height of 1.3 m above ground. During the mobile measurements, geographical coordinates were recorded using a smartphone GPS tracker app (CycleDroit, version 1.9.9) that logged the location every 1 s. Air temperature, relative humidity, and wind speed were measured every 1 s with a climate measuring instrument (Testo 480) comprising a Pt100 resistance thermometer and a hot-wire anemometer with integrated thermohygrometer (Testo SE & Co. KGaA, Germany). The technical information of all instruments are listed in table 2.1. The climate measuring instrument including all sensors was mounted on a bicycle. The measurement height was about 80 cm above ground. The temperature sensor was shielded against global radiation and was passively ventilated by the movement of the bicycle. According to manufacturer information it takes 75 s for the air temperature sensor to detect 90 % of a temperature difference when it is ventilated with about 2 m s^{-1} (t_{90}). I determined the response time with a ventilation of 3 m s^{-1} and measured a time constant of 27 s. This is the time needed until 63 % of a change in signal was detected. Adding a radiation shield to the ventilated sensor prolonged the time constant to about 55 s (Fig. 2.2). Without ventilation the change in signal was detected much later (163 s unshielded and 247 s with a radiation shield, respectively).

Table 2.1.: Technical information of the instruments used in the case study according to the manufacturer specifications

parameter	instrument/sensor	accuracy	resolution
T_{air}	Testo (0614 0072): Pt100	$\pm (0.15 \text{ K} + 0.05 \% \text{ of } mv)$	0.01 K
rH	Testo (0635 1543): hot wire probe	$\pm (1.8 \% + 0.7 \% \text{ of } mv)$	0.1 %
u	Testo (0635 1543): hot wire probe	$\pm (0.03 \text{ m s}^{-1} + 4 \% \text{ of } mv)$	0.01 m s^{-1}
$T_{surface}$	IR camera Optris PI 640	$\pm 2 \text{ K}$ or $\pm 2 \%$	optical: 640x480 px thermal: 75 mK

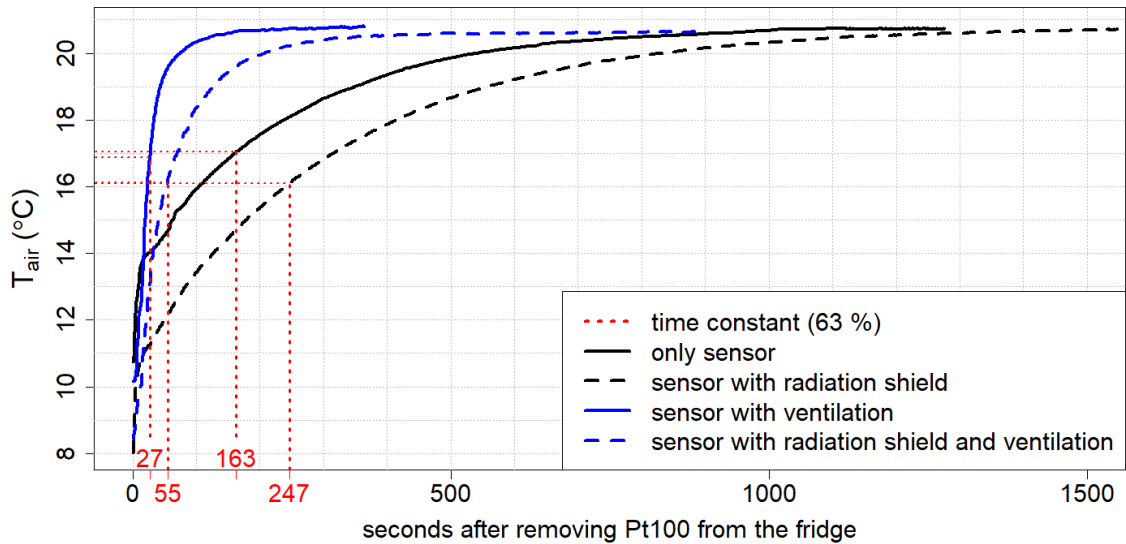


Figure 2.2.: Response time of the mobile air temperature sensor (Pt100) with and without radiation shield and ventilation (3 m s^{-1}); time constant = time to detect 63 % of the temperature difference

2.1.2. Study area

The case study was conducted in the Hofgarten, an urban park in the city centre of Bayreuth (Fig. 2.1). The atmospheric conditions in this park are of high interest, as the Hofgarten is a very famous location for urban recreation and much frequented. Most parts of the about 13 ha large park area are shaded by trees except for a large meadow in the centre of the park. The Hofgarten is surrounded by houses and several partially high-traffic streets.

As it was the objective of this approach to quantify the spatial variability of temperature on a small scale perceivable for humans, the relevant meteorological parameters were observed in the Hofgarten and the surrounding streets. Two measurement concepts were realized: Along three transects, crossing the park and the surrounding streets and housing areas (Fig. 2.3, transect 1 to 3), the air temperature was measured spatially continuously. Furthermore, point measurements were conducted at seven sites in and around the park. At each point, the humidity, surface temperature, and wind speed were determined in addition to the air temperature (Fig. 2.3 point A to G).

2.1.3. Spatially continuous measurements (transects)

The spatially continuous measurements were conducted along three transects. Each transect had a length of about 400 m. The first transect (T1) went from an urban street (Rathstraße) through a mixed area with houses and trees into the shaded part of the Hofgarten. The intent of this transect was to show the thermal differences between the street, mixed, and park areas. To additionally investigate the park's internal differences, a second transect (T2) was picked, covering some shaded park areas and the meadow as well as another urban street with houses. In the neighbourhood of the Hofgarten, a second smaller park is located. The two parks are only separated by a high-traffic street (Cosima-Wagner-Straße). The third transect (T3) led through both parks by crossing that street to detect the thermal effect of the street.

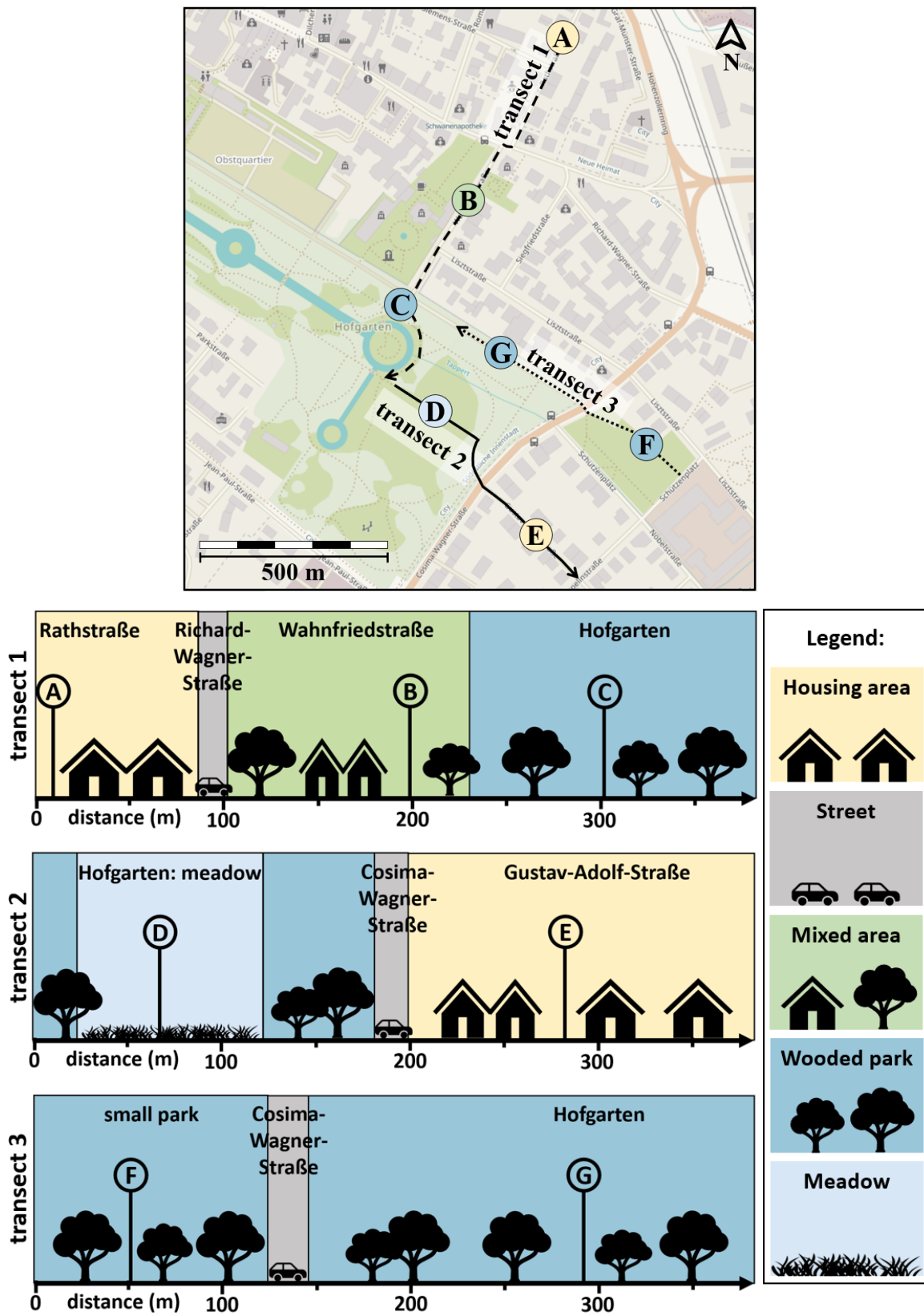


Figure 2.3.: Map and schematic of the urban surroundings of the three transects and the measuring points A to G; The colours and symbols represent the different types of urban surroundings (housing area, street, wooded park, meadow, mixed area) (map: OpenStreetMap)

During biking or walking along these transects at a speed of about 3 m s^{-1} , the air temperature was logged every 1 s. All transects were visited in sequence, beginning with T1 and ending with T3. This process will be referred to as *continuous transect run*.

Due to a non-constant driving speed, the collected data points were spatially not evenly distributed along the transects. In order to compare individual transect runs to each other, they had to be harmonized. First, the three transects were transformed to straight line segments. By projecting the measurement coordinates orthogonally onto those line segments and determining the length of the (sub)segments, the coordinates were converted into *distances along the transect*. Afterwards, the data were aggregated and linearly interpolated. For each run, data were now available for every meter.

The measurements were made on temporal as well as on spatial scales. For comparability reasons, the data were split into mean and perturbation on both scales. Therefore, the following symbols were used:

$$\begin{aligned}
 & \text{value} = \text{mean} + \text{perturbation} \\
 \text{temporal scale : } X &= \bar{X} + X' \\
 \text{spatial scale : } X &= \langle X \rangle + \hat{X}
 \end{aligned} \tag{2.1}$$

This nomenclature was consistently used for all spatio-temporal measurements that were made for this study. Regarding the spatial data, \hat{X} , which is the deviation from the spatial mean, should not be confused with ΔX , the difference of a parameter between two sites such as ΔT_{UHI} .

2.1.4. Point measurements

Between the continuous transect runs, stationary measurements were made at seven points in and around the park. The purpose was to determine thermal differences by using the radiative and perceived temperatures in addition to the air temperature.

All measuring points were located along the transects (Fig. 2.3). There were two points in tarred side streets with cars, houses, and small gardens along the street (street points: A and E). Three points were situated inside the Hofgarten: two of them (park points: C and G) under trees and one in the middle of the meadow (meadow point: D). The remaining points are located in a mixed area with houses, cars, and large trees (mixed point: B) and inside the small park beside the Hofgarten (small park point: F).

At each point, air temperature, relative humidity, and wind speed were measured for about 20 s. The radiative temperature at each site was estimated by measuring the surface temperature of the surrounding surfaces with the IR camera. To get continuous 360° temperature information, six single images were taken. As the human body has in an upright posture a larger dimension vertically than horizontally, only vertical pictures were made. The sky and ground surface temperatures directly above and underneath the measuring point were neglected. Information about the cloudiness and whether the measuring point was exposed to direct shortwave radiation were observed by eye and recorded.

During the data processing, the median of the air temperature and the maximum of the wind speed were calculated out of the 20 1-Hz data for each point measurement. The temperature-dependent relative humidity rH was converted into absolute humidity a (Eq. 2.3) before calculating the median. For this conversion the Magnus equation (Eq. 2.2) was used to calculate the vapour pressure e .

$$e = \frac{rH}{100 \%} \times C_1 \times \exp\left(\frac{C_2 \times T_{air}}{C_3 + T_{air}}\right) \quad (2.2)$$

$$a = \frac{e}{R_W \times T_{air}} \quad (2.3)$$

with $C_1 = 6.108$ hPa, $C_2 = 17.081$, $C_3 = 234.175$ °C and $R_W = 461.50$ J kg⁻¹ K⁻¹

$$T_{surface_point} = \text{mean} \left(\sum_{i \in I_{point}} \sum_{p \in P_i} T_{surface_p} \right) \quad (2.4)$$

with $I_{point} = \{Image_1 \dots Image_6\}$; $P_i = \{pixel_1 \dots pixel_{640 \times 480}\}$

At every measuring point six abutting IR-images of 640x480 pixels each were taken covering the horizontal 360° view of the surrounding environment. The mean surface temperature $T_{surface_point}$ at a measuring point was calculated as the mean value of the temperature for each pixel p of every image i taken at that point (Eq. 2.4).

The perceived temperature was estimated using the concept of the Universal Thermal Climate Index (UTCI). The UTCI is a temperature scale index: the value indicates an air temperature under reference conditions causing the same thermal strain as the actual meteorological conditions (Jendritzky et al., 2002). For modelling this thermal index all significant heat exchange mechanisms are considered. The metabolic rate and clothing insulation are taken into account as well as the meteorological parameters air temperature, relative humidity, and mean radiative temperature, all at 2 m height, and the wind velocity at 10 m height. In this study the concept of the UTCI was used with a few modifications regarding the input data. The wind velocity was determined at 2 m instead of 10 m height and the mean radiative temperature was estimated with the mean 360° surface temperature. Therefore, the resulting values are not called UTCI, but perceived temperatures, as they may not exactly comply with the described thermal index. The values were determined using the R package *rBiometeo* (Crisci and Morabito, 2016).

2.1.5. Sampling routine

On three days in summer 2018 (08.08., 28.08. and 19.09.) measurements were made in the Hofgarten and the surrounding streets. As the largest temperature differences are expected to occur under clear and calm conditions, the measurements were conducted during bright summer days with little advection (Tab. 2.2). Nevertheless, the conditions, especially regarding the soil moisture, were slightly different: the two days in August were part of a dry period while a few days prior to the measuring day in September there was some precipitation. On the first measuring day, some smaller parts of the Hofgarten were irrigated.

Each of the three measuring days was split into four times of day: morning (9 am), midday (12 am), afternoon (3 pm), and evening (6 pm). During every time of day the following measurement routine was executed consecutively:

1. continuous transect run (T1 → T2 → T3) (10 min)
2. point measurements (A → B → C → D → E → F → G) (75 min)
3. continuous transect run (T1 → T2 → T3) (10 min)

Hence, measurements were made along each transect eight times per day and at every measuring point four times per day. The duration of one complete measuring routine was on average 95 min.

Table 2.2.: Mean rural weather conditions during the measuring days (data from EBG using the day-time condition $K \downarrow > 10 \text{ W m}^{-2}$; measuring heights: radiation and temperature at 2 m, wind at 17 m; weather type classification by DWD (2019): SWZ = South-West cyclonic; WA = West anticyclonic; SWA = South-West anticyclonic)

date	weather type	T_{air} ($^{\circ}\text{C}$)	u (m s^{-1})	$K \downarrow$ (W m^{-2})
08.08.2018	SWZ	27.26	2.4	356
28.08.2018	WA	20.36	1.4	384
19.09.2018	SWA	22.46	1.7	298

2.1.6. Quality assessment

Several errors impaired the data quality of the mobile measurements. Table B.1 in the appendix summarizes all conducted measurements of this approach marking which data was used in the further analysis.

During the transect measurements two technical problems occurred: First, the determination of the position via GPS was not constantly possible, as the GPS tracker not always received GPS signals. Secondly, the air temperature device logged incorrect readings during several rounds. The problems occurred mostly during the first measuring day (08.08.2018). As only three out of eight transect runs delivered complete data sets on that day, all transects of that day were discarded. Regarding the other two days, only one transect run had to be excluded. As consequence, only two out of three measuring days were used for the analysis of the transect data.

Due to faulty operation and internal instrument errors, there were also some data missing for the point measurements: The surface temperature data of the first measuring day have a large uncertainty as no flag was applied for calibration before the measurements. This handling error was eliminated after the first measuring point of the evening round. Furthermore, measuring at a sunny or shady spot had an influence of on average 2 K on the air temperature measurements (Fig. B.1), since the sensor was not ventilated properly. Each day some of the midday and afternoon measurements are affected by this radiative error, mostly those at the measuring points on the meadow (D) and in the street (E) (Fig. B.3). Only the measurements conducted in the evening generated a completely available and valid data set. Therefore, all results of the

measuring points refer to the evening round, if not stated otherwise.

For the analysis of the point measurements, the temporal offset between the points had to be considered. As the measurements took about 10 min at each point, the time difference between the measurements at the first (A) and the last (G) point was about 1 to 1.5 h. Some of the determined temperature differences between two points are caused by the non-simultaneity of the measurements. To eliminate that inaccuracy, the ΔT_{PCI} was calculated as the difference between the street point E and the mean of the park points C and G (Eq. 1.2). The measurements in the street (E) were always made temporally between the two park points (C and G). The two park points are spatially not far from one another and are both located in the forested part of the Hofgarten.

As a comparison between the transect and point data of the evening rounds revealed, the transect measurements could not show all extrema of the air temperature, but only a damped amplitude along the transects (Fig. B.2). Fritschen and Gay (1979) described the relation between the dampened amplitude and the measurement lag of a sensor (Fig. 2.4a). This artefact is called *dynamic error*. Being placed in an environment of different temperature, a sensor approaches this new temperature asymptotically. The time needed to reach the correct value is given by the time constant τ , which was experimentally determined to be 55 s for the used sensor with radiation shield and ventilation (see Fig. 2.2). To create continuous measurements it was not applicable to wait at each point of the transects until the sensor reached the environmental temperature.

Fritschen and Gay (1979) stated, that a temporally changing temperature signal can be described by an oscillating signal. The temperature T at a certain time step t depends thereby on the amplitude T_1 and the angular frequency oscillation ω (Eq. 2.5).

$$T = T_1 * \sin(\omega t) \quad (2.5)$$

The *detected* change in signal per time step dT/dt is given by equation 2.6 using the time constant τ .

$$\frac{dT}{dt} + \frac{T}{\tau} = \left(\frac{T_1}{\tau}\right) \sin(\omega t) \quad (2.6)$$

Since the signal along T3 resembles an oscillating signal most closely, it is used as an example to show the effect of the dynamic error (Fig. 2.4b). By rearranging equation 2.6 the real temperature during the measurements can be calculated, since the measured values and the time constant of the sensor are known. The estimated real temperature was then modelled with a linear regression of the first two iterations of the Fourier series, a sum of in total 4 sine and cosine waves. This additionally yielded approximations for ω . With the angular frequency of the modelled signal the attenuation α , the factor how much the measured temperature underestimated, the correct values can be determined (Eq. 2.7). For T3 an α of 0.6 was calculated, meaning the amplitude of the measured signal was 0.16 K smaller than the real temperature.

$$T_{measured} = \alpha T_1 \quad \text{with } \alpha = [1 + (\omega \tau)^2]^{-1/2} \quad (2.7)$$

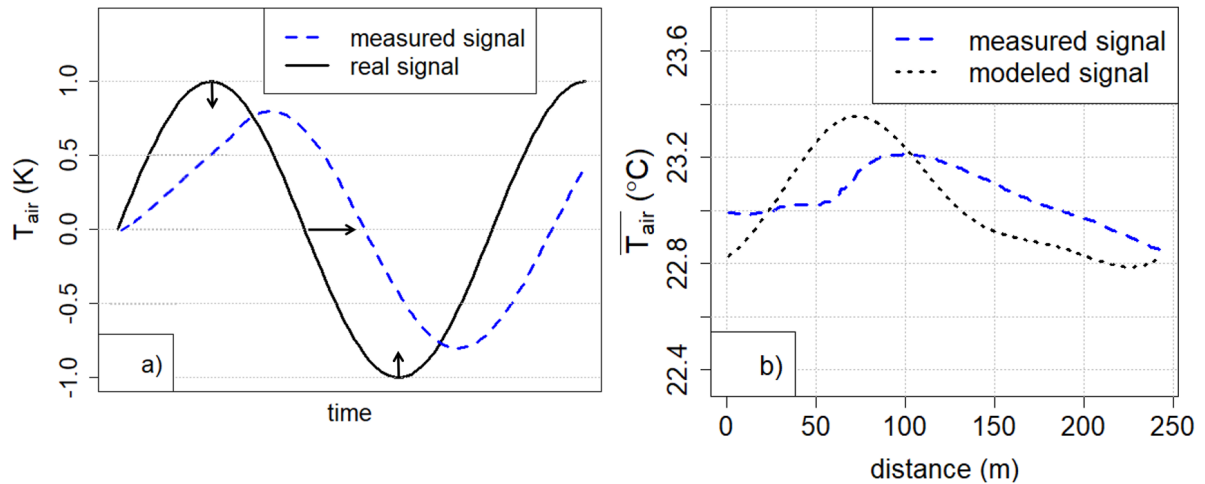


Figure 2.4.: a) Scheme of the dynamic error occurring during the determination of an oscillating signal with a sensor with a certain time constant.
 b) Example for the dynamic error occurring during the air temperature measurements along the transects (example: crossing the Cosima-Wagner-Str. along T3). The maximum air temperature at the street was underestimated by 0.16 K.

As figure 2.2 showed, the time constant of a sensor is influenced by ventilation. For the aforementioned calculations to be applicable, the sensor has to be ventilated with a constant velocity. This was not the case during the transect measurements, because the layout of the transects required varying driving speeds and multiple stops during the route, for example at traffic lights. This means that the lag between the measured and real signal varies along the transects. For example the areas with the shortest lag are the locations of stops during the transect, since the sensor had time to catch up to the real signal. Since the time constant influences the the angular frequency, which in turn is used to calculate the attenuation, it can be concluded that there is a varying dampening effect for the data. It should be kept in mind that the real temperature differences were more pronounced than it could be observed in the transect data, presented in chapter 3.1.1.

Due to these inaccuracies the transect measurements are further used as a qualitative indication of the location of hot and cool spots along the transects while the point measurements are used for exact quantifications of the real thermal differences.

2.2. City-wide approach

The second measuring approach was performed on a larger, city-wide scale. The meteorological conditions at eleven structurally different urban sites were determined over a time period of seven months. In contrast to the mobile measurements around the Hofgarten, the devices used for this approach were installed stationarily at the chosen sites.

2.2.1. Instruments

At each site a micro weather station (ATMOS41) with data logger (EM60G) (METER Group, Inc. USA) was installed, mostly mounted at streetlights at a height of 3.5 m above ground. With those stations the most relevant meteorological parameters were measured and logged with a temporal resolution of 5 min. In this thesis the measurements of air temperature T_{air} , wind speed u , and direction φ were used (Tab. 2.3). A field evaluation of those weather stations that was conducted by Thomas et al. (2019) revealed a precision of the air temperature measurements of 0.05 K. The anemometer overestimated the wind velocity on average by 24 %. Regarding the determination of the wind direction, Thomas et al. (2019) found large deviations between the tested stations for low wind speeds ($u < 1 \text{ m s}^{-1}$). For larger wind speeds, this error diminished.

Table 2.3.: Technical information for the micro weather station ATMOS41 according to the manufacturer specifications

parameter	sensor	accuracy	resolution
T_{air}	Pt100	$\pm 0.6 \text{ K}$	0.1 K
u	2D sonic anemometer	$\pm 3\%$ (min. 0.3 m s^{-1})	0.01 m s^{-1}
φ	2D sonic anemometer	$\pm 5^\circ$	1°

A comparison of the weather stations used in this study was performed for 17 d in July 2018 at the campus of the University of Bayreuth (Fig. B.4). The measurements showed an average deviation of 0.1 K or 0.06 m s^{-1} , respectively (Fig. B.5, Fig. B.6). A linear regression analysis of the air temperature and wind measurements of each station in comparison to the mean of all stations is shown in the appendix (Fig. B.7, Fig. B.8).

End of August 2018, the devices were installed in the city. The coordinates of the measuring sites were determined using a GPS sensor (Geo 7X Handheld GNSS System, Trimble, USA). In this thesis, the time series recorded from 01.09.2018 to 31.03.2019 were analysed. About two month after the installation, one of the initially twelve stations overestimated the air temperature due to technical malfunctions. The measuring error increased with time. As the air temperature was the most important parameter for this thesis, the whole dataset of this site was excluded from the analysis. Consequently, the analysis of the urban heat conditions contained eleven urban sites and, for comparison, the rural site at the EBG.

For information about the large scale weather situation during the measurement period the weather type classification provided by the DWD (2019) was used.

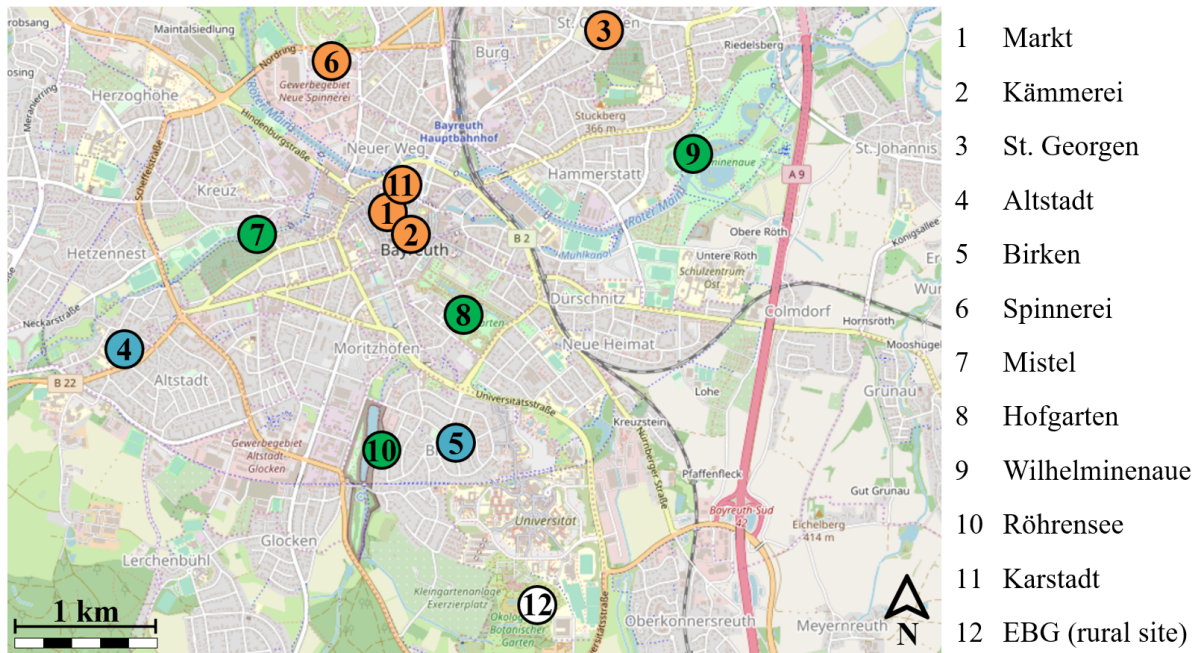


Figure 2.5.: Locations of the permanent meteorological measurements in Bayreuth. Highly sealed sites (orange): 1 Markt, 2 Kämmerei, 3 St. Georgen, 6 Spinnerei, and 11 Karstadt; Vegetated sites (green): 7 Mistel, 8 Hofgarten, 9 Wilhelminenaue, and 10 Röhrensee; Housing areas (blue): 4 Altstadt and 5 Birken; Rural reference site: 12 EBG (map: OpenStreetMap)

2.2.2. Measuring sites

The city-wide measurements were designed to reveal the spatial meteorological variabilities in the city. Therefore, the measurement sites (Fig. 2.5) were chosen intending to represent the most important urban designs adequately. To achieve this, the sites' grade of sealing and building density were considered during the site selection, as well as the water and vegetation cover ratios. Three stations were installed in the city centre of Bayreuth: one station was set up directly on the town square (station #1 **Markt**), one in a narrow alley (station #2 **Kämmerei**) and one at about 20 m height on a roof deck on top of a building near the market-place (station #11 **Karstadt**). In addition to these three sites, two other highly sealed places were chosen, located in the northern parts of Bayreuth: the **Spinnerei** (station #6), which is an industrial park, and **St. Georgen** (station #3), an densely built district of Bayreuth, which has a similar structure as the city centre. In comparison to these highly sealed sites, five parks and green areas should represent the meteorological conditions at green urban sites. Among those were two forested sites: the **Hofgarten** (station #8), the urban park near the city centre, which was also used for the mobile measurements, and the **Röhrensee** (station #10), a park with an artificial lake in the southern part of the city. Bayreuth is traversed by some creeks and a small river. To capture the influence of the urban riverbeds, one station was installed where the Roter Main river enters the urban area (station #9 **Wilhelminenaue**) and one station at the small creek **Mistel** (station #7) in the west of the city centre. These are open-spaced sites with grass-covered river banks, water bodies, and trees or shrubs in the near surroundings. As many inhabitants spend their time at home, especially in the evening and at night, the residential districts **Altstadt** (station #4) and **Birken** (station #5) were

chosen as site for the last two stations. Detailed information about all measuring sites can be found in the appendix A.

2.2.3. Multiresolution Decomposition

The analysis of the meteorological time series recorded by the city-wide measuring network included a multi-resolution decomposition (MRD) (Howell and Mahrt, 1997). This method was applied to the time series of air temperature. By calculating the spatial two-point correlation coefficients at different temporal scales, coherences between all stations should be revealed. The MRD was performed using a software code written in Matlab (Thomas, 2011).

The dataset was divided into increment periods using dyadic time steps of the width 2^n ; with n ranging from 0 to M , where $n = 0$ was the signal at recorded original resolution and M the longest time interval, which was 24 h in this study. Each of the MRD modes M contained 2^{M-n} data points per interval. Initially, each of the not overlapping 24 h intervals contained 288 data points, since the original dataset had a temporal resolution of 5 min. But as the largest averaging interval was supposed to be 24 h, the original 5 min data had to be transformed into time series with a 5.625 min resolution, to have $2^8 = 256$ records per 24 h interval.

After the MRD was performed, the two-point correlation coefficients between the stations were calculated for every MRD time scale using the whole dataset or, respectively, only parts of it (Tab. 2.4): First the correlation coefficients were determined using all available data (211 d; 24 h intervals from 10 am to 10 am) in $M = 9$. In a second step, daytime and nighttime data of all 211 d were analysed separately. Daytime was defined from 10 am to 4 pm and nighttime from 10 pm to 4 am. As the intervals had now a length of 6 h, only $M = 6$ were needed. Additionally, the correlation coefficients were determined using only data of nights that showed extremely high spatial temperature differences (Fig. 3.9).

Table 2.4.: Summary of the four variations, the two-point correlation coefficients were determined.

data	number of days	time interval	number of MRD modes	max. average interval
a) all days and nights	211	10 am to 10 am	$M = 9$	24 h
b) all days	211	10 am to 4 pm	$M = 6$	6 h
c) all nights	211	10 pm to 4 am	$M = 6$	6 h
d) extreme nights	53	10 pm to 4 am	$M = 6$	6 h

3. Results

3.1. Street-canyon scale approach

3.1.1. Spatially continuous measurements (transects)

With the spatially continuous, mobile measurements in and around the Hofgarten, thermal differences on the spatial scale of a street canyon were investigated. In the housing area Rathstraße, it was on average 0.8 K warmer than in the park (T1, Fig. 3.1a). Within the mixed area between the housing area and the park, the Richard-Wagner-Straße (90 m), trees (140 m), and houses (160 m) caused slight horizontal temperature variations (< 0.1 K). The meadow (90 m) and the Cosima-Wagner-Straße (190 m), which were crossed by the second transect (T2, Fig. 3.1b), showed on average similar air temperatures. In comparison to these two areas, the housing area in the Gustav-Adolf-Straße (350 m) was 1 K warmer. The lowest temperatures were measured under the trees of the Hofgarten, even at the about 60 m long forested segment between the warmer meadow and street (175 m). The comparison of the two parks separated by a high-traffic road (T3, Fig. 3.1c) showed an influence of the street (130 m) of at least 0.2 K. In the small park (60 m) it was about 0.3 K warmer than in the larger Hofgarten (325 m). Taken all transects, the measurements indicated a daytime average ΔT_{PCI_air} of almost 1 K between the Richard-Wagner-Straße (T1) and the forested parts of the Hofgarten (T2/T3).

The differences between air temperatures along the transects changed as the day progressed. As the temperatures along T1 show, the distinction between different structures evolved with the course of the day (Fig. 3.2). In the morning around 9 am, an almost linear decrease of the air temperature was observed along the transect with a total difference of 0.4 K between the street and the park. The spatial small-scale temperature perturbations occurring later in the day showed an increasing magnitude. The largest temperature difference of 1.2 K between the street and the Hofgarten were observed in the evening around 6 pm. Regarding the mean temperatures along T2, the air was evenly warm at the meadow and in the street. Including the times of day into that comparison revealed that in the morning and evening the meadow was 0.2 K cooler than the street, whereas during midday at 12 am and afternoon at 3 pm, it was warmer (about 0.1 K to 0.2 K). Within the park, the temperature difference between the meadow and the trees was largest during midday and afternoon as well (0.2 K to 0.4 K).

Comparing the two measuring days revealed only few variabilities (Fig. 3.3). For each transect the ΔT_{PCI} was about 0.1 K larger during the warmer and moister measuring day (19.09.2018), whereas on 28.08.2018 the spatial small-scale temperature perturbations were more distinct. The different structures along T2 (meadow \rightarrow trees \rightarrow street) showed the most interesting variations (Fig. 3.3b): During the measurements on 19.09.2018, the meadow was 0.1 K warmer

than the forested area and the street was 0.1 K warmer than the meadow. On 28.08.2018, however, the air at the meadow was 0.1 K warmer than in the street and 0.2 K warmer than under the trees.

For the interpretation of all these temperature differences, it has to be considered that the amplitudes of the signals were damped by about 40% due to the dynamic error, as explained in chapter 2.1.6. The thermal differences along the transects were even more pronounced than the determined values shown here. Warm spots such as streets or housing areas are likely to be even hotter, while cool spots like the forested parts of the Hofgarten were cooler than the measurements indicated.

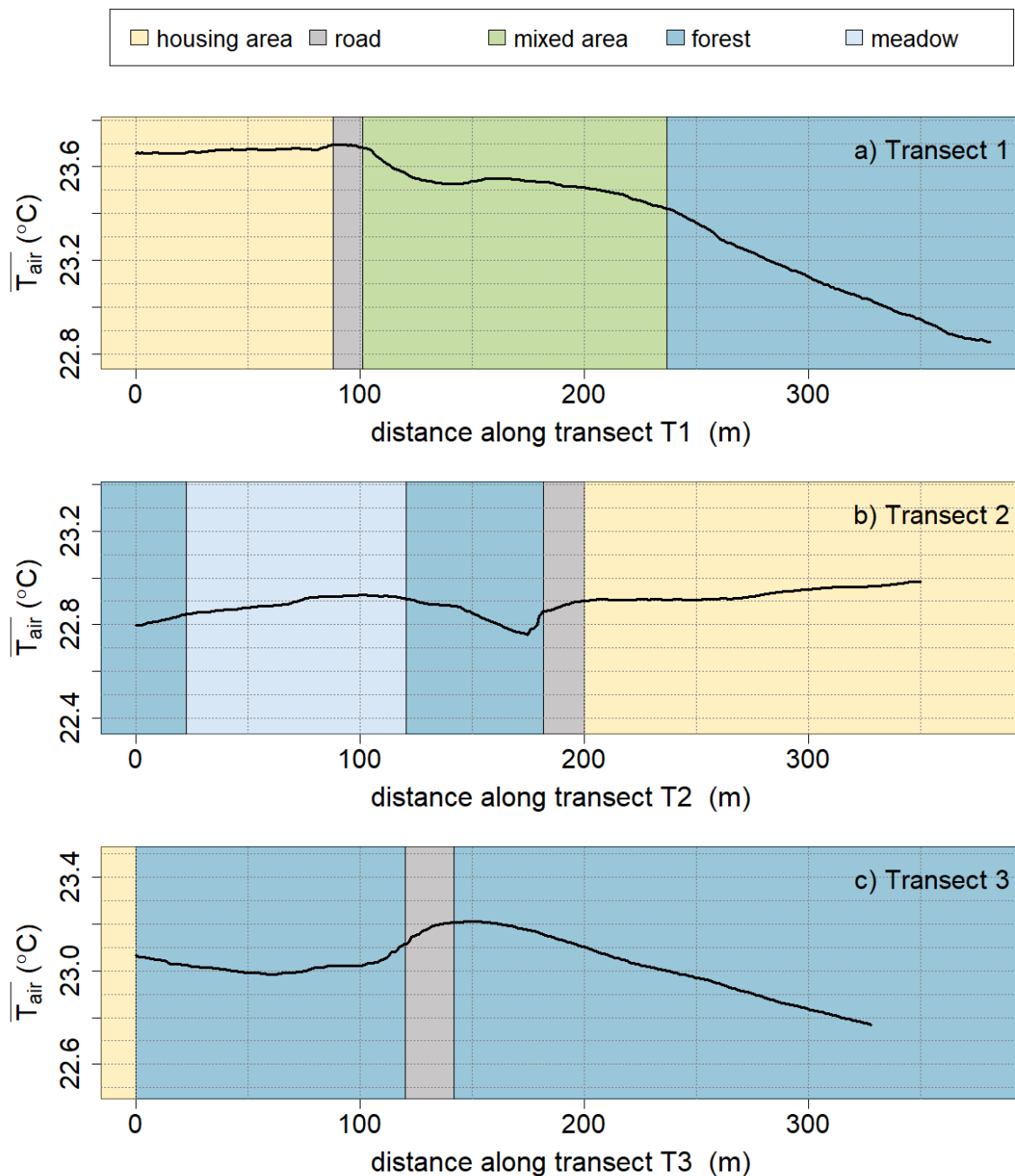


Figure 3.1.: Daily mean air temperature \overline{T}_{air} along the three transects T1 (a), T2 (b), and T3 (c). (data: temporal mean of 15 transect measurements per transect, spatial resolution: 1 m)

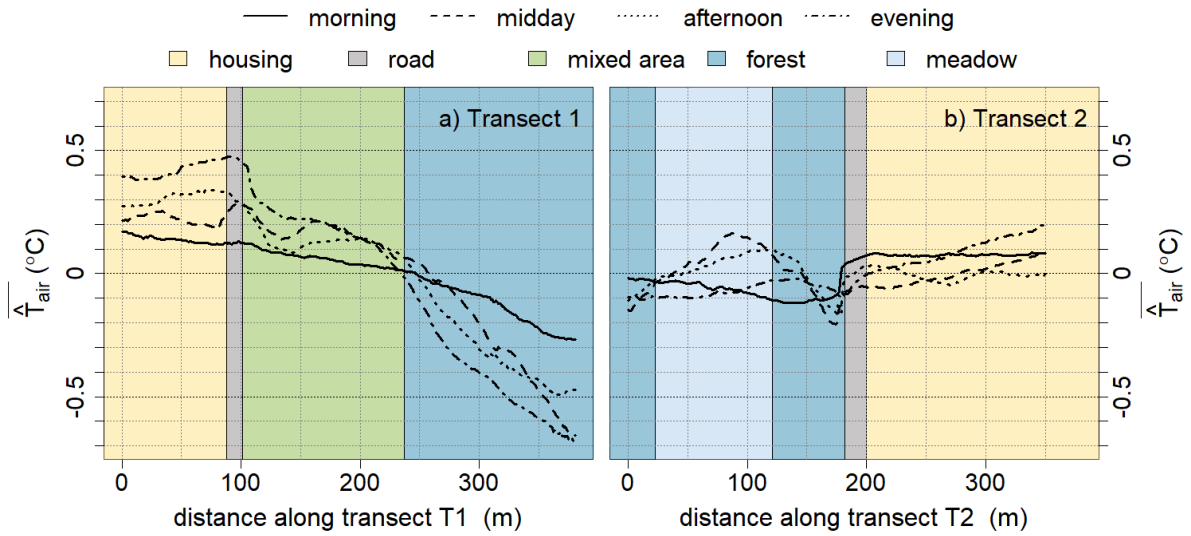


Figure 3.2.: Comparison of the spatial perturbation of the air temperature \widehat{T}_{air} along the transects T1 (a) and T2 (b) during the different times of day (data: temporal mean of 4 transect measurements per time of day, or, respectively 3 measurements for the midday round)

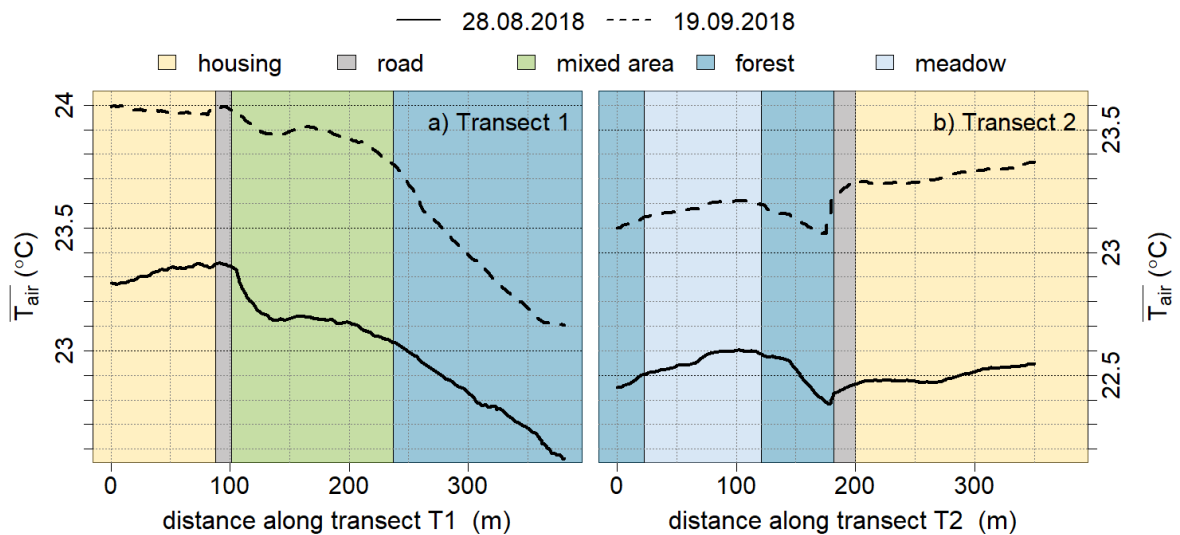


Figure 3.3.: Comparison of the daily mean air temperature \overline{T}_{air} along the transects T1 (a) and T2 (b) during the two analysed measuring days (temporal mean of 7 (28.08.2018) or 8 (19.09.2018) transect measurements per day)

3.1.2. Point measurements

Based on the spatially continuous air temperature information along the transects, the thermal conditions in and around the Hofgarten were further investigated with the point measurements. The thermal differences were quantified regarding the air temperature as well as the surface temperature and perceived temperature. Therefore, measurements of air temperature T_{air} , surface temperature $T_{surface}$, relative humidity rH , and wind speed u were analysed. As explained in chapter 2.1.4, the absolute humidity a and the perceived temperature T_{felt} were calculated.

Differences between the measuring points were observed for all parameters during the evening round (Fig. 3.4). Compared to the points located in streets, the park points were on average characterised by lower air temperatures (-1 K to -2.9 K), surface temperature (-0.1 K to -3.5 K), and perceived temperatures (-0.8 K to -2.3 K) (Fig. 3.4a/b/e). Regarding the surface temperature, the measuring point B, located in a traffic-calmed street lined with houses and large trees, was remarkable warm ($\widehat{T}_{surface} = 1.9\text{ K}$), whereas in the Hofgarten (points D and G) the lowest surface temperatures were measured ($\widehat{T}_{surface} = -1.5\text{ K}$). Furthermore, the surface temperature at the two street points A and E differed, as well as the two park points. Altogether, there were larger differences between surface temperatures at different points compared to air temperatures. The spatial perturbations of the measurements of absolute humidity and wind speed (Fig. 3.4c/d) showed an almost inverse behaviour. Although those parameters varied during the different measuring days, the vegetated park was on average moister and calmer than the open-spaced streets. The other measuring points were characterized by average absolute humidities, while the wind speed was also reduced in the small park (point F).

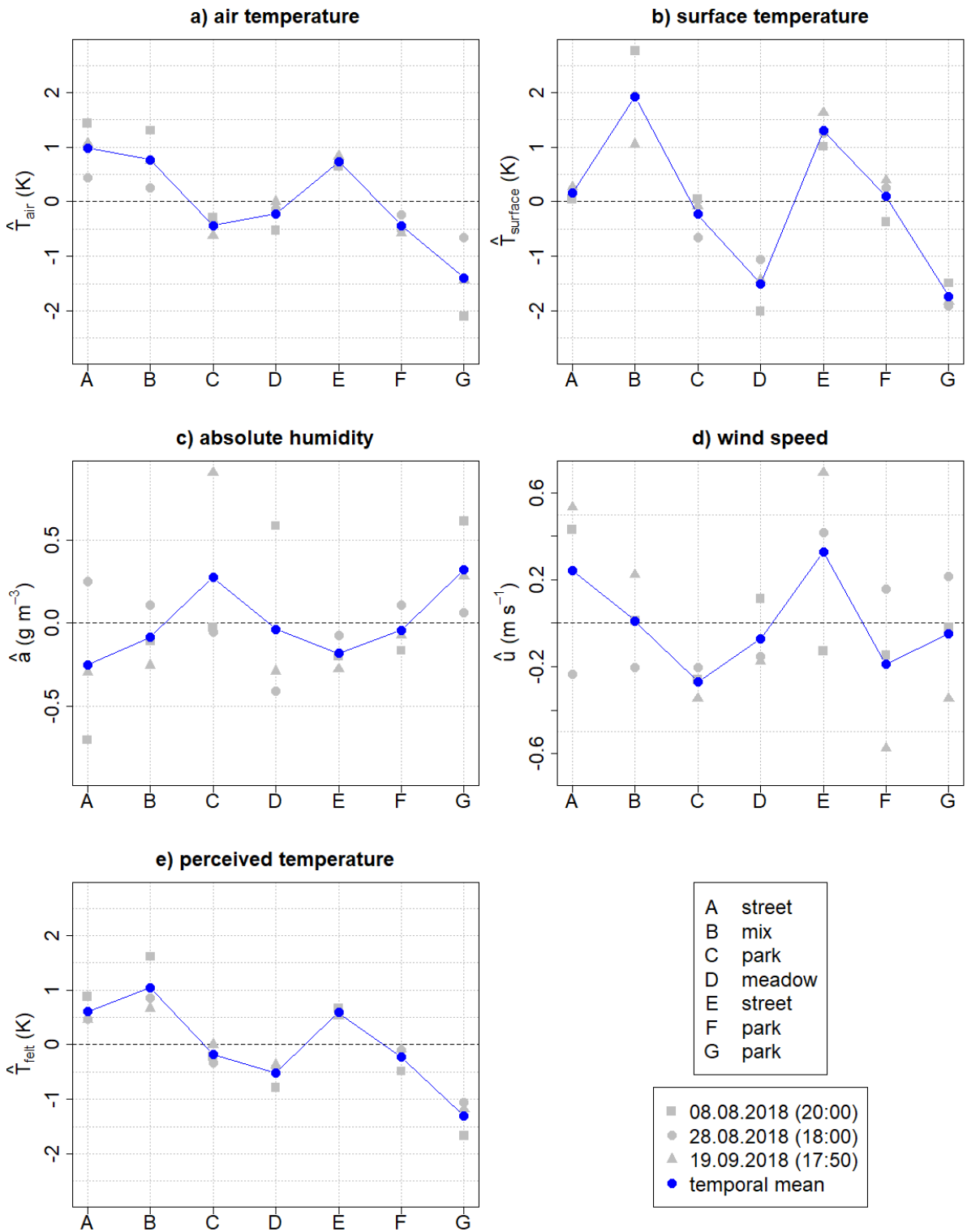


Figure 3.4.: Overview of the determined parameters air temperature (a), surface temperature (b), absolute humidity (c), wind speed (d), and perceived temperature (e) at all measuring points in the evening of all three measuring days. The perceived temperature was estimated with the UTCI (chapter 2.1.4). Each grey data point is the temporal mean over 20s of 1 Hz measurements at one measuring point. The blue data points are the temporal mean over all measuring days. All parameters are plotted as spatial perturbation.

The air temperature readings recorded during the point measurements were compared to the thermal conditions at the rural reference station in the EBG. The morning and evening round were used, since only the air temperature measurements were compared with the rural measurements. ΔT_{UHI} was determined as the difference between the urban and rural temperatures that were measured at the same time (Eq. 1.1). The urban point E was used for the quantification, as that point showed the largest differences to the rural reference (Fig. 3.5). The mean difference between the urban and rural air temperature was 1.5 K: 1.6 K in the morning and 1.4 K in the evening (Tab. 3.1). A comparison between the three measuring days showed an influence of the time of the measurements for the evening round: The later in the evening the measurements were made, the larger was the difference between the urban and rural area. However, the different times of sunset should be considered while interpreting this temporal pattern.

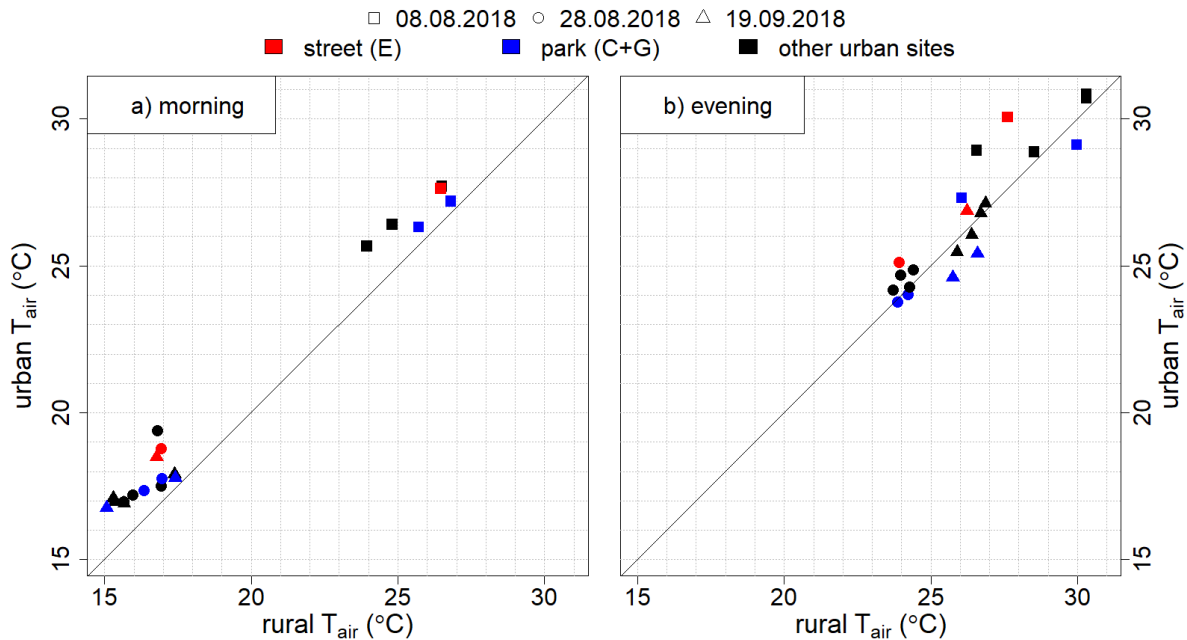


Figure 3.5.: Comparison of the air temperatures in the city and in the rural reference area (EBG) in the morning (a) and evening (b). Red dots represent the measuring points in housing areas (A and E). Point E was used for the quantification of the ΔT_{UHI_air}

Table 3.1.: Air temperature difference ΔT_{UHI_air} between the urban street measuring point E and the rural EBG

	morning	evening	morning & evening
08.08.2018	1.2 K (10:00)	2.4 K (20:10)	1.8 K
28.08.2018	1.9 K (09:40)	1.2 K (18:20)	1.5 K
19.09.2018	1.7 K (08:50)	0.7 K (18:00)	1.2 K
all days	1.6 K	1.4 K	1.5 K

A comparison between the streets and the park was made by using data from the measuring points E (housing area), C, and G (both park) (for further explanations see chapter 2.1.6. The results from the transect measurements showed that the largest air temperature differences between the park and the surrounding streets occurred in the evening. The point measurements confirmed this result for all three temperature definitions (Fig. 3.6a). Therefore, only the evening data will be used for the following quantifications (Fig. 3.6b). In the park, the temperature of the surrounding surfaces was on average 2.3 K lower than in the street, whereas the air was 1.7 K cooler (Tab. 3.2). The difference between perceived temperatures at the points was with -1.3 K on average the smallest. A comparison of the three days with the slightly different measuring times indicated a coherence of the time with the $T_{surface}$ results: the later the measurements were made, the smaller was the difference between the street and the park. The reverse pattern occurred for the perceived temperature. The air temperature data did not show a temporal pattern.

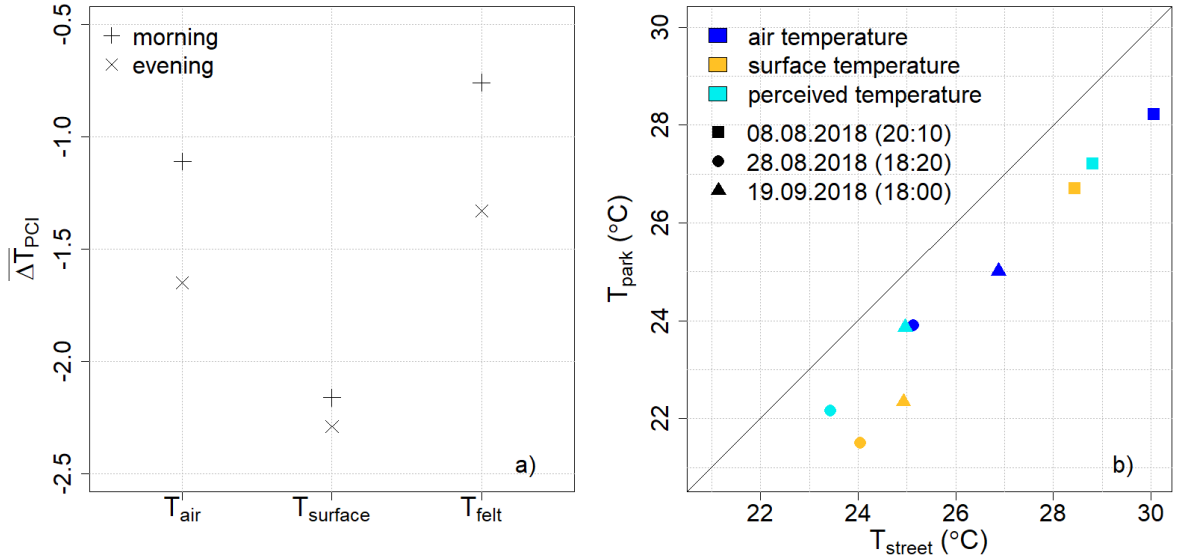


Figure 3.6.: a) Temporal mean of the temperature differences $\overline{\Delta T_{PCI}}$ between the park (C and G) and the street (E) in the morning and evening (mean values of 3 days);
 b) Direct comparison of the evening temperatures at the street point E (T_{street}) and the mean temperature at the park points C and G (T_{park})

Table 3.2.: Temperature differences between the park (C and G) and the street (E) in the evening

	ΔT_{air}	$\Delta T_{surface}$	ΔT_{felt}
08.08.2018 (20:10)	-1.9 K	-1.7 K	-1.6 K
28.08.2018 (18:20)	-1.2 K	-2.5 K	-1.3 K
19.09.2018 (18:00)	-1.9 K	-2.6 K	-1.1 K
all days	-1.7 K	-2.3 K	-1.3 K

3.2. City-wide approach

3.2.1. Overview of the rural weather conditions during the measuring period

During the 7-month observational period from September 2018 to March 2019, the meteorological conditions in Bayreuth were controlled by 20 different weather types. The air temperature at the EBG varied between -12°C in September 2018 and 29°C in January 2019 (Fig. 3.7). Between November 2018 and February 2019, there were only small differences between daytime and nighttime air temperature ($< 5\text{ K}$). The meteorological data that were used for this analysis were averaged over 10 min intervals. The wind at the EBG came mostly from westerly and southerly directions with an average velocity of 2.7 m s^{-1} during daytime and 1.8 m s^{-1} at night (Fig. 3.8). The strongest winds came with velocities up to 12 m s^{-1} from westerly directions.

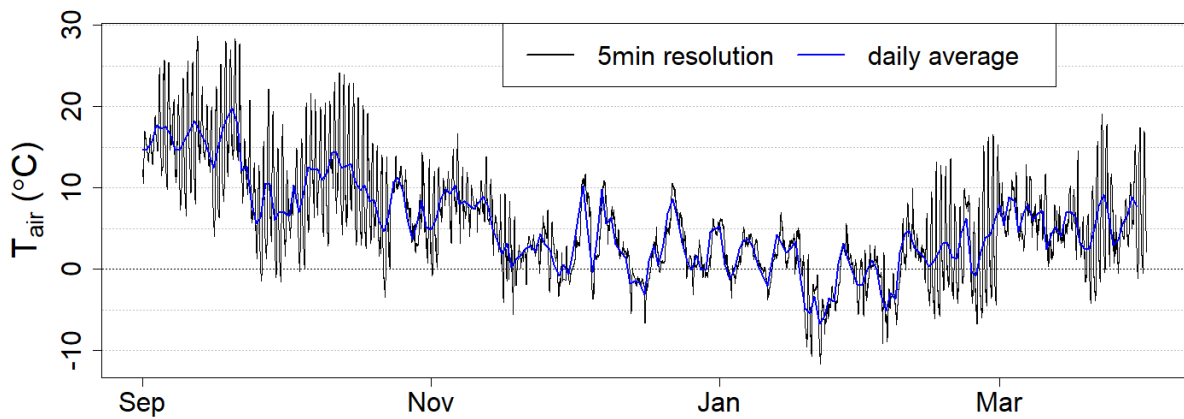


Figure 3.7.: Time series of the air temperature at the rural site in the EBG at 2 m height during the measuring period of the city-wide measurements (data: 10 min resolution, $N = 30.528$)

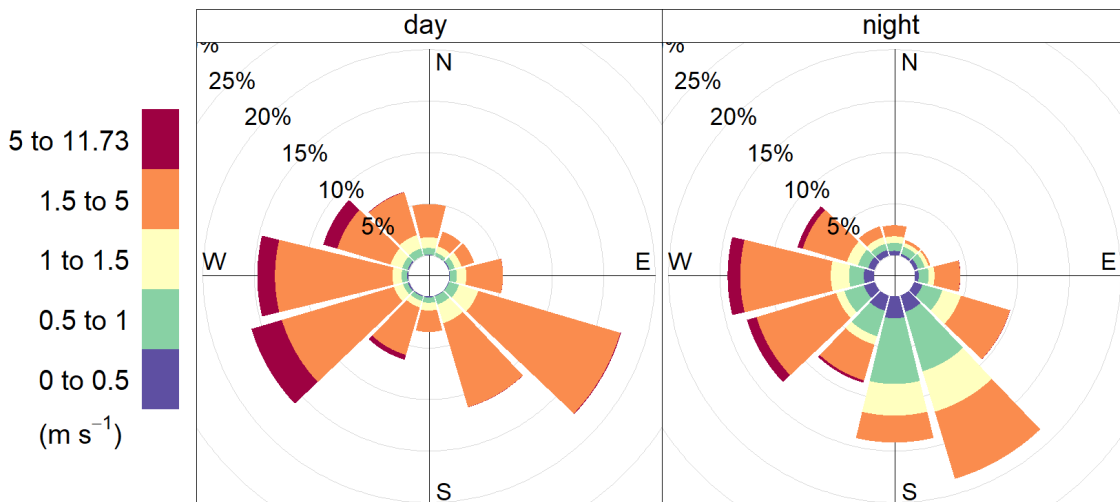


Figure 3.8.: Wind roses for daytime (10 am to 4 pm) and nighttime (10 pm to 4 am) for the rural site in the EBG at 17 m height (data: 10 min resolution, $N = 30.528$)

3.2.2. Daily mean thermal differences

For a first impression of the variability of heat within the city, the maximum temperature difference within the network was determined for each 5 min time step ts by subtracting the lowest urban temperature from the highest (Eq. 3.1). The measured thermal phenomena do not align with the time span of a day, from midnight to midnight: Some processes start in the beginning of the night and carry over to the next morning. To better analyse these effects, the daily median was calculated for each 24 h interval from 10 am to 10 am.

$$\Delta T_{PCI,air,ts} = \max(T_{air,ts}) - \min(T_{air,ts}) \quad (3.1)$$

$$\text{with } ts = 1 \dots 211 * 288$$

The warmest site was on daily average up to 4.8 K, but at least 0.4 K, warmer than the coolest (Fig. 3.9). Comparing all 211 days, the city-internal $\Delta T_{PCI,air}$ was on average 1 K. The 25 % quantile was 0.8 K and the 75 % quantile was 2.5 K. The smallest city-internal temperature differences were mostly detected in December and January, while in September, October and late February the largest differences occurred. The periods with large city-internal temperature differences will be referred to as *extreme days* hereafter. When the whole measuring period is referenced, the term *all days* will be used. Extremely high city-internal temperature differences were mostly caused by high air temperatures in the Kämmereigasse in the city centre and in contrast to that, low temperatures at the Mistel site. Less often the Wilhelminenaue or the Röhrensee was the coolest site or St. Georgen the warmest. One of the most important forcings was the advection (Fig. 3.10): The wind measurements in the EBG showed average velocities of 0.6 m s^{-1} on days with large temperature differences. On days with low city-internal differences, however, the weather was characterized by average wind speeds of 1.4 m s^{-1} . The $\Delta T_{PCI,air}$ was significantly correlated with the average wind speed with a rank correlation coefficient r of -0.60 (p - value $\ll 0.01$).

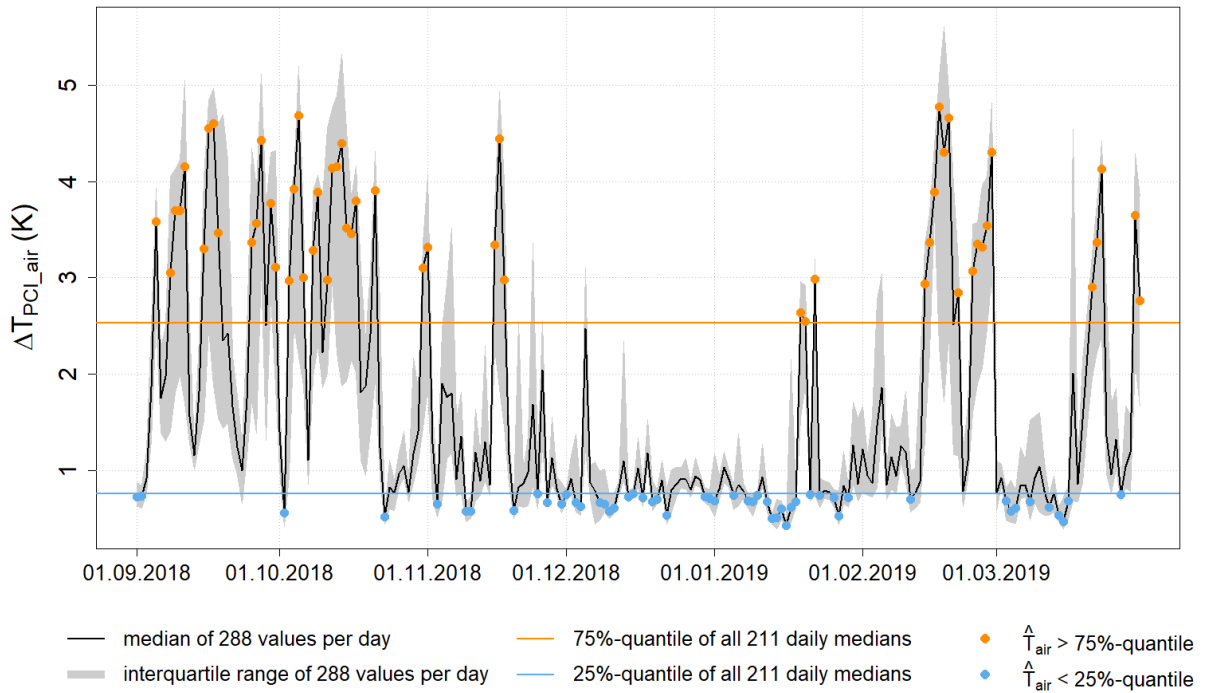


Figure 3.9.: Time series of the daily median and interquartile range of the city-internal air temperature difference $\Delta T_{PCI,air}$ during the whole sampling period (211 days, each day from 10 am to 10 am). The blue and orange lines indicate the 1. and 3. quartile of all air temperature differences; i. e. 50% of all days showed mean differences between these lines, 25% had larger (orange dots) or smaller differences (blue dots)

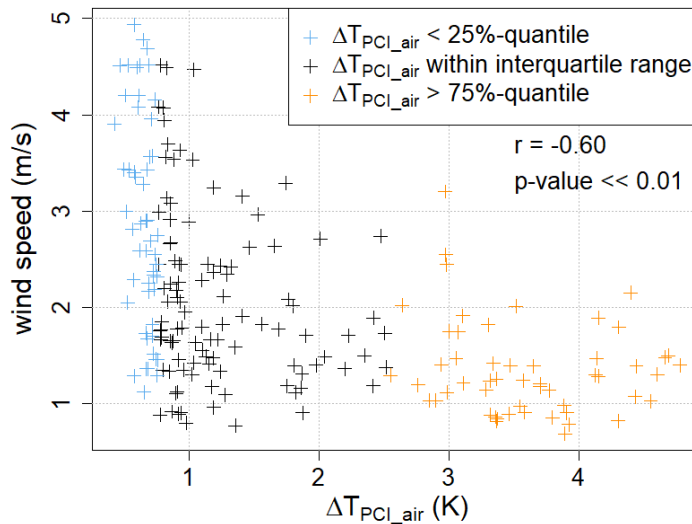


Figure 3.10.: Relation between the city-internal air temperature difference and the wind speed, both on daily average. The variables show a significant rank correlation of $r = -0.60$ ($p\text{-value} \ll 0.1$)

The intensity of the city-internal temperature differences depended on the large scale weather type (Fig. 3.11). The weather of most of the *extreme days* was subject to anticyclonic forcing including weather types characterized by anticyclones above Central Europe (weather types HM and BM), as well as westerly (WA) and north-westerly (NWA) weather conditions. Sometimes also southerly conditions (SA, TRW, SEA) led to high differences. Tendentially, anticyclonic weather conditions caused larger city-internal differences than cyclonic conditions. Extremely small temperature differences occurred mostly during north-westerly conditions (NWZ, NWA), but also on days under westerly (WW, WZ) and south-westerly (SWZ) influence.

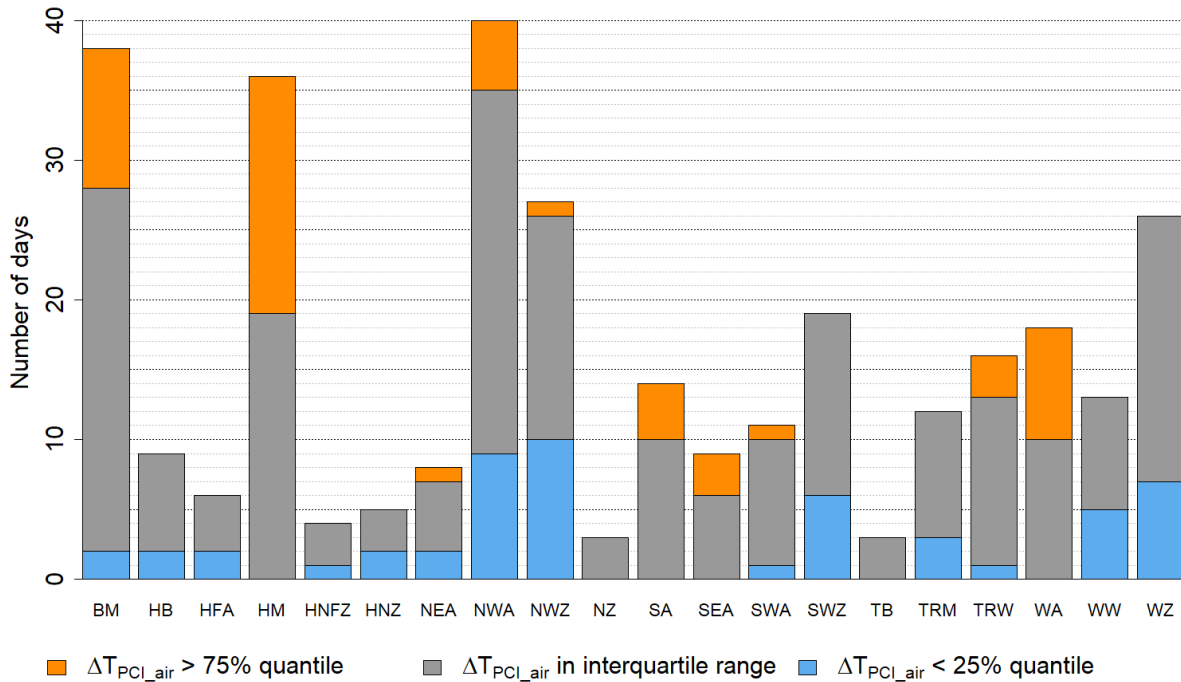


Figure 3.11.: Weather types during the sampling period. Blue: number of days with a certain weather type which showed small city-internal air temperature differences (in total 53 d); orange: number of days with a certain weather type which showed large city-internal air temperature differences (in total 53 d; *extreme days*)

For each measuring site the spatial perturbations of the air temperature \widehat{T}_{air} were determined by subtracting the spatial mean $\langle T_{air} \rangle$ from the air temperature data (Eq. 2.1). The temporal mean was calculated for each site using the whole dataset of 211 d (*all days*) and, additionally, only for the 53 d with extremely large city-internal temperature differences (*extreme days*). The site-specific values of $\overline{\widehat{T}_{air}}$ are listed in table 3.3. The Kämmerei was on average the warmest site with a $\overline{\widehat{T}_{air}}$ of +0.7 K (*extreme days*: +1.3 K). The lowest temperatures were – apart from the EBG – measured at the Mistel (*all days*: –0.5 K, *extreme days*: –1.1 K).

To investigate the causes of these thermal differences, a correlation analysis was conducted with the mean spatial air temperature (*all days*) and several elements of the urban design. The urban design in the surroundings of each site was classified by estimating the ground cover rations of pavement, buildings, water, and vegetation within a 20 m perimeter around the weather station (Tab. 3.3). For the correlation analysis the Spearman’s rank correlation was used, which is, in contrast to the Pearson correlation, also suitable for non-linear relations. The results of the correlation analysis are shown in figure 3.12. Except for the water cover, all elements of urban design had a significant influence on the site-specific air temperature perturbation (p – values < 0.05). The pavement cover ratio at a site correlated with the temperature with a correlation coefficient r of 0.7. A similar positive correlation was determined for the building cover ratio. The amount of vegetation at a site showed a highly significant, negative correlation to the temperature ($r = -0.91$, p – value < 0.001). A significant, negative correlation coefficient was also determined for the percentile of the sky view of a site that is covered by trees ($r = -0.60$). In addition to the influence of these five elements of urban design, the impact of the distance of a site to the city centre (Markt) was investigated. A significant, negative correlation with the air temperature perturbation was found ($r = -0.66$).

Table 3.3.: Classification of the measuring sites, which were used for the correlation analysis. The temporal mean of the spatial perturbation of the air temperature $\overline{\widehat{T}_{air}}$ was determined using the whole dataset of 211 days and for the 53 days, which showed extremely large differences. The percentiles of the 20 m perimeter, which were covered by pavement, buildings, vegetation, or trees were estimated using aerial photos of the sites (appendix A)

site	ground cover (%)				sky cover (%)	distance to the city centre (m)	$\overline{\widehat{T}_{air}}$	$\overline{\widehat{T}_{air}}$
	pavement	building	water	vegetation	trees		(all days)	(extreme days)
Altstadt	40	30	0	30	5	1660	-0.1	-0.3
Birken	40	20	0	40	5	1370	-0.1	-0.1
EBG	0	0	0	100	20	2410	-0.6	-1.3
Hofgarten	0	0	10	70	95	680	0.0	0.0
Kämmerei	18	80	0	2	2	120	0.7	1.3
Karstadt	75	25	0	0	0	63	0.3	0.8
Markt	85	15	0	0	0	0	0.4	0.7
Mistel	0	0	8	92	20	705	-0.5	-1.1
Röhrensee	0	0	30	55	85	1300	-0.4	-0.8
Spinnerei	94	1	0	5	2	870	0.2	0.3
St. Georgen	53	45	0	2	0	1670	0.3	1.0
Wilhelminenaue	15	0	10	75	0	1730	-0.3	-0.6

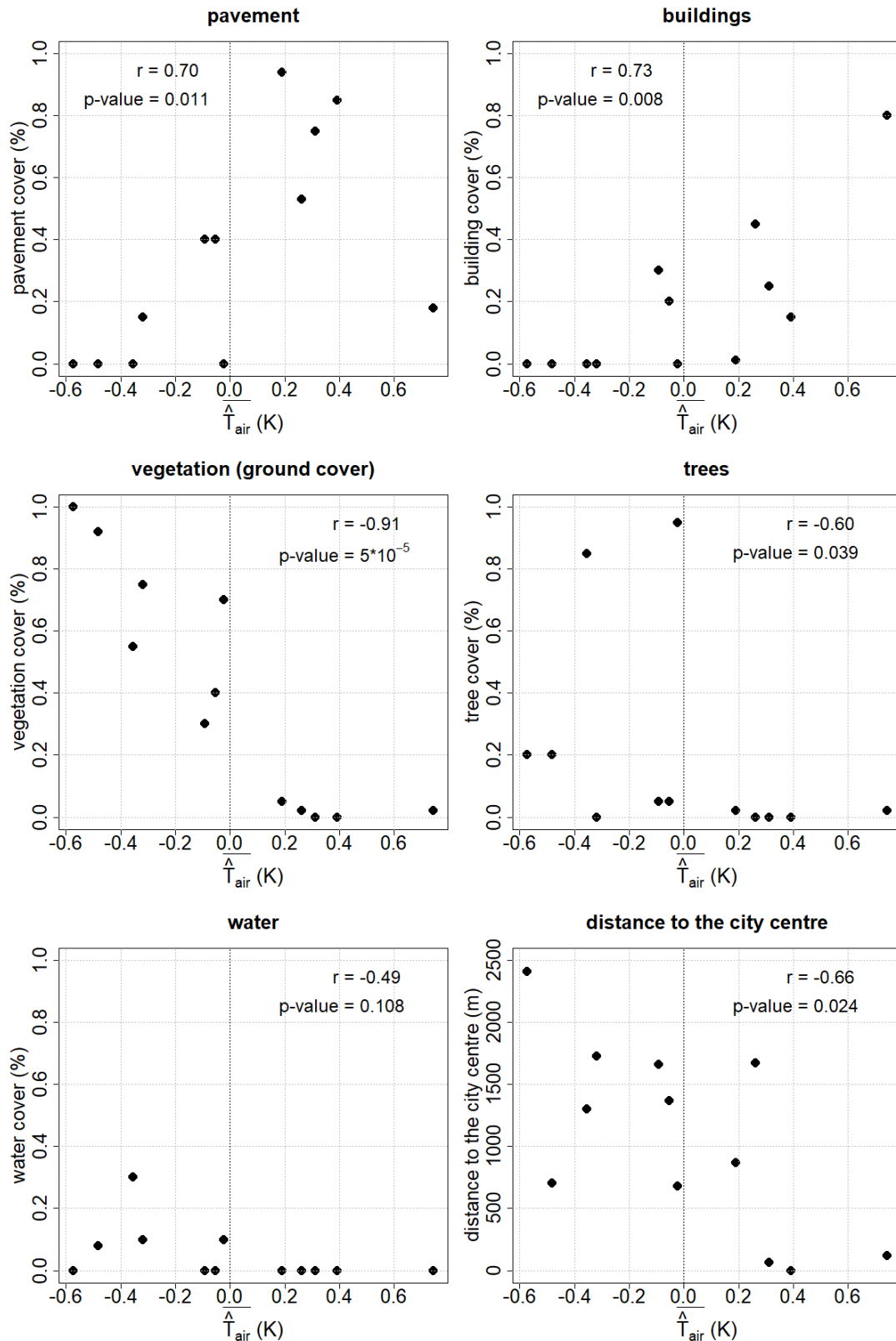


Figure 3.12.: Scatterplots of the temporal mean of the spatial perturbation of the air temperature \hat{T}_{air} vs. the percentile of the 20 m perimeter, which is covered by pavement, buildings, vegetation, or trees or, respectively, vs. the distance to the city centre. *Vegetation* relates in this context to the ground covered by vegetation, while the *tree cover* quantifies the sky view covered by tree crowns. The value r represents the Spearman's rank correlation coefficient, while the p-value is an indication for the significance of the correlation.

3.2.3. Diurnal course of the thermal differences

To investigate the temporal variation of the city-internal differences between different times of day, the mean diurnal course of the spatial perturbation of the air temperature was determined for each site (Fig. 3.13).

The diurnal courses showed differences between daytime and nighttime: While some sites were on average up to 1.2 K warmer or cooler than the mean of all stations during nighttime, the air temperature during daytime deviated maximal 0.5 K from the mean. This referred to the temporal mean \widehat{T}_{air} of the whole sampling period (Fig. 3.13a). Regarding only the 53 *extreme days* both, day- and nighttime showed greater deviations from the mean: $\widehat{T}_{air} \leq 1$ K during daytime and $\widehat{T}_{air} \leq 2.8$ K at night (Fig. 3.13b). The distinctions between the times of day were even more pronounced, too. By contrast, days with extremely small differences on daily average showed almost even deviations of maximal 0.4 K at day- and nighttime (Fig. 3.13c). Only the station in the Kämmereigasse measured on average higher air temperatures at nighttime on these days ($\widehat{T}_{air} \approx 0.5$ K). The Kämmerei was generally the warmest site during nighttime, independent from the actual temperature difference. The sites Markt, Karstadt, and St. Georgen were, with up to 1.5 K, also warmer than the other sites at night, while during the day, the Spinnerei and St. Georgen were the warmest sites (maximum +1 K). During nighttime, however, the \widehat{T}_{air} at the Spinnerei was close to zero. A similar behaviour was observed at the Hofgarten ($\approx +0.2$ K) and the two housing districts Altstadt and Birken (-0.2 K). The Hofgarten, however, was together with the Röhrensee the coolest site during daytime (-0.3 K). The coolest sites at night were the EBG (-2.8 K) and the Mistel (-2 K), followed by the Wilhelminenaue and the Röhrensee (both maximal -1.5 K). While the air temperature at the EBG, Mistel, and Wilhelminenaue did not deviate from the spatial mean during daytime, the Röhrensee stayed up to 1 K cooler than the rest of the sites.

With the dataset of the city-wide measuring network the average UHI and PCI were determined (Tab. 3.4). The city was on average 0.5 K warmer than the EBG during daytime and 2 K warmer at night. During periods of extreme temperature differences the UHI increased to 1 K during daytime and 4.8 K at night. Within the city, the parks were on average 0.8 K cooler than the other urban areas during daytime and 2 K cooler at night. On *extreme days* this PCI reached values of -2 K (day) and -4.2 K (night).

Table 3.4.: Quantification of the UHI and PCI for daytime and nighttime using the city-wide measurements. The determination was made for the whole measuring period (*all days*) and only for days showing extremely large differences (*extreme days*).

	<i>all days</i> day	<i>all days</i> night	<i>extreme days</i> day	<i>extreme days</i> night
UHI	0.5 K	2 K	1 K	4.8 K
PCI	-0.8 K	-2 K	-2 K	-4.2 K

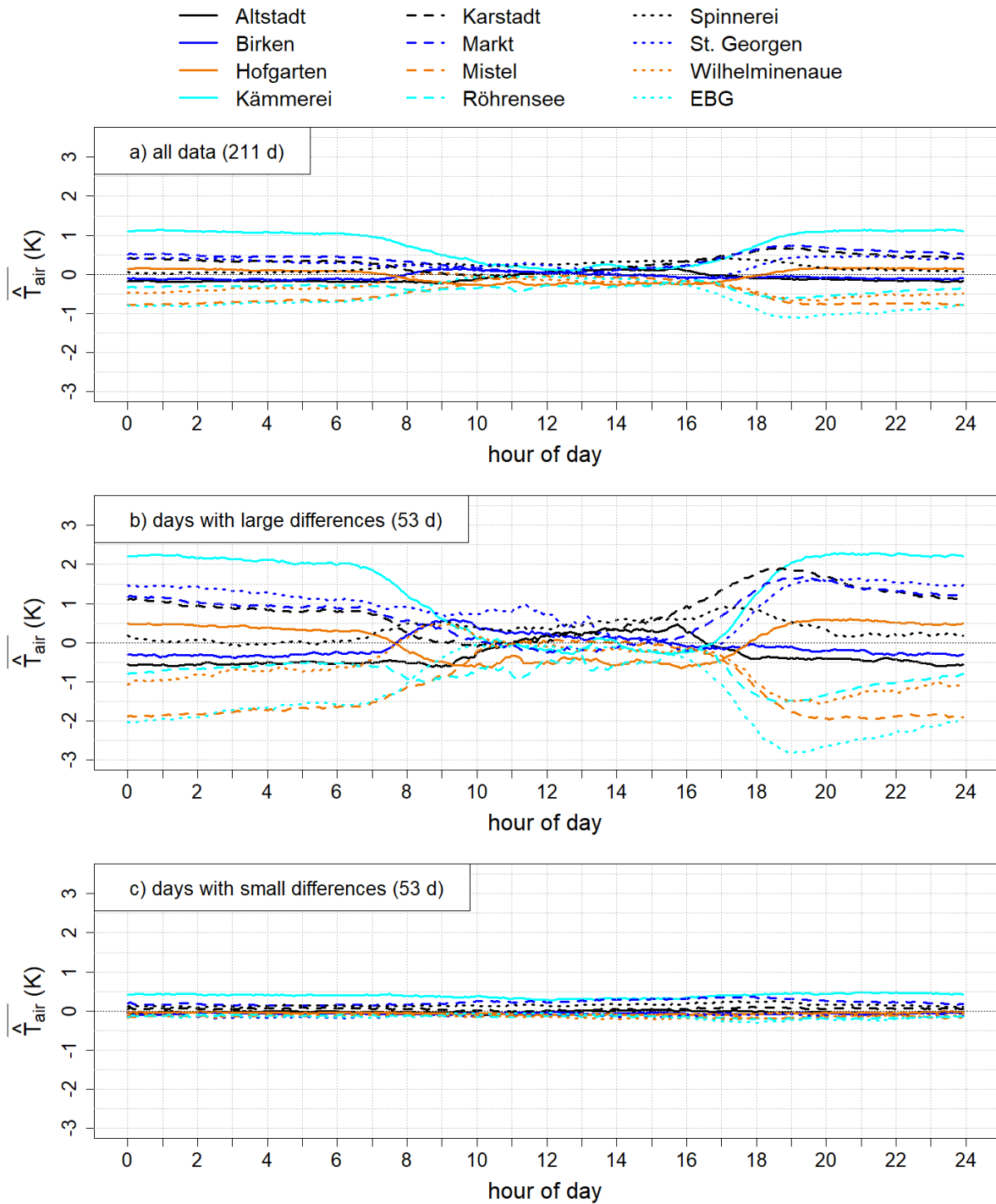


Figure 3.13.: Ensemble-averaged diurnal courses of the spatial perturbation of the air temperature $\overline{\hat{T}_{air}}$ at all stations regarding a) *all days* from September 2018 to March 2019, b) only *extreme days* with large differences (53 d; $\Delta T_{PCI,air} > 75\% - \text{quantile}$), or c) only days with small differences (53 d; $\Delta T_{PCI,air} < 25\% - \text{quantile}$), respectively. Temporal resolution: 5 min

In the following, the mean diurnal courses of the air temperature at selected sites are compared directly. The additionally determined heating and cooling rates at each site are shown in the appendix (Tab. B.2).

The three measuring sites Markt, Karstadt, and Kammerei were the warmest sites in Bayreuth, especially during nighttime. Those three stations were all installed in the city centre within a spatial distance of 200 m, though at structurally different sites. Despite the small horizontal distance, the air temperature differed between those three sites most of the time. To avoid errors by different measuring heights, the temperature differences were calculated using the potential temperature Θ (Eq. 3.2), which takes account of the altitude of the measurement.

$$\Theta = T \left(\frac{p_0}{p} \right)^{\kappa_L} \quad (3.2)$$

with $p_0 = 1000 \text{ hPa}$ and $\kappa_L = \frac{2}{7}$

During extreme nights the air in the Kammerei was on average about 1 K warmer than at the Markt, while in the afternoon the narrow Kammereigasse was up to 0.5 K cooler than the open-spaced market place (Fig. 3.14a). Around 11 am, the two sites were evenly warm and additionally just as warm as the air at the top of the Karstadt building. For this site at about 20 m height generally similar potential temperatures were determined as for the nearby station at the market place (Fig. 3.14b). Only between 10 am and 7 pm, the potential temperature was up to 0.9 K warmer on top of the building than at the ground. In comparison to these highly sealed sites, the Hofgarten was on daily average constantly between 0.2 K and 1.2 K cooler than the Markt site (Fig. 3.14c). The largest difference occurred around 6 pm and in the morning at 9 am, while the difference was the smallest at noon. In the Spinnerei, which is equally sealed as the Markt but located at the edge of the built-up area, the air temperature was also lower than at the Markt during night (1 K to 1.5 K) (Fig. 3.14d). During daytime on the contrary, it was 0.7 K warmer in the Spinnerei. At the Spinnerei the highest cooling rate was reached 20 min later in the morning than at the Markt. In the evening, the cooling rate was larger at the Spinnerei (-2.9 K h^{-1} ; Markt: -2.5 K h^{-1})

The coolest urban measuring site was not located at the edge of the built-up area, but quite near the city centre: the river bank at the Mistel. Even on *extreme days* the air temperature at this site was on average similar to the T_{air} at the rural reference station in the EGB (Fig. 3.15). The only differences occurred in the morning and in the evening: The air at the EGB heated up 30 min earlier after sunrise and cooled down 40 min earlier with sunset and showed a larger cooling rate (EBG: -3.9 K h^{-1} ; Mistel: -3.3 K h^{-1}). The maximum T_{air} at the Mistel was reached with a delay of about 1.5 h. This resulted in temperature differences of 1 K. More pronounced differences to the rural site showed the sealed Markt in the city centre: The cooling rate at the Markt was particularly at night smaller than at the rural site (EBG: -3.9 K h^{-1} ; Markt: -2.5 K h^{-1}) and the maximum daily T_{air} was reached about 1 h later.

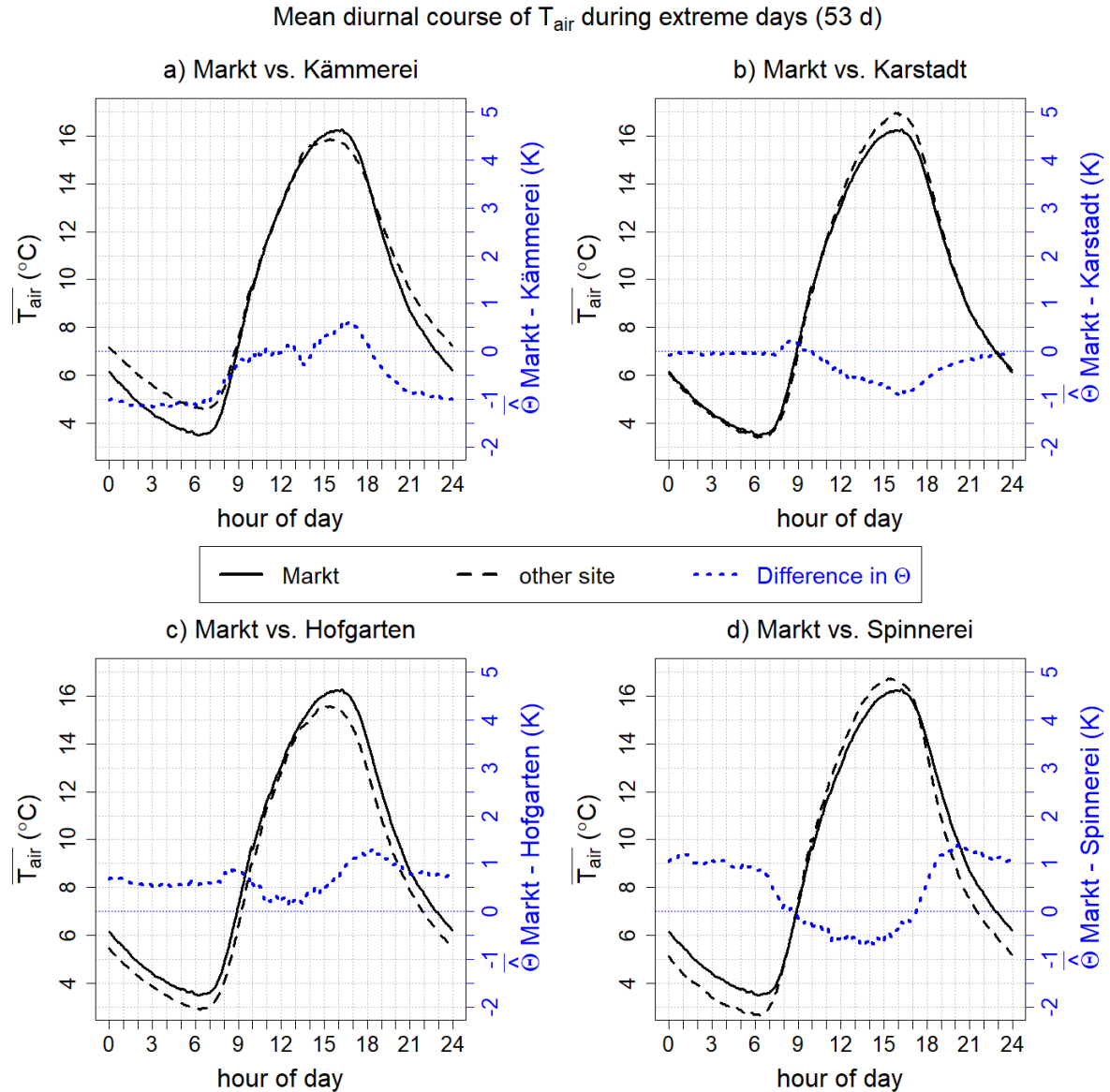


Figure 3.14.: Direct comparison of the mean diurnal course of the air temperature at the Markt with four other stations for showing the influence of the following elements of the urban design: a) building density (Kämmerei), b) height of the measurements above ground (Karstadt), c) vegetation with trees (Hofgarten), and d) large distance from the city centre (Spinnerei); The ensemble average was calculated using only days with large city-internal differences ($\geq 75\%$ quantile; 53 d); The dotted blue lines indicate the difference between potential temperatures at the Markt and the other station. (temporal resolution: 5 min)

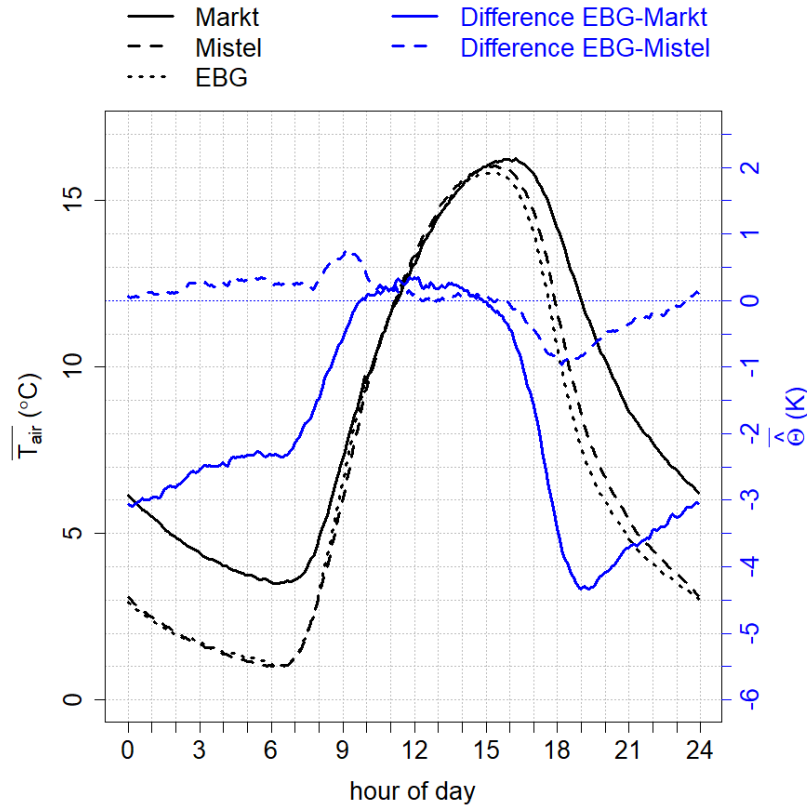


Figure 3.15.: Direct comparison of the mean diurnal course of the air temperature at the Markt with the coolest urban station (Mistel) and the rural reference station (EBG); The ensemble average was calculated using only days with high city-internal differences ($\geq 75\%$ quantile; 53 d); The blue lines indicate the difference between potential temperatures at the Markt and the other two stations (temporal resolution: 5 min)

As ventilation with rural or urban air can influence the site-specific heating, the wind direction is of relevance for the city-internal temperature differences. The most relevant wind directions at each site were determined for daytime (10 am to 4 pm) and nighttime (10 pm to 4 am). The wind was often channelled along the directions of street canyons or valleys. At the following sites the wind direction changed as the day progressed: The Altstadt was at night mostly ventilated from southerly direction, while during the day the wind came more frequently from north-east. During daytime, more air from the city centre reached the site (Fig. 3.16). The Mistel, by contrast, was most of the time ventilated from the west. Only during daytime the wind came partly from easterly direction, where the city centre is located. The varying wind direction at the Röhrensee during the day contrasted clearly with the constant nocturnal ventilation from the south. Only nocturnal ventilation towards the city occurred also in the north of Bayreuth at the Spinnerei.

At the mentioned sites, the wind was at night often directed towards the city. These were also the sites, which showed a more intense nocturnal cooling than other sites. The windroses for all other sites are shown in the appendix (Fig. B.9 and Fig. B.10).

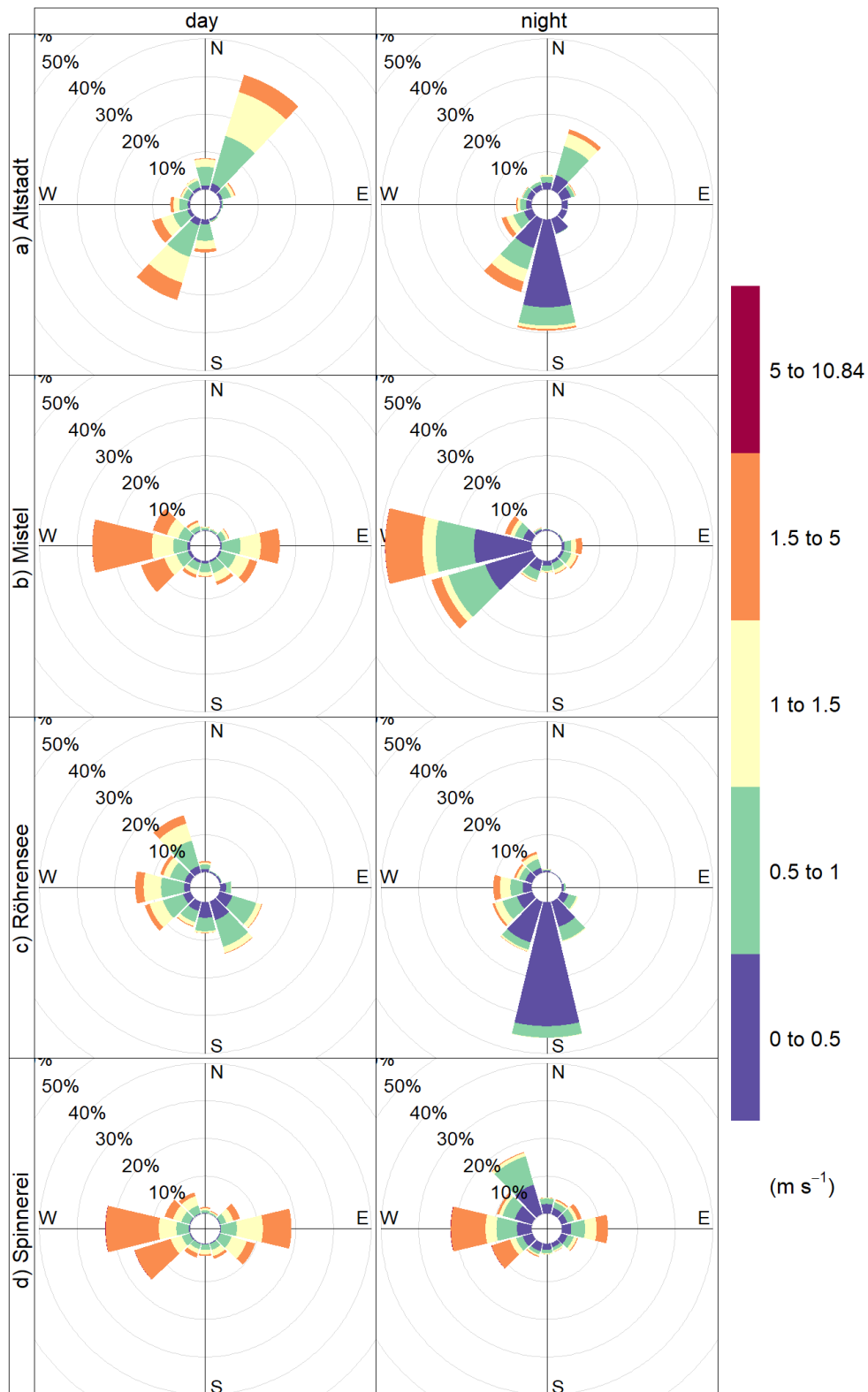


Figure 3.16.: Wind roses for the three sites Altstadt (a), Mistel (b), Röhrensee (c), and Spinnerei (d) parted for daytime (10 am to 4 pm) and nighttime (10 pm to 4 am). Data: 211 d, temporal resolution: 5 min. Wind roses for all other sites are shown in the appendix (Fig. B.9)

3.2.4. Multiresolution Decomposition

To reveal similarities or differences regarding the meteorological behaviour, spatial two-point correlation coefficients were calculated using the time series of air temperature on several temporal scales (chapter 2.2.3). For simplicity, the correlations presented here were determined primarily with the Markt site as reference, so all correlation coefficients refer to the Markt if not stated otherwise.

The correlation between the T_{air} at different sites was generally smaller, the higher the temporal resolution of the time series was. Regarding the whole data set (211 d; 24 h), the correlation coefficients of the air temperature time series R_T ranged on spatial average between 0.71 for the 5.625 min resolution and almost 1 for the 24 h resolution (Fig. 3.17a). The daytime data correlated to a slightly higher degree (0.77 (5.625 min) to 1 (6 h); Fig. 3.17b). Generally smaller correlations between 0.60 (5.625 min) and 0.99 (6 h) occurred when only nighttime data were compared (Fig. 3.17c). During extreme nights the correlations were with 0.38 (5.625 min) to 0.97 (6 h) on average even smaller (Fig. 3.17d). The magnitude of R_T within one temporal scale was the largest for high resolutions. These large spatial correlation differences occurred especially at night, when additionally the correlation coefficients depended on the separation distance. For the data of the lowest resolutions and daytime, this distance dependency was less distinct.

Independent of the temporal resolution, correlation coefficients of at least 0.65 could be observed. The Kämmerei, Hofgarten, and Mistel overall correlated best with the Markt, closely followed by the Karstadt and the Spinnerei. At night, the T_{air} at the Markt showed the highest correlation to the nearby sites Kämmerei and Karstadt. Unlike the daytime, the Markt site was during night more correlated with the Karstadt than with the Kämmerei. While the daytime data of the sites Hofgarten, Mistel, and Spinnerei correlated almost equally well with the Markt, the correlation coefficients of the nighttime data differed: regarding the time series of the 5.625 min to 22.5 min resolutions for these three sites, the R_T decreased with increasing separation distance. For lower resolutions the Mistel, which is located closer to the Markt than the Spinnerei but more distant than the Hofgarten correlated less with the Markt than the other two stations.

The two sites Röhrensee and Birken were almost equidistant from the Markt site and correlated during daytime almost equally, whereby the high resolution daytime data (5.625 min to 22.5 min) of the Birken showed slightly higher R_T than the Röhrensee. At night, by contrast, when larger differences occurred, the Röhrensee showed a higher correlation with the Markt at least for the low resolution time scales of less than 1 h. Regarding the data of higher resolutions, the Markt was more correlated with the Birken during night and with the Röhrensee during day.

Apart from the reference station in the EGB, the Altstadt, St. Georgen, and Wilhelminenaue were the sites located farthest from the Markt. In spite of being located at opposite sides of the city, the T_{air} at the districts Altstadt and St. Georgen correlated equally with the Markt temperature regarding all 24 h data. Partitioning the data into day and night revealed smaller R_T of the St. Georgen data during day and slightly higher R_T at night in comparison to the Altstadt data. The Wilhelminenaue was overall less correlated with the Markt, whereby this

effect was mostly induced by rather low R_T of the nocturnal temperatures. Only the T_{air} at the EBG showed smaller correlation with the Markt temperature at night. Regarding the daytime data, the EBG correlated with the Markt to a slightly lower degree as the Wilhelminenaue.

The correlations of the air temperatures during extreme nights behaved in this relative spatial comparison similar to the correlations that were determined for the data of all nights, though with larger differences. Only the 11.25 min and 3 h data showed smaller discrepancies to the all night results as the Markt T_{air} was for these two time scales less correlated with the Röhrensee than with the Birken. The 11.25 min data of the Wilhelminenaue were during extreme nights additionally decorrelated from the Markt, even more than the 5.625 min data.

Similarities and dissimilarities of sites were highlighted by looking at the spatial two-point correlation coefficients of the air temperature of every site in comparison to all other sites. To minimize the spatial effects of the distance, the 6 h time scale was used for this comparison. With the R_T that were calculated using all data (211 d; 10 am to 10 am) two groups with opposite behaviour could be detected (Fig. 3.18): The T_{air} at the Markt, Karstadt, and Kämmerei were well correlated among each other as mentioned before and additionally showed similar behaviour regarding the correlations with all other sites. The EBG, Mistel, and Wilhelminenaue on the contrary were combined to a second group as they showed generally an opposite behaviour to the city centre sites. These two groups could be well separated based on their R_T for all sites but the Spinnerei. The T_{air} at the Birken, Röhrensee, and Altstadt were more correlated with the EBG, Mistel, and Wilhelminenaue, than with the city centre, while the Hofgarten and St. Georgen showed by contrast higher R_T with the Markt, Karstadt, and Kämmerei.

With the correlation coefficients of the nocturnal air temperatures (211 d; 10 pm to 4 am; 6 h resolution) some sites could be aggregated to pairs of similar behaviour, though all correlations were with $R_T > 0.95$ quite large (Fig. 3.19): As for the 24 h intervals the nocturnal correlations of the EBG with all other sites were quite similar to those of the Mistel with the highest correlations with the Röhrensee, Birken, Wilhelminenaue, and Altstadt and the lowest with St. Georgen and the Kämmerei. The latter sites themselves showed similar correlations. Only the Birken correlated almost equally with the two pairs EBG/Mistel and Kämmerei/St. Georgen. Finally, the Röhrensee and the Altstadt could be paired up, as those two sites showed generally high correlations with all other sites.

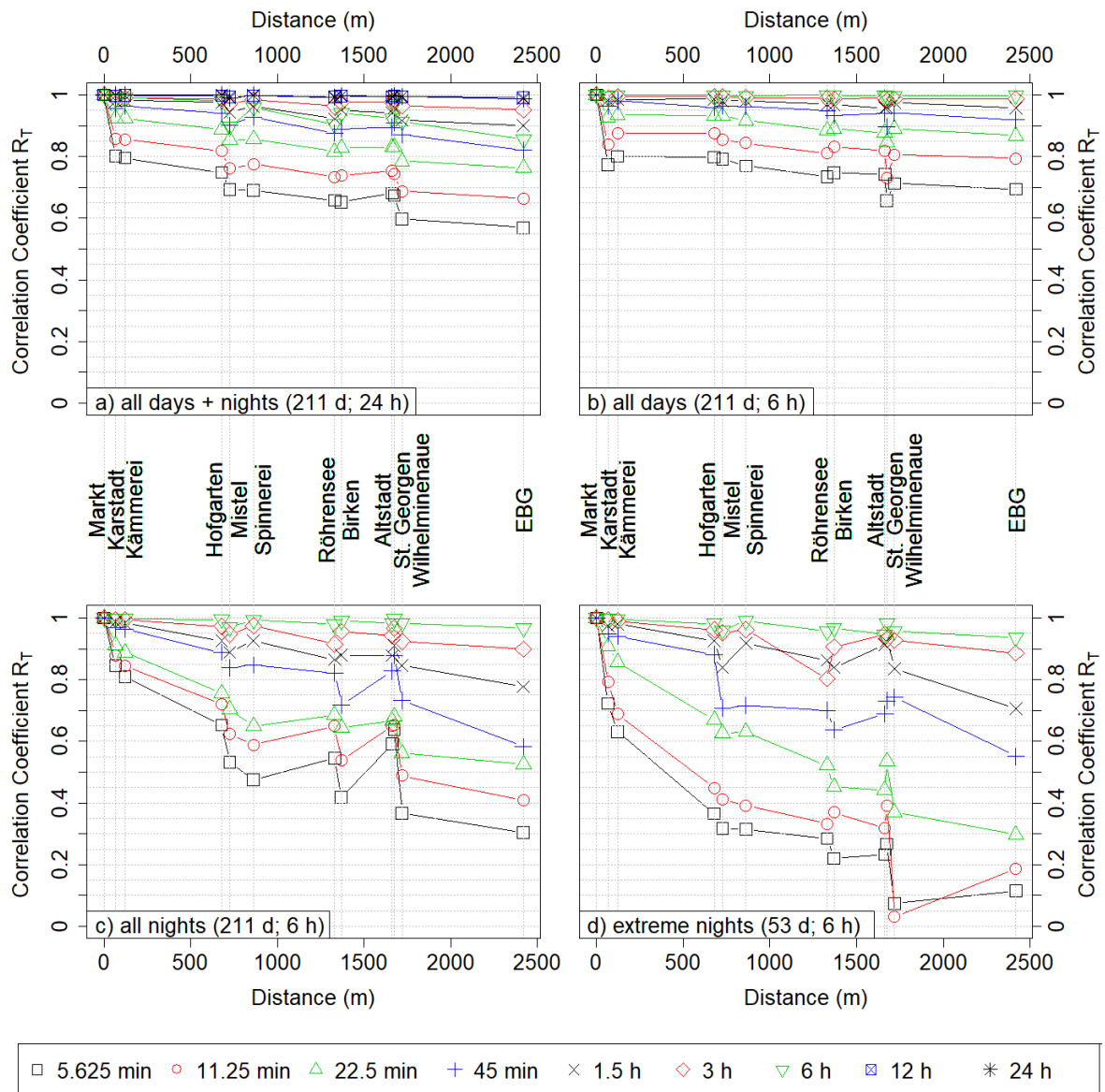


Figure 3.17.: Spatial two point correlation coefficient R_T of the air temperature at the Markt in comparison to all other stations in dependency of the separation distance between the Markt and the comparison stations. The various time scales are represented by graphs in different colours. R_T was determined for a) all data of all days (211 d; 10 am to 10 am), b) only daytime of all days (211 d; 10 am to 4 pm), c) only nighttime of all days (211 d; 10 pm to 4 am), and d) only nighttime of *extreme days* (53 d; 10 pm to 4 am)

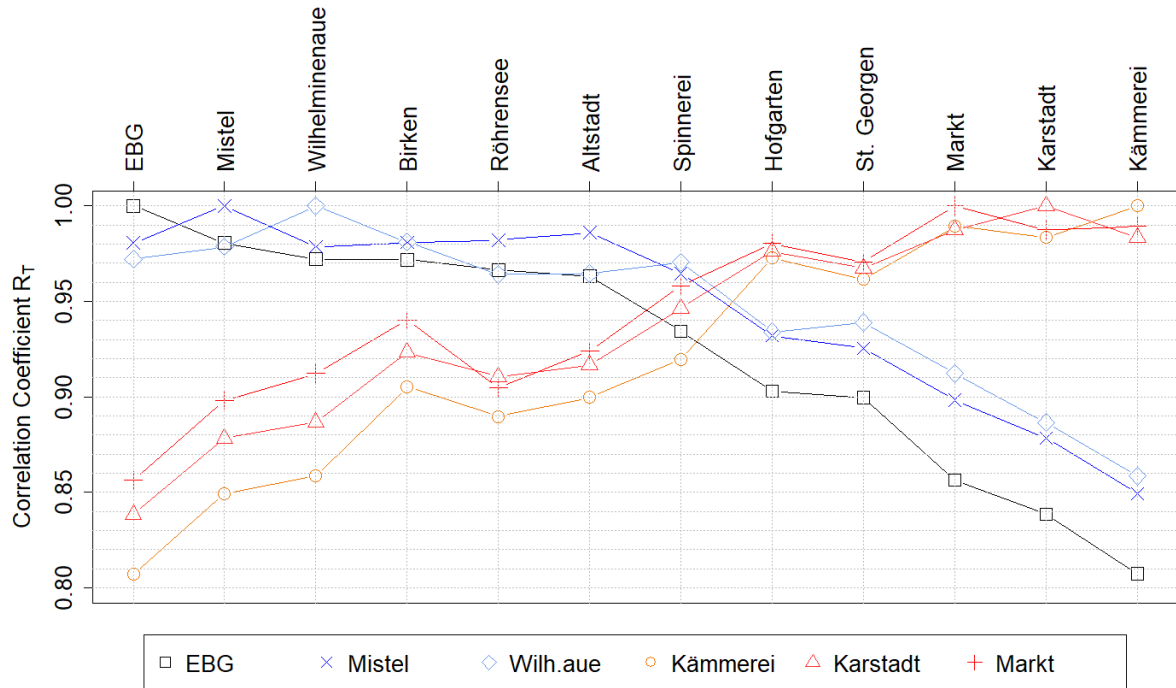


Figure 3.18.: Spatial two point correlation coefficient R_T of the air temperature at six selected stations in comparison to all other stations for the time scale of 6 h. These R_T were determined using all available data (211 d; 10 am to 10 am). This selection highlights similar or distinct correlation coefficients of the T_{air} at the selected sites.

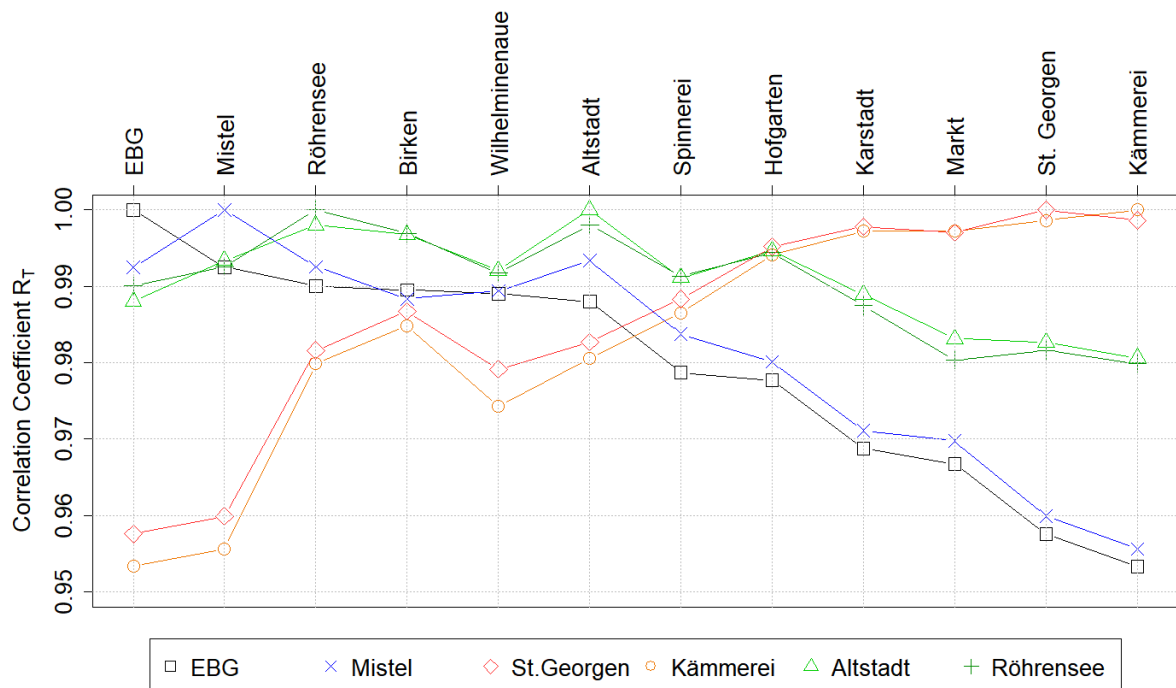


Figure 3.19.: Spatial two point correlation coefficient R_T of the air temperature at six selected stations in comparison to all other stations for the time scale of 6 h. These R_T were determined using only nighttime data of *all days* (211 d; 10 pm to 4 am). This selection highlights similar or distinct correlation coefficients of the T_{air} at the selected sites.

4. Discussion

4.1. Quantification of the thermal differences

The first objective of this study was to quantify the heat differences in a medium-sized city. Meteorological data were collected and analysed on different temporal and spatial scales to determine city-internal thermal differences (PCI) and the additional heat load in the city in comparison to the rural surroundings (UHI). It was expected, that urban parks are characterized by similar thermal conditions as the rural surroundings of the city ($\rightarrow |UHI| = |PCI|$).

4.1.1. Urban Heat Island

The city-wide meteorological measurements in Bayreuth and the surroundings revealed average urban-rural air temperature differences of 0.5 K during the day and about 2 K at nighttime. These averages included *all days* of the measuring period between September and March. Regarding only the *extreme days*, the average urban-rural temperature difference ranged from 1 K during daytime to 4.8 K at night.

As numerous studies have been made on the UHI and its variability in many cities of different size, climate, and latitude, different quantitative values were reported for the magnitude of the UHI. Oke (1973) estimated a maximal UHI magnitude of 5 to 6 K for an European city with a population of less than 10^5 . For larger European cities like Stuttgart, Berlin, or Vienna other studies reported *average* urban-rural air temperature differences of up to 2 K and maximal UHI intensities of, for example, 12 K (Böhm (1998); Gabriel and Endlicher (2011); Szymanowski and Kryza (2012); Ketterer and Matzarakis (2014)). Although Bayreuth has a significantly smaller area, the average temperature difference ranges within the UHI magnitudes of these larger cities. An inter-city comparison of UHI magnitudes is, however, rated to be inconclusive, because of the numerous influencing factors and the heterogeneity of cities (Stewart, 2011).

Regarding the diurnal evolution of the UHI, consistent results were reported from different cities. At night, the temperature differences are generally the largest, as the UHI intensifies around sunset and peaks around midnight (Oke and East, 1971). In Bayreuth the UHI was most pronounced earlier: at about 7 pm in the evening, when the air temperature at the rural EBG already decreased with sunset, while the cooling in the city had not yet begun. After the nocturnal peak the UHI diminishes and reaches its minimum extent during daytime with on average 0.5 to 1 K in Bayreuth. In other cities the temperature difference completely decays with sunrise or even changes the sign, so the city becomes a cool island in a warmer surrounding rural area (Runnalls and Oke (2000); Bhargava et al. (2017)). Such an *Urban Cool Island* was not observed in Bayreuth, as the EBG never was the warmest site during the measurement period. Further measurements during the summer months will be of interest as this Urban

Cool Island was reported to occur mostly on summer days, when the urban geometry shadows the surface, while the open-spaced rural site is exposed to intense global radiation (Runnalls and Oke, 2000).

In this study the location of hot and cool spots changed as the day progressed: In the morning St. Georgen was the warmest site, while after midday it was warmer at the Spinnerei. Afterwards the city centre showed on average the highest temperatures: first high up on the Karstadt building and after sunset in the Kämmergeigasse, which stayed the warmest site for the whole night. This observation confirms and refines former studies, which found, that the UHI determination with a single fixed urban station underestimates the intensity in comparison to mobile measurements (e.g. Runnalls and Oke (2000)). The core of the Heat Island changes its spatial location with the time of the day. This variation may not be captured even by mobile measurements, as, also because of the temporal and spatial differences between the cooling and heating rates at different sites, only simultaneous observations allow a direct comparison.

This point impedes the interpretation of the $\Delta T_{UHI,air}$, which were determined with the case study measurements. The housing area near the Hofgarten was in the evening of the three measuring days on average 1.4 K warmer than the EBG, though this result was only a snapshot in comparison to the city-wide measurements. The temperature difference between the housing area and the EBG increased towards late afternoon and early night. This result is consistent with the peak UHI intensity in the evening or early night that was shown by the city-wide mean diurnal course of the UHI intensity.

4.1.2. Park Cool Island

The case study measurements were more useful for the quantification of small-scale temperature differences within the urban area of Bayreuth and, more precisely, for the quantification of the PCI as they were made around the Hofgarten. The transect measurements showed that the spatial air temperature differences increased with the course of the day. In the evening they peaked, according to the point measurements, with a $\Delta T_{PCI,air}$ of -1.7 K. Although the surface temperature showed a larger PCI of -2.3 K, the differences between perceived temperatures at the points were with -1.3 K on average smaller than the $\Delta T_{PCI,air}$. Such an increase of the PCI_{air} over the day as the transect measurements indicated could not be detected by the city-wide measurements. Those measurements showed constant average air temperature differences within the city during daytime (*all days*: $\Delta T_{PCI,air} = -0.8$ K; *extreme days*: $\Delta T_{PCI,air} = -2.0$ K). In the evening, however, the differences increased fast and reached on average -2.0 K or, regarding only the *extreme days*, -4.2 K. These variabilities of the PCI intensity between day and night were also observed by others, though with smaller differences: a review by Bowler et al. (2010) summarized several studies to an average daytime PCI of -0.9 K vs. a PCI of -1.2 K at night.

The site showing the minimum air temperature changed in the course of the day: While the open-spaced site at the Mistel was the coolest the whole night trough, during daytime the lowest temperatures were measured in the two forested parks Hofgarten and Röhrensee. This result is consistent: the largest daytime PCI form at forested parks due to shading, whereas at night the cooling is more intense at open-spaced lawn sites than at their built-up surroundings

because of unimpeded longwave emission (Spronken-Smith et al., 2000). The size of the park is an additional parameter controlling the intensity of the PCI (Bowler et al., 2010). This relationship could not be verified with this study, since the Hofgarten was the only forested park investigated near the city centre.

As the PCI was determined without regard to the separation distance between the compared sites, it is necessary to discuss the term Park Cool Island in this context. Spronken-Smith and Oke (1998) defined the PCI as “area of lower temperature associated with a park”. Therefore, the naming of city-internal temperature differences as PCI is only appropriate for differences between a park and the *nearby* surroundings without the typical park structures. Large temperature differences between the sites St. Georgen and Mistel are not necessarily a PCI, but simply a city-internal spatial temperature difference, as the sites are wide apart. However, the lower air temperatures at Mistel indicate a PCI, but the exact *quantification* should be made in comparison to a nearby urban site.

4.1.3. Comparison UHI vs. PCI

The qualitative relation of the UHI and the PCI can be illustrated by comparing the average diurnal courses of the two island effects (Fig. 4.1). This comparison is based on the results of the city-wide measurements in Bayreuth. During daytime, the magnitude of the PCI is almost twice as large as the UHI. The reason for this relation lies in the fact that there are sites in the city, e.g. the Röhrensee, which are cooler than the rural reference site. The relation between the UHI and PCI changes before or around sunset, when the cooling rates are larger at the rural reference site than at the urban green sites. The UHI intensity increases faster than the PCI. The magnitude of the PCI is smaller than the magnitude of the UHI. Around midnight, the magnitudes converge as the UHI decreases due to urban cooling. Afterwards, the average UHI and PCI magnitudes are almost even until sunrise, as the PCI stays almost constant during the whole night.

However, these schematic diurnal courses distort the result by ignoring the fact that with the course of the day, different sites showed the extreme temperatures, which were used for the UHI and PCI determination. This distortion is especially important for the PCI: during the day the lowest temperatures were measured in the shadow of the forested parks Röhrensee and Hofgarten and at night at the open-spaced lawn site Mistel. Because of this fact, in this comparison the PCI is as large as the UHI after midnight and larger than the UHI during the day. A comparison of the UHI and PCI between sites with a similar sky view is regarded as more consistent.

This thesis showed that the first hypothesis, stating that urban parks show similar conditions as the rural surroundings, applies for the time between midnight and sunrise. At daytime, urban parks can be even cooler than rural areas. During the first nighttime hours, however, even in medium-sized cities urban parks are affected by urban heating.

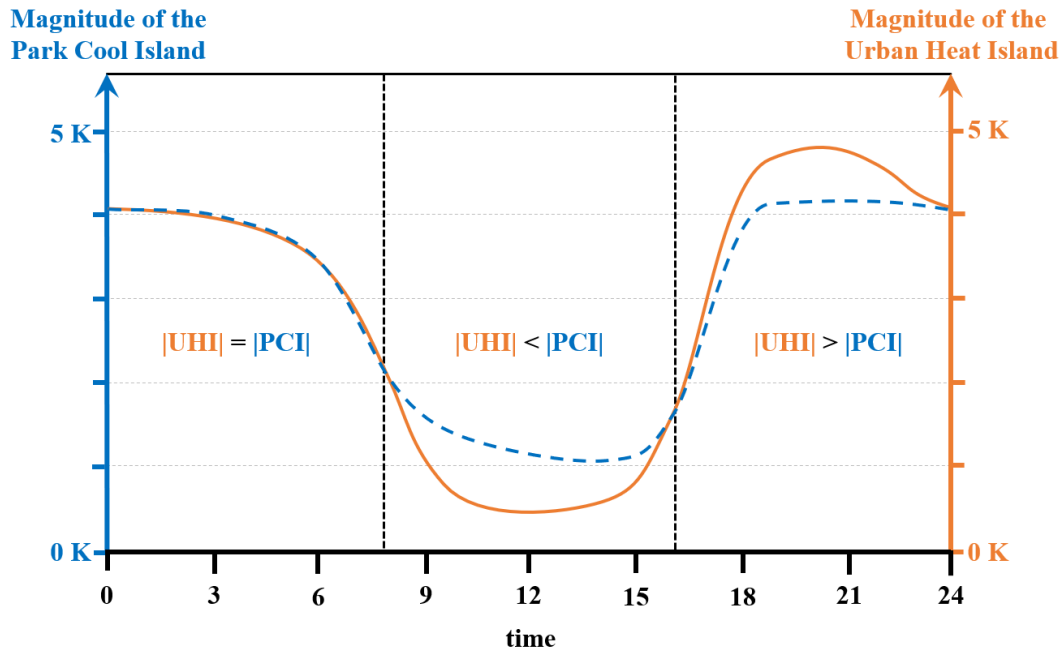


Figure 4.1.: Qualitative comparison of mean diurnal courses of the UHI (solid, orange graph) and the PCI (dashed, blue graph). As the PCI in this study is defined as a negative value, for comparability both temperature differences were plotted as magnitude. The vertical black lines indicate the time of day when the relation of the two island effects changed. As scale for the y-axis, the temperature differences on *extreme days* was chosen as an example.

4.2. Explanation of the thermal differences

The second objective of this study was to explain the thermal differences. Therefore, the most important factors, which induce or intensify the variabilities, had to be determined. External forcings like the weather were considered as well as different elements of urban design, which vary spatially between the different sites.

It was expected that the largest city-internal temperature differences occur under calm, anticyclonic conditions as the highly sealed sites form warm spots, while cool spots evolve at vegetated urban sites.

4.2.1. Influence of external forcings

The transect measurements on two days with different moisture conditions showed that, under dry conditions, the air temperature above a meadow can exceed the air temperature over asphalt. Local properties like the soil moisture have an important influence on variabilities on a small spatial scale. Additionally, the thermal effectiveness of parks, especially of open-spaced green areas, is influenced as the cooling by evapotranspiration depends on the water availability. The ET in urban parks can exceed the ET in streets and even at rural fields, but only under the condition that enough water is available (Spronken-Smith et al., 2000). The intensity and horizontal extent of the ET-induced PCI depend on the horizontal advection. In Bayreuth extremely large temperature differences were linked to low average wind speeds. That relation is also the reason for the smaller correlation coefficients R_T of the air temperature data of the 53 extreme nights in comparison to the R_T determined for the temperature data of all nights.

The passage of weather fronts is reflected in the distance dependency of the correlation coefficients of the high-resolution data. These fronts can induce large short-time differences within the city. But also the UHI intensity can be affected by weather fronts, as shown by Gedzelman et al. (2003): the UHI intensity in New York was largest two to three nights after a cold front passage. Highest UHI intensities are often recorded during high mean sea level atmospheric pressure, whereby the location of the centre of the anticyclone is relevant for the genesis and development of the UHI (Morris and Simmonds (2000); Ivažnšič and Žiberna (2019)).

Regarding the weather types, extremely large average ΔT_{air} occurred in Bayreuth mostly during anticyclonic conditions. Cyclonic conditions led to smaller differences. But also under anticyclonic conditions these small differences occurred. Consequently, the weather type can be used as an indication for the occurrence of large or small temperature differences. However, one weather type can effect urban air temperature differences in different ways. This effect arose in Bayreuth with the weather type NWA, which describes north-westerly, anticyclonic conditions. It has to be considered that the weather type classification by Hess and Brezowsky (1969) only gives a general classification of the circulation pattern in the atmosphere above Europe during a day. But depending on the season, the location, and the exact form of the conditions, one weather type can lead to various effects. With a dataset comprising several years, the season-dependent effects of most weather types can be statistically evaluated for one city.

4.2.2. Influence of the urban design

The external forcings provide the general potential for the formation of large temperature differences. Where hot and cool spots evolve, however, is controlled by urban design.

The largest impact of urbanization consists in the replacement of vegetation and soil by urban structures such as buildings and streets made of artificial materials. The city-wide measurements showed that, as expected, the highly sealed sites in Bayreuth were the warmest: Kämmerei, Karstadt, Markt, St. Georgen, and Spinnerei. These sites are characterized by a low amount of permeable surfaces with a capacity for water storage. There is almost no water available for evaporative cooling, which could, together with transpiration by plants, contribute to the reduction of daytime heating intensity (Ryu and Baik, 2012). Regarding urban surfaces, in addition to the grade of sealing, the paving material is relevant. The heating potential of a site is controlled by the absorption, heat storage, and longwave emission of a surface, which are given by the material properties. Increasing the albedo of pavement material, e.g. by replacing black asphalt by brighter concrete, could reduce the temperature of those horizontal surfaces significantly (Wang et al., 2016). At the measuring sites in Bayreuth, this albedo effect could not be seen since all highly sealed sites are paved with similar dark materials.

The 3D urban geometry and the amount of vertical surfaces are another important parameters. During daytime, buildings can inhibit the site-specific heating by shading horizontal surfaces. This shading especially reduces the surface temperature of the horizontal surfaces (Ryu and Baik, 2012). The impact on the air temperature is, however, disputed (Armson et al., 2012). In Bayreuth, the site at St. Georgen, for example, showed increased air temperatures in the morning hours, when the site was exposed to direct global radiation. Later in the day, when

the buildings along the street shaded the site, the spatial temperature deviation sank to almost 0 K. Shading effects by buildings also occurred in the narrow alley of the Kämmereigasse. There, the daytime temperature was on *extreme days* on average even reduced in comparison to the spatial mean temperature, as other, not-shaded sites were more heated. At night, however, the buildings narrowing the Kämmereigasse had an opposite effect. Buildings inhibit cooling by absorbing and reemitting longwave emission (Oke, 1981). As a result, the air at the Kämmerei cooled down even slower than the air at the nearby Markt. Consequently, at night the Kämmereigasse was constantly hotter than the Markt, while during daytime the Markt was warmer. The correlation analysis revealed significant correlations with the air temperature for the cover ratio of pavement as well as for the building density around a site. In comparison to modern districts, the heating effect in the city centre could be additionally intensified due to increased heat storage and release by the building walls partly made of sandstone. The thermal properties of walls influence the heat conduction and longwave emission of buildings and are therefore important factors for urban heating (Arnfield and Grimmond (1998); Lemonsu and Masson (2002)).

Reduced nocturnal longwave emission occurs in street canyons as well as at forested sites due to insulation by the tree crowns (Bowler et al., 2010). The forested Hofgarten was, nevertheless, on average constantly cooler than the open-spaced Markt, even at night, when the cooling in the park by ET and outgoing longwave emission should be minimal. Longwave emission of urban materials are an important contribution to nocturnal urban heating. Similar to buildings, trees also inhibit daytime heating by shading horizontal surfaces. The effectiveness of shading by trees increases with the tree cover ratio, which depends on the size of the crowns and on the density of the vegetation (Wang and Akbari, 2016). Lin et al. (2017) even showed that for a significant reduction of the daytime air temperature in small urban parks a tree cover ratio of more than 42% is needed. The effect of vegetation is not limited to the area of the park, but can expand into built-up areas. Ca et al. (1998) found that a 0.6 km² park showed a cooling effect of -1.5 K in up to 1 km in lee.

In Bayreuth, it could clearly be seen, that the open-spaced sites without nearby buildings like the sites Mistel and Wilhelminenaue were the coolest sites at night, whereas during daytime, it was coolest at the densely forested sites Hofgarten and Röhrensee. According to the results of the correlation analysis, the ground cover of vegetation as well as the amount of trees has a significant influence on the site-specific air temperature.

Despite the high tree cover ratio and the large water body, which could also store heat like buildings, the air at the Röhrensee cooled down at night. The air in the Hofgarten, however, that has similar site characteristics was warmer. As the correlations between the time series of air temperature showed additionally, the temperature at the Hofgarten was more related to the city centre than to the other green sites. This nocturnal temperature difference between the Hofgarten and the Röhrensee is a result of the different structure of the urban surroundings or, respectively, the distance to the city centre. Even in smaller cities like Bayreuth, urban districts near the city centre are often more densely built than housing areas at the periphery. The effect of inhibited cooling by outgoing longwave emission is increased near the city centre (Tan et al. (2010); Franck et al. (2013)). Additionally, cooling by fresh rural air is more likely

in outer districts. The different ventilations are regarded to be the most important cause for the temperature difference between the sites Hofgarten and Röhrensee. These effects of a large separation distance to the city-centre are also the reasons for the housing districts Altstadt and Birken to be, despite the high grade of sealing, surprisingly cool at night. On extreme nights, the two sites were on average 1.5 K cooler than the Markt. For the city of Stuttgart Ketterer and Matzarakis (2014) found similar average air temperature differences of 1.7 K between the city centre and the suburban areas. The nocturnal influence of rural air could be seen in the wind directions, especially at the sites Altstadt and Spinnerei, both located near rural areas. A significant correlation was found between the distance of a site to the city centre and the \widehat{T}_{air} at the site. However, the air at the Mistel was at night about 1 K cooler than the air at the other, eastern side of the city at the Wilhelminenaue, which is about 1.5 times as far from the city centre as the Mistel. As the two sites are structurally similar, this difference is caused by different ventilation. The main wind direction is relevant, as Bayreuth is generally influenced by westerly or southerly winds. More rural, cool air reaches the southern and western parts of the city, for example the Mistel. The ventilation of the Wilhelminenaue with cool air is limited by the motorway separating the site from nearby rural areas.

4.2.3. Impact on heating and cooling mechanisms

Single design parameters have the potential for heating or cooling a site, sometimes with opposite effects during day and night. An example is the narrowing of sites by buildings or trees. A reduced sky view inhibits heating during days with intense global radiation. At night, however, outgoing longwave radiation is absorbed and reemitted by the building walls or tree crowns. These effects of design parameters are of less importance under cloudy conditions, as clouds reduce the incoming shortwave radiation during daytime as well as the longwave outgoing radiation at night. As clouds increase the incoming longwave radiation by omnidirectional longwave emissions, they additionally inhibit the near-surface cold-air formation. Clouds suppress heating during the day and cooling at night, just as buildings and trees.

The nocturnal heating effect of inhibited outgoing longwave radiation is increased by heat storage in artificial materials. Sites, which are narrowed by walls built of materials like sandstone, additionally have an increased nocturnal heating potential. In Bayreuth, this effect arose at the Kämmereigasse. Increased heat storage can also occur at large urban water bodies. The city-wide measurements in Bayreuth in the analysed period from September to March did not show such an effect. However, it is expected that this effect is more important in the summer months.

Vegetated, moist sites have the potential to be cooled by evapotranspiration. In Bayreuth, the vegetated sites were cooler than the highly sealed sites. But this result is interpreted to be mostly an effect of increased heating at the sealed sites and to a lower degree the result of increased cooling by ET in the parks. This could be different in the summer months, when more energy is available. But, as the case study measurements showed, ET is only possible, if enough water is available.

The general ventilation of the city with fresh rural air largely depends on the meteorological conditions, mainly on the wind. Strong synoptical forcing can even suppress the formation of an

UHI by enhancing the mixing between urban and rural air masses. The main wind direction is of importance for the variability of heat within the city. Depending on the main wind direction and the exact location of e.g. a housing area, different air masses are transported towards the houses. At irrigated rural fields and urban parks, the wind speed additionally influences the cooling by ET. The transport of cooled park air contributes to the cooling of urban sites in the lee of the park (Ca et al. (1998); Spronken-Smith et al. (2000)). The transport of fresh rural or cooled park air masses is, however, influenced by the urban roughness, which depends on the building density. The ventilation of a site with rural air increases with the separation distance to the city centre. But also the location in regard to the main wind direction has to be considered.

In this thesis, it was hypothesized that the largest temperature differences occur under calm, anticyclonic conditions. Based on the results of the weather type analysis, this hypothesis was accepted. Regarding the site-specific heating, it was additionally hypothesised that the heating increases with the grade of sealing and decreases with the amount of vegetation. The results of the correlation analysis of the mean air temperature perturbation and the cover ratios of pavement, buildings, and vegetation at each site, supported this hypothesis. With the city-wide measurements, it was shown that sealing contributes to urban heating, while vegetated sites stay on average cooler. However, it is stated that the ventilation of a site is an additional, very important parameter for explaining the site-specific heating.

The schematic summarizing the important factors and mechanisms that was shown in the introduction (Fig. 1.1), was supplemented based on the results of this study (Fig. 4.2): Regarding the general potential for urban heating, the importance of the seasonal variability of the weather type was highlighted. For the site-specific urban heating, however, this study showed the additional influence of the inner-urban location of the site in relation to the mean wind direction.

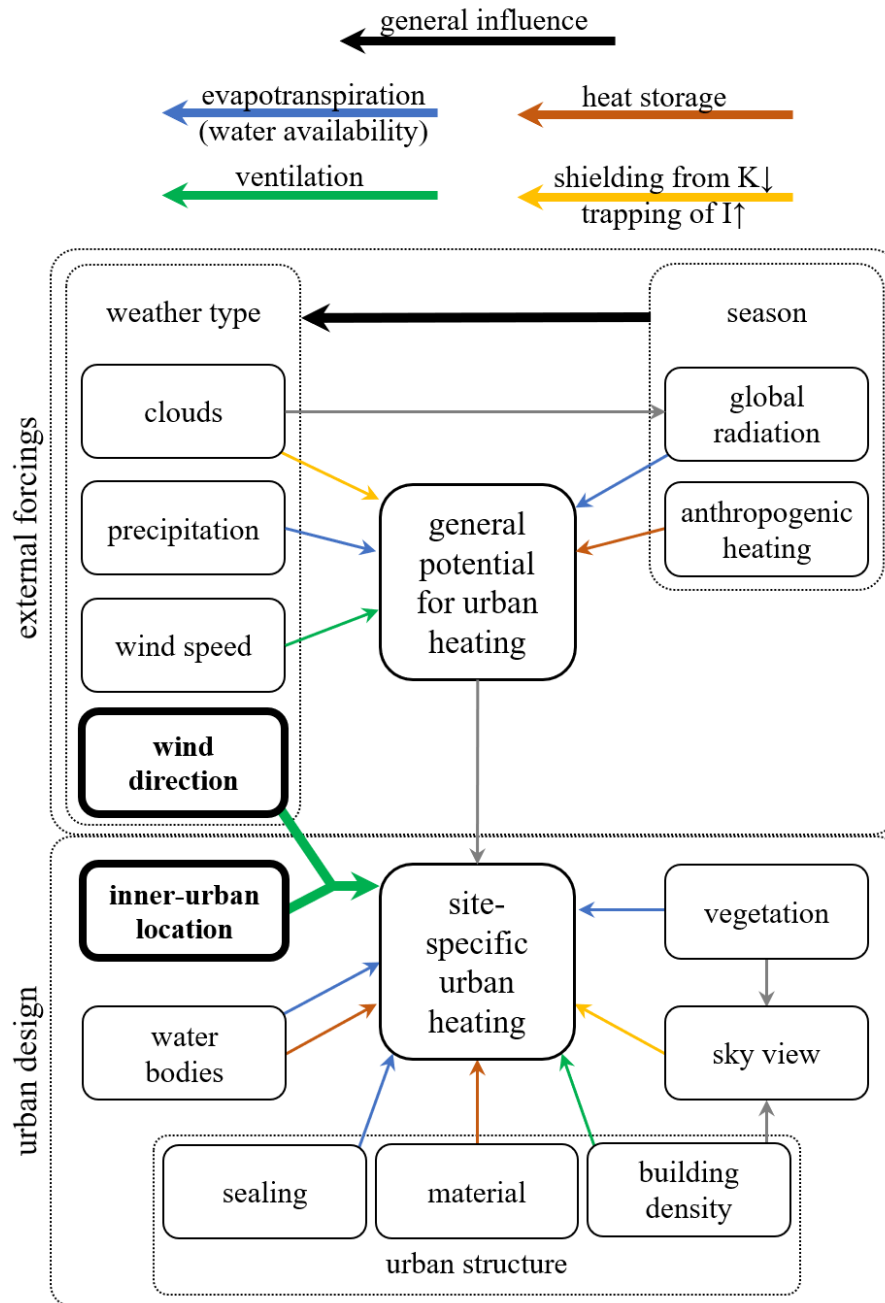


Figure 4.2.: Adapted schematic of the parameters and mechanisms that influence the urban heating. The external forcings that influence the general potential for urban heating are presented in the upper part. The lower part shows the factors that are important for the site-specific heating. The schematic was supplemented with the results of this thesis (bold arrows and text boxes).

5. Conclusions

In this study, the urban heating in a medium-sized city was evaluated to generate a reliable data basis for sustainable urban planning. To quantify the magnitude of thermal differences and to ascertain the main reasons for their formation, meteorological measurements were made on a street-canyon scale as well as with a city-wide network of weather stations.

It was shown that the urban heating in medium-sized cities like Bayreuth can be similar to the heating magnitude in larger European cities, especially under calm, anticyclonic weather conditions. Nevertheless, the urban area contains some sites, which show similar thermal conditions as a rural reference area. In addition to the vegetation, effective ventilation was most relevant for the cooling in these cases. Therefore, it is concluded, that the investigated urban area is small enough for heat mitigation strategies such as ventilation paths and urban vegetation to have a significant impact on the urban climate. This is most relevant for sustainable urban planning. Implementing such strategies additionally contributes to an increased air quality. People, who are most vulnerable to heat and pollution, should therefore preferentially chose such well ventilated districts as housing area.

By using a stationary measuring network, this study revealed that the locations of urban hot and cool spots vary spatially within the city with the course of the day. This variability could be resolved neither with a single urban station nor with mobile measurements, as the different heating and cooling rates impede the comparability of sequentially sampled observations. This information is relevant for further quantifications of thermal differences. Additionally, the comparability of sites has to be considered, especially with regard to the sky view: For evaluating the impact of urban heating on a forested urban park, the rural comparison site has to be a site with a similar tree density.

For a better understanding of the meteorological variabilities within the city of Bayreuth it would be of further interest to analyse the occurrence of extreme air temperatures on the basis of single events: How do the thermal differences change during summer heat waves? Which urban areas provide the potential for nocturnal cold air drainage? And do the rivers traversing the city provide sufficient ventilation with fresh, rural air?

Urban climate – just warm streets and cool parks? This statement is an extremely simplified, but nevertheless mostly applicable, estimation. With this thesis it was shown that the air temperature is the result of many forcings: The amount of vegetation and ground properties such as the grade of sealing are relevant. Additionally, the sky view, material, and ventilation potential as well as the temporal variation with the time of day, weather type, and season have to be considered, too. A sealed, but well-ventilated, housing area in the suburban area can be even cooler than a wooded park in the city centre, especially at night. This observation, however, does not diminish the positive effect of the park regarding the matter of urban recreation!

Acknowledgements

I like to thank everyone, who contributed to my master thesis:

Special thanks to Prof. Dr. Christoph Thomas and Dr. habil. Johannes Lüers for organizing and coordinating this practice-oriented project, for the motivation and the time for discussions and feedback; Johann Schneider and Johannes Olesch for their technical help during the preparation of all measurements and Dr. Brigitte John for providing the GPS device.

Thanks to all, who gave us the permission to install measurement devices on their properties.

I want to thank the whole Micrometeorology group for the constant feedback - especially to Lena Pfister, who additionally helped me with the MRD.

Many thanks to Lena Brüggewirth, Ursula Bundschuh and Elena Loos for the support during the mobile measurements.

The MiSKOR project, which this thesis is a part of, was supported by the Bayerisches Landesamt für Gesundheit und Lebensmittelsicherheit.

Bibliography

- Armson, D., Stringer, P., and Ennos, A.: The effect of tree shade and grass on surface and globe temperatures in an urban area, *Urban Forestry & Urban Greening*, 11, 245–255, 2012.
- Arnfield, A.: Two decades of urban climate research: a review of turbulence, exchanges of energy and water, and the urban heat island, *International Journal of Climatology*, 23, 1–26, 2003.
- Arnfield, A. J. and Grimmond, C.: An urban canyon energy budget model and its application to urban storage heat flux modeling, *Energy and Buildings*, 27, 61–68, 1998.
- Bhargava, A., Lakmini, S., and Bhargava, S.: Urban heat island effect: it’s relevance in urban planning, *Journal of Biodiversity & Endangered Species*, 5, 5–187, 2017.
- Böhm, R.: Urban bias in temperature time series—A case study for the city of Vienna, Austria, *Climatic Change*, 38, 113–128, 1998.
- Bowler, D., Buyung-Ali, L., Knight, T., and Pullin, A.: Urban greening to cool towns and cities: A systematic review of the empirical evidence, *Landscape and Urban Planning*, 97, 147–155, 2010.
- Buchin, O., Hoelscher, M.-T., Meier, F., Nehls, T., and Ziegler, F.: Evaluation of the health-risk reduction potential of countermeasures to urban heat islands, *Energy and Buildings*, 114, 27–37, 2015.
- Ca, V., Asaeda, T., and Abu, E.: Reductions in air conditioning energy caused by a nearby park, *Energy and Buildings*, 29, 83–92, 1998.
- Coutts, A. M., Beringer, J., and Tapper, N. J.: Impact of increasing urban density on local climate: Spatial and temporal variations in the surface energy balance in Melbourne, Australia, *Journal of Applied Meteorology and Climatology*, 46, 477–493, 2007.
- Crisci, A. and Morabito, M.: rBiometeo: Biometeorological Functions in R, URL <https://github.com/alfcrisci/rBiometeo>, R package version 0.1, 2016.
- DePaul, F. and Sheih, C.: Measurements of wind velocities in a street canyon, *Atmospheric Environment*, 20, 455–459, 1986.
- DWD: Deutscher Wetterdienst, Großwetterlagenklassifikation, URL <https://www.DWD.de>, accessed: 05.04.2019, 2019.
- Eliasson, I., Offerle, B., Grimmond, C., and Lindqvist, S.: Wind fields and turbulence statistics in an urban street canyon, *Atmospheric Environment*, 40, 1–16, 2006.

- Fanger, P.: Thermal comfort. Analysis and applications in environmental engineering., Copenhagen: Danish Technical Press., 1970.
- Franck, U., Krüger, M., Schwarz, N., Grossmann, K., Röder, S., and Schlink, U.: Heat stress in urban areas: Indoor and outdoor temperatures in different urban structure types and subjectively reported well-being during a heat wave in the city of Leipzig, *Meteorologische Zeitschrift*, 22, 167–177, 2013.
- Fritschen, L. J. and Gay, L. W.: Environmental instrumentation, Springer Science & Business Media, 1979.
- Gabriel, K. and Endlicher, W.: Urban and rural mortality rates during heat waves in Berlin and Brandenburg, Germany, *Environmental Pollution*, 159, 2044–2050, 2011.
- Gaffen, D. J. and Ross, R. J.: Increased summertime heat stress in the US, *Nature*, 396, 529, 1998.
- Gedzelman, S., Austin, S., Cermak, R., Stefano, N., Partridge, S., Quesenberry, S., and Robinson, D.: Mesoscale aspects of the urban heat island around New York City, *Theoretical and Applied Climatology*, 75, 29–42, 2003.
- Haeger-Eugensson, M. and Holmer, B.: Advection caused by the urban heat island circulation as a regulating factor on the nocturnal urban heat island, *International Journal of Climatology: A Journal of the Royal Meteorological Society*, 19, 975–988, 1999.
- Hathway, E. and Sharples, S.: The interaction of rivers and urban form in mitigating the Urban Heat Island effect: A UK case study, *Building and Environment*, 2012.
- Hess, P. and Brezowsky, H.: Katalog der grosswetterlagen Europas, 1969.
- Howard, L.: Climate of London deduced from meteorological observation, *Harvey and Darton*, 1, 1–24, 1833.
- Howell, J. and Mahrt, L.: Multiresolution flux decomposition, *Boundary-Layer Meteorology*, 83, 117–137, 1997.
- Ivajnsič, D. and Žiberna, I.: The effect of weather patterns on winter small city urban heat islands, *Meteorological Applications*, 26, 195–203, 2019.
- Jendritzky, G., Maarouf, A., Fiala, D., and Staiger, H.: An update on the development of a Universal Thermal Climate Index, in: 15th Conf. biomet. aerobiol. and 16th ICB02, vol. 27, pp. 129–133, 2002.
- Kalkstein, L. S. and Davis, R. E.: Weather and human mortality: an evaluation of demographic and interregional responses in the United States, *Annals of the Association of American Geographers*, 79, 44–64, 1989.
- Ketterer, C. and Matzarakis, A.: Human-biometeorological assessment of the urban heat island in a city with complex topography—The case of Stuttgart, Germany, *Urban Climate*, 10, 573–584, 2014.

- Kloog, I.: Air pollution, ambient temperature, green space and preterm birth, *Current Opinion in Pediatrics*, 31, 237–243, 2019.
- LDBV: Bayerisches Landesamt für Digitalisierung, Breitband und Vermessung, BayernAtlas, URL <https://geoportal.bayern.de/bayernatlas/>, accessed: 08.09.2019.
- Lemonsu, A. and Masson, V.: Simulation of a summer urban breeze over Paris, *Boundary-Layer Meteorology*, 104, 463–490, 2002.
- LfStat: Bayerisches Landesamt für Statistik, Genesis-Online Datenbank, URL <https://www.statistikdaten.bayern.de>, accessed: 24.07.2019, 2018.
- Lin, P., Lau, S., Qin, H., and Gou, Z.: Effects of urban planning indicators on urban heat island: a case study of pocket parks in high-rise high-density environment, *Landscape and Urban Planning*, 168, 48–60, 2017.
- Morris, C. and Simmonds, I.: Associations between varying magnitudes of the urban heat island and the synoptic climatology in Melbourne, Australia, *International Journal of Climatology*, 20, 1931–1954, 2000.
- Morris, C., Simmonds, I., and Plummer, N.: Quantification of the influences of wind and cloud on the nocturnal urban heat island of a large city, *Journal of Applied Meteorology*, 40, 169–182, 2001.
- Nunez, M. and Oke, T. R.: The energy balance of an urban canyon, *Journal of Applied Meteorology*, 16, 11–19, 1977.
- Oke, T.: Towards a more rational understanding of the urban heat island, *McGill Climatology Bulletin*, 5, 1–21, 1969.
- Oke, T.: City size and the urban heat island, *Atmospheric Environment*, 7, 769–779, 1973.
- Oke, T.: The distinction between canopy and boundary-layer urban heat islands, *Atmosphere*, 14, 268–277, 1976.
- Oke, T.: Canyon geometry and the nocturnal urban heat island: comparison of scale model and field observations, *Journal of Climatology*, 1, 237–254, 1981.
- Oke, T.: *The energetic basis of the urban heat island*, vol. 108, Wiley Online Library, 1982.
- Oke, T.: The heat island of the urban boundary layer: characteristics, causes and effects, in: *Wind climate in cities*, pp. 81–107, Springer, 1995.
- Oke, T. and East, C.: The urban boundary layer in Montreal, *Boundary-Layer Meteorology*, 1, 411–437, 1971.
- Park, J., Kim, J.-H., Lee, D., Park, C., and Jeong, S.: The influence of small green space type and structure at the street level on urban heat island mitigation, *Urban Forestry & Urban Greening*, 21, 203–212, 2017.

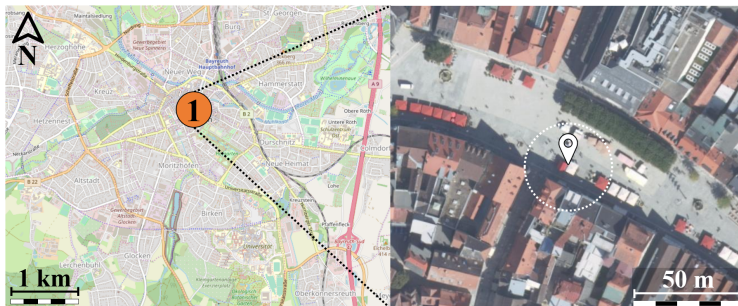
- Peterson, T. C. and Owen, T. W.: Urban heat island assessment: Metadata are important, *Journal of Climate*, 18, 2637–2646, 2005.
- Runnalls, K. and Oke, T.: Dynamics and controls of the near-surface heat island of Vancouver, British Columbia, *Physical Geography*, 21, 283–304, 2000.
- Ryu, Y.-H. and Baik, J.-J.: Quantitative analysis of factors contributing to urban heat island intensity, *Journal of Applied Meteorology and Climatology*, 51, 842–854, 2012.
- Spronken-Smith, R. and Oke, T.: The thermal regime of urban parks in two cities with different summer climates, *International Journal of Remote Sensing*, 19, 2085–2104, 1998.
- Spronken-Smith, R., Oke, T., and Lowry, W.: Advection and the surface energy balance across an irrigated urban park, *International Journal of Climatology*, 20, 1033–1047, 2000.
- Stewart, I.: A systematic review and scientific critique of methodology in modern urban heat island literature, *International Journal of Climatology*, 31, 200–217, 2011.
- Stone, B., Hess, J. J., and Frumkin, H.: Urban form and extreme heat events: are sprawling cities more vulnerable to climate change than compact cities?, *Environmental Health Perspectives*, 118, 1425–1428, 2010.
- Szymanowski, M. and Kryza, M.: Local regression models for spatial interpolation of urban heat island – an example from Wrocław, SW Poland, *Theoretical and Applied Climatology*, 108, 53–71, 2012.
- Taha, H.: Urban climates and heat islands: albedo, evapotranspiration, and anthropogenic heat, *Energy and Buildings*, 25, 99–103, 1997.
- Tan, J., Zheng, Y., Tang, X., Guo, C., Li, L., Song, G., Zhen, X., Yuan, D., Kalkstein, A. J., Li, F., et al.: The urban heat island and its impact on heat waves and human health in Shanghai, *International Journal of Biometeorology*, 54, 75–84, 2010.
- Thomas, C. K.: Variability of Sub-Canopy Flow, Temperature, and Horizontal Advection in Moderately Complex Terrain, *Boundary-Layer Meteorology*, 139, 61–81, 2011.
- Thomas, C. K., Linhardt, T., Schneider, J., and Olesch, J.: Field evaluation of the micro-weather station MA-4100 (ATMOS-41) - Comparison of the observational device used in the Trans-African HydroMeteorological Observatory (TAHMO) against WMO-grade instruments at the Ecological Botanical Gardens, University of Bayreuth, Germany, *Arbeitsergebnisse*, Universität Bayreuth, Mikrometeorologie, ISSN 1614-8926, 2019.
- Thorsson, S., Lindqvist, M., and Lindqvist, S.: Thermal bioclimatic conditions and patterns of behaviour in an urban park in Göteborg, Sweden, *International Journal of Biometeorology*, 48, 149–156, 2004.
- Tobias, A., Armstrong, B., Zuza, I., Gasparrini, A., Linares, C., and Diaz, J.: Mortality on extreme heat days using official thresholds in Spain: a multi-city time series analysis, *BMC Public Health*, 12, 133, 2012.

- Tsuzuki, K., Okamoto-Mizuno, K., and Mizuno, K.: Effects of humid heat exposure on sleep, thermoregulation, melatonin, and microclimate, *Journal of Thermal Biology*, 29, 31–36, 2004.
- Wang, Y. and Akbari, H.: The effects of street tree planting on Urban Heat Island mitigation in Montreal, *Sustainable Cities and Society*, 27, 122–128, 2016.
- Wang, Y., Berardi, U., and Akbari, H.: Comparing the effects of urban heat island mitigation strategies for Toronto, Canada, *Energy and Buildings*, 114, 2–19, 2016.
- Wong, K. V., Paddon, A., and Jimenez, A.: Review of world urban heat islands: Many linked to increased mortality, *Journal of Energy Resources Technology*, 135, 022 101, 2013.
- Yang, C., He, X., Wang, R., Yan, F., Yu, L., Bu, K., Yang, J., Chang, L., and Zhang, S.: The effect of urban green spaces on the urban thermal environment and its seasonal variations, *Forests*, 8, 153, 2017.
- Zacharias, J., Stathopoulos, T., and Wu, H.: Microclimate and downtown open space activity, *Environment and Behavior*, 33, 296–315, 2001.

A. Site descriptions (city-wide measurements)

1 Markt: city centre

Location: Maximilianstr. 55
 Distance to the Markt: 0 m
 Latitude: 49.944790
 Longitude: 11.573609
 Altitude: 339 m
 Height above ground: 4.2 m
 ATMOS ID: ATM41 000 2922



Approx. land use cover ratio in a 20 m perimeter:

land use	cover ratio
pavement	85 %
buildings	15 %
water	0 %
vegetation (ground cover)	0 %
tree cover	0 %

2 Kämmerei: city centre

Location: Kämmereigasse 6
 Distance to the Markt: 120 m
 Latitude: 49.943828
 Longitude: 11.574383
 Altitude: 339 m
 Height above ground: 3.6 m
 ATMOS ID: ATM41 000 2906



Approx. land use cover ratio in a 20 m perimeter:

land use	cover ratio
pavement	20 %
buildings	80 %
water	0 %
vegetation (ground cover)	2 %
tree cover	2 %

Figure A.1.: Description of the sites Markt and Kämmererei. (map: OpenStreetMap)

3 St. Georgen

Location: St. Georgen 23
 Distance to the Markt: 1670 m
 Latitude: 49.953989
 Longitude: 11.592095
 Altitude: 360 m
 Height above ground: 3.1 m
 ATMOS ID: ATM41 000 2932



Approx. land use cover ratio in a 20 m perimeter:

land use	cover ratio
pavement	53 %
buildings	45 %
water	0 %
vegetation (ground cover)	2 %
tree cover	0 %

4 Altstadt

Location: Wallstr. 8
 Distance to the Markt: 1660 m
 Latitude: 49.937801
 Longitude: 11.552973
 Altitude: 343 m
 Height above ground: 3.5 m
 ATMOS ID: ATM41 000 2912



Approx. land use cover ratio in a 20 m perimeter:

land use	cover ratio
pavement	40 %
buildings	30 %
water	0 %
vegetation (ground cover)	30 %
tree cover	5 %

Figure A.2.: Description of the sites St. Georgen and Altstadt. (map: OpenStreetMap)

5 Birken

Location: Hegelstr. 18
Distance to the Markt: 1370 m
Latitude: 49.932985
Longitude: 11.579128
Altitude: 348 m
Height above ground: 3.5 m
ATMOS ID: ATM41 000 2914



Approx. land use cover ratio in a 20 m perimeter:

land use	cover ratio
pavement	40 %
buildings	20 %
water	0 %
vegetation (ground cover)	40 %
tree cover	5 %

6 Spinnerei

Location: Spinnereistr. 5
Distance to the Markt: 870 m
Latitude: 49.952024
Longitude: 11.569168
Altitude: 334 m
Height above ground: 3.5 m
ATMOS ID: ATM41 000 2911



Approx. land use cover ratio in a 20 m perimeter:

land use	cover ratio
pavement	94 %
buildings	1 %
water	0 %
vegetation (ground cover)	5 %
tree cover	2 %

Figure A.3.: Description of the sites Birken and Spinnerei. (map: OpenStreetMap)

A. Site descriptions (city-wide measurements)

7 Mistel: river bank

Location: Mistel (Kreuz)
 Distance to the Markt: 705 m
 Latitude: 49.943543
 Longitude: 11.563788
 Altitude: 336 m
 Height above ground: 3.5 m
 ATMOS ID: ATM41 000 2916

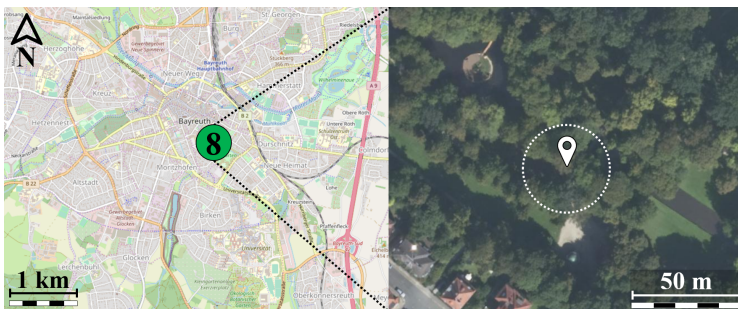


Approx. land use cover ratio in a 20 m perimeter:

land use	cover ratio
pavement	0 %
buildings	0 %
water	8 %
vegetation (ground cover)	92 %
tree cover	20 %

8 Hofgarten: city centre

Location: Parkstr. / Im Hofgarten
 Distance to the Markt: 680 m
 Latitude: 49.940236
 Longitude: 11.579736
 Altitude: 343 m
 Height above ground: 3.2 m
 ATMOS ID: ATM41 000 2917



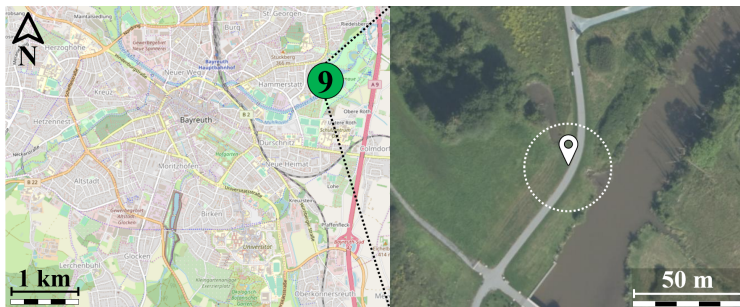
Approx. land use cover ratio in a 20 m perimeter:

land use	cover ratio
pavement	0 %
buildings	0 %
water	10 %
vegetation (ground cover)	70 %
tree cover	95 %

Figure A.4.: Description of the sites Mistel and Hofgarten. (map: OpenStreetMap)

9 Wilhelminenaue: river bank

Location: Roter Main
(Hammerstatt)
Distance to the Markt: 1730 m
Latitude: 49.946422
Longitude: 11.597638
Altitude: 341 m
Height above ground: 3.5 m
ATMOS ID: ATM41 000 2925



Approx. land use cover ratio in a 20 m perimeter:

land use	cover ratio
pavement	15 %
buildings	0 %
water	10 %
vegetation (ground cover)	75 %
tree cover	0 %

10 Röhrensee: lake

Location: near Birken (Kantstr. 2)
Distance to the Markt: 1300 m
Latitude: 49.932762
Longitude: 11.573291
Altitude: 341 m
Height above ground: 3.1 m
ATMOS ID: ATM41 000 2908



Approx. land use cover ratio in a 20 m perimeter:

land use	cover ratio
pavement	0 %
buildings	0 %
water	30 %
vegetation (ground cover)	55 %
tree cover	85 %

Figure A.5.: Description of the sites Wilhelminenaue and Röhrensee. (map: OpenStreetMap)

A. Site descriptions (city-wide measurements)

11 Karstadt: city centre

Location: Maximilianstr. 42
 Distance to the Markt: 63 m
 Latitude: 49.945373
 Longitude: 11.573903
 Altitude: 338 m
 Height above ground: 23.1 m
 ATMOS ID: ATM41 000 2902



Approx. land use cover ratio in a 20 m perimeter:

land use	cover ratio
pavement	75 %
buildings	25 %
water	0 %
vegetation (ground cover)	0 %
tree cover	0 %

12 EBG: rural reference

Location: Campus of the University of Bayreuth
 Distance to the Markt: 2410 m
 Latitude: 49.924586
 Longitude: 11.586108
 Altitude: 355 m
 Height above ground: 2 m



Approx. land use cover ratio in a 20 m perimeter:

land use	cover ratio
pavement	0 %
buildings	0 %
water	0 %
vegetation (ground cover)	100 %
tree cover	20 %

Figure A.6.: Description of the sites Karstadt and EBG. (map: OpenStreetMap)

B. Additional tables and figures

Quality assessment (street-canyon scale approach)

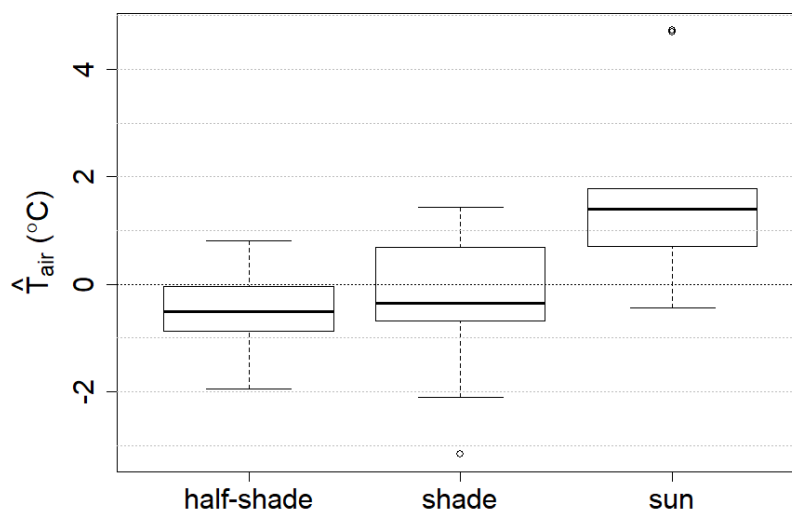


Figure B.1.: Influence of direct solar radiation on air temperature measurements

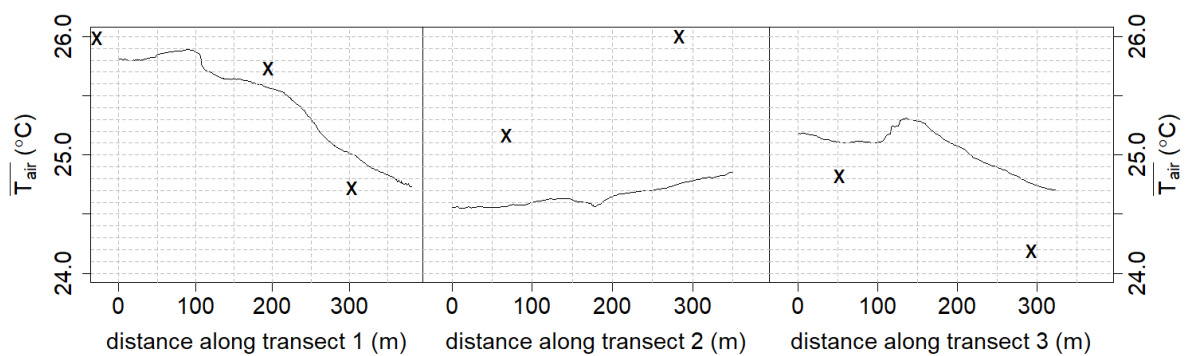


Figure B.2.: Comparison of the transect and point measurements in the evening. (data: mean of 4 transects or 2 point measurements, respectively)

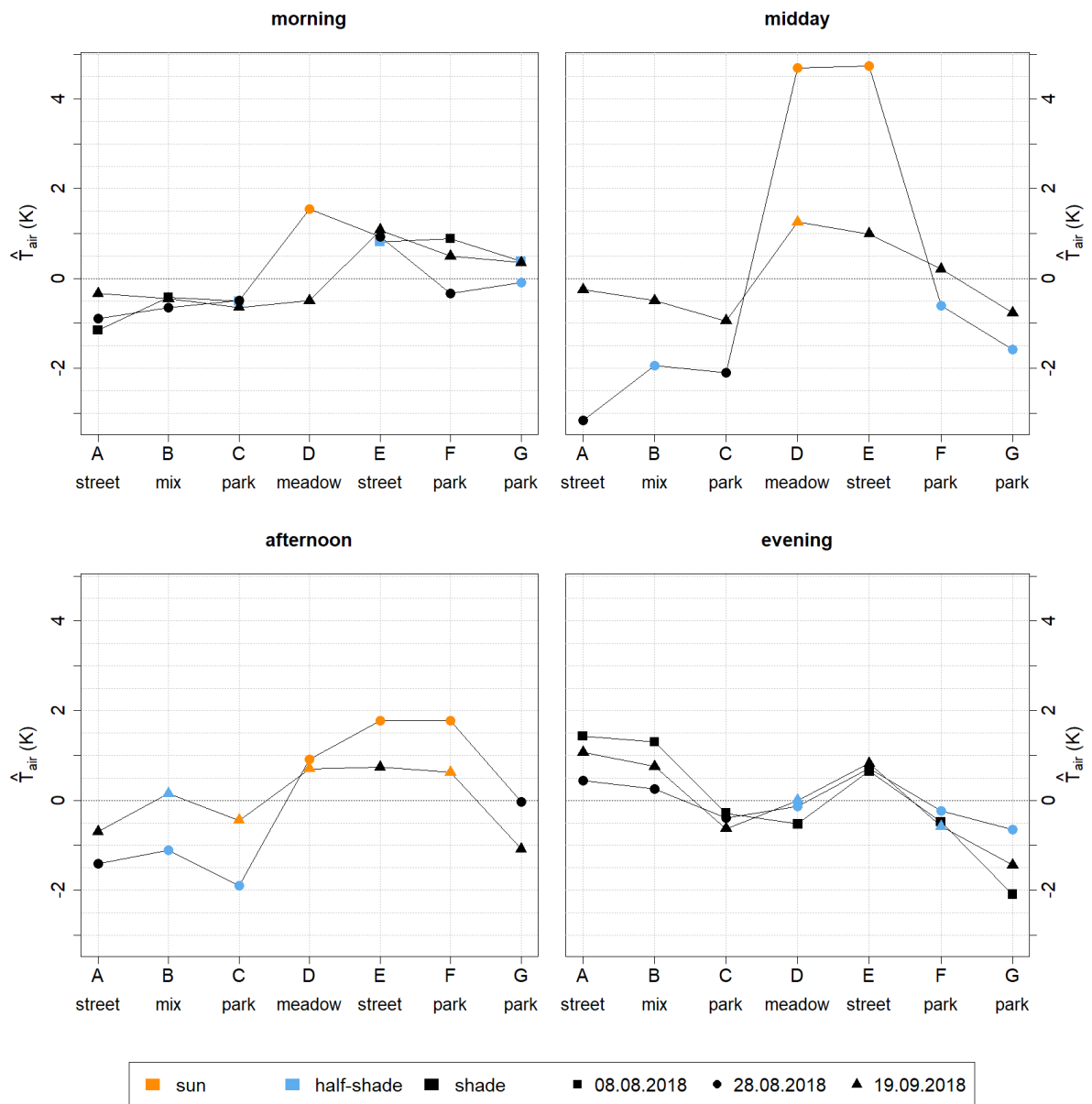


Figure B.3.: Spatial perturbation of the air temperature at the measuring points during the four times of day. The different symbols represent the three measuring days; the colour marking indicates whether the measurements were made in the sun or shade.

Table B.1.: Summary of the measurements made in the Hofgarten

day	start	end	measurements	quality flag 0 = invalid 1 = valid	error			data used for the analysis
					IR-camera	Testo	GPS	
08.08.2018	08:40	08:50	transects	1				-
	09:15	10:30	MP	0	no flag	radiative error (point D)		✓
	10:45	11:00	transects	0			no signal	-
	11:30	11:45	transects	1				-
	12:00	13:15	MP	0	no flag	incorrect or no readings		-
	13:20	13:30	transects	0			no signal	-
	15:20	15:30	transects	0				-
	15:45	17:00	MP	0	no flag	incorrect or no readings		-
	17:30	17:45	transects	1				-
	19:00	19:15	transects	1				-
	19:30	20:45	MP	1				✓
	20:50	21:00	transects	0			no signal	-
28.08.2018	08:00	08:10	transects	1				✓
	08:40	10:10	MP	0		radiative error (point D)		-
	10:20	10:30	transects	1				✓
	11:15	11:25	transects	1				✓
	11:35	12:45	MP	0		radiative error (points D + E)		-
	13:00	13:10	transects	0			incorrect or no readings	-
	14:55	15:05	transects	1				✓
	15:15	16:30	MP	0		radiative error (points D + E + F)		-
	16:40	16:50	transects	1				✓
	17:15	17:25	transects	1				✓
	17:30	18:45	MP	1				✓
19:00	19:10	transects	1				✓	
19.09.2018	07:20	07:30	transects	1				✓
	08:00	09:15	MP	1				✓
	09:30	09:40	transects	1				✓
	11:00	11:10	transects	1				✓
	11:20	12:30	MP	0		radiative error (point D)		-
	12:35	12:45	transects	1				✓
	14:30	14:40	transects	1				✓
	14:50	16:00	MP	0		radiative error (points C + D + F)		-
	16:15	16:25	transects	1				✓
	17:00	17:10	transects	1				✓
	17:20	18:20	MP	1				✓
18:35	18:45	transects	1				✓	

Quality assessment (city-wide approach)

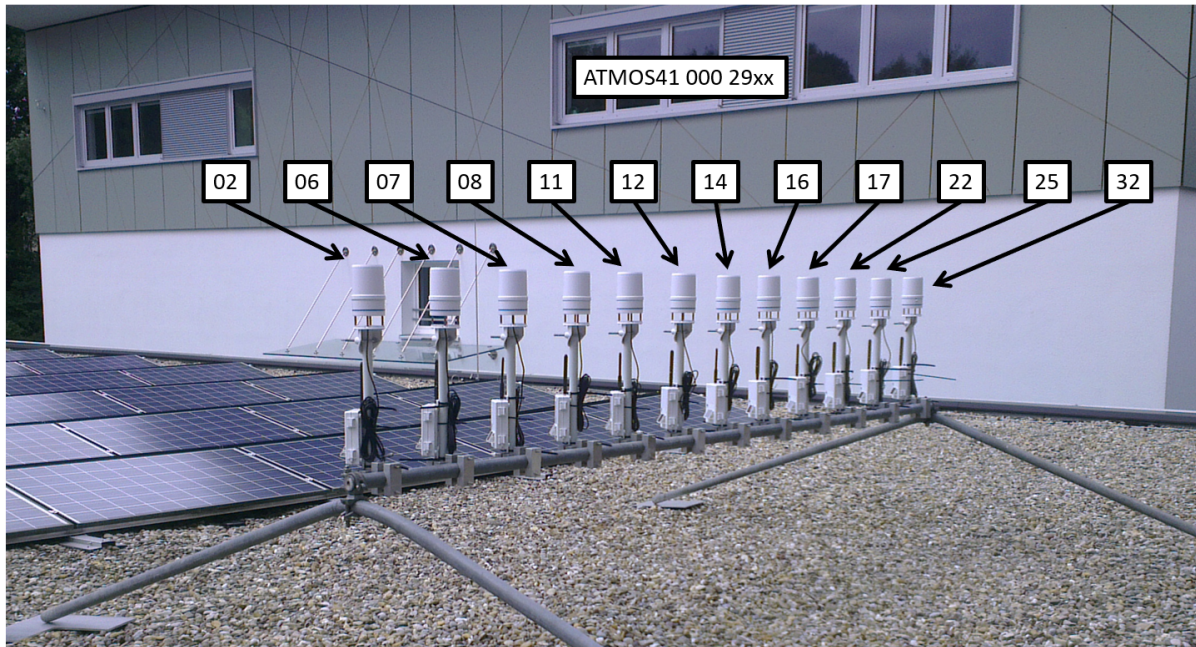


Figure B.4.: Set-up of the instrument comparison conducted in July 2018 at the Campus of the University of Bayreuth.

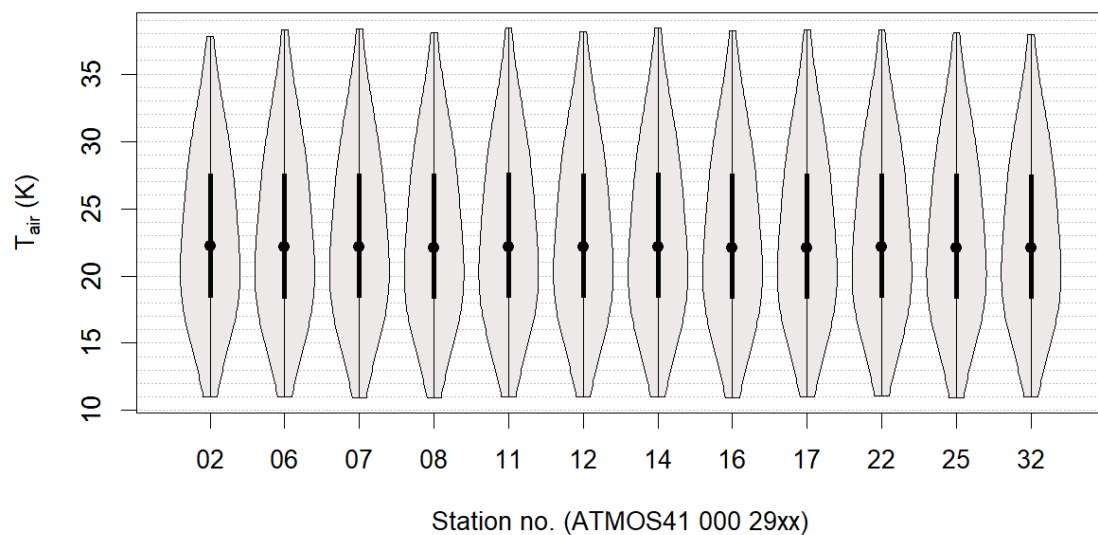


Figure B.5.: Comparison of the measurements of air temperature of all weather stations (data: 17d with 5 min resolution $\rightarrow N = 4837$)



Figure B.6.: Comparison of the wind measurements of the micro weather stations; (data: 17 days with 5 min resolution $\rightarrow N = 4837$)

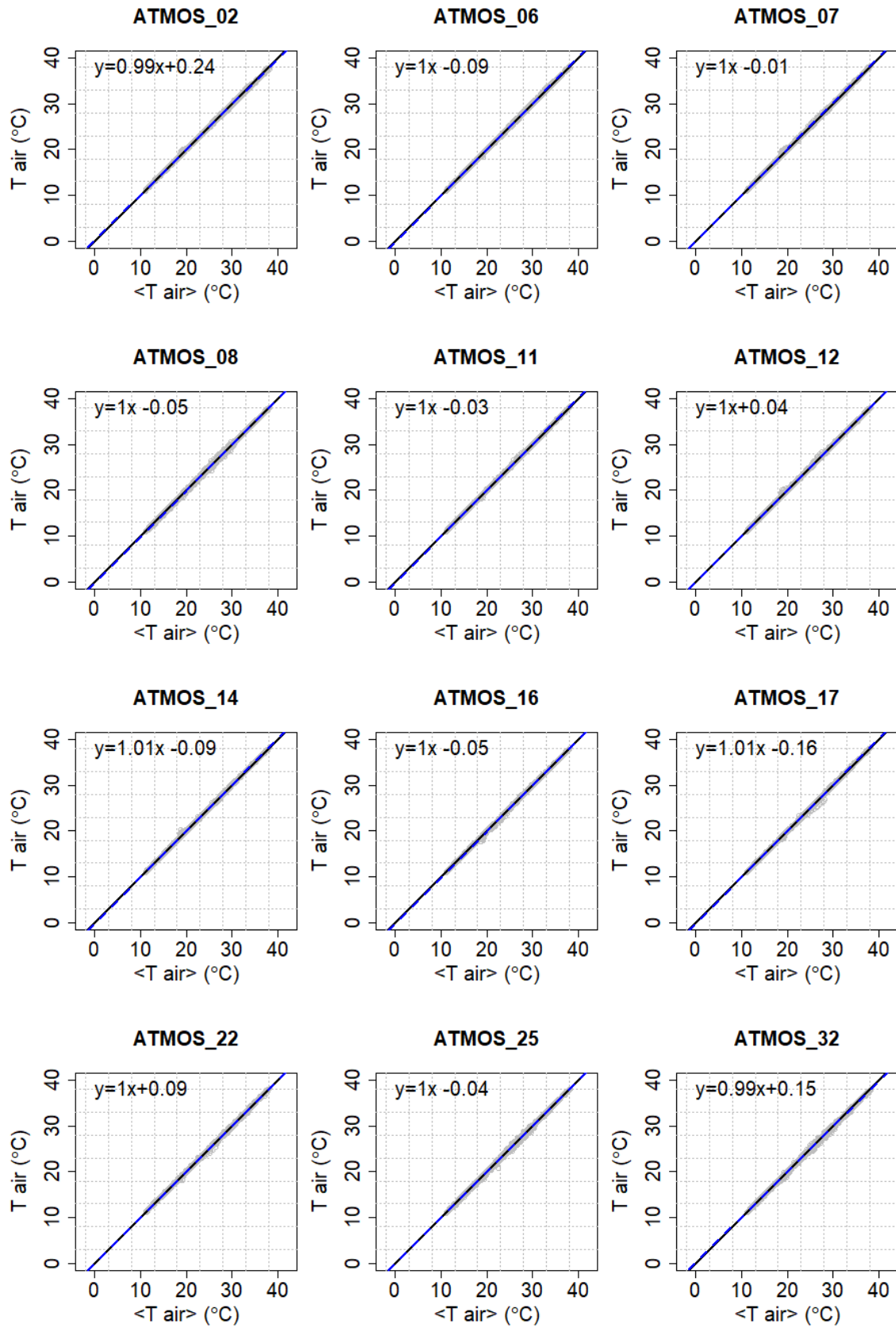


Figure B.7.: Instrument comparison of the micro weather stations regarding the air temperature T_{air} . Each station was compared to the mean value of all 12 stations $\langle T_{air} \rangle$. (data: 17 d with 5 min resolution $\rightarrow N = 4837$)

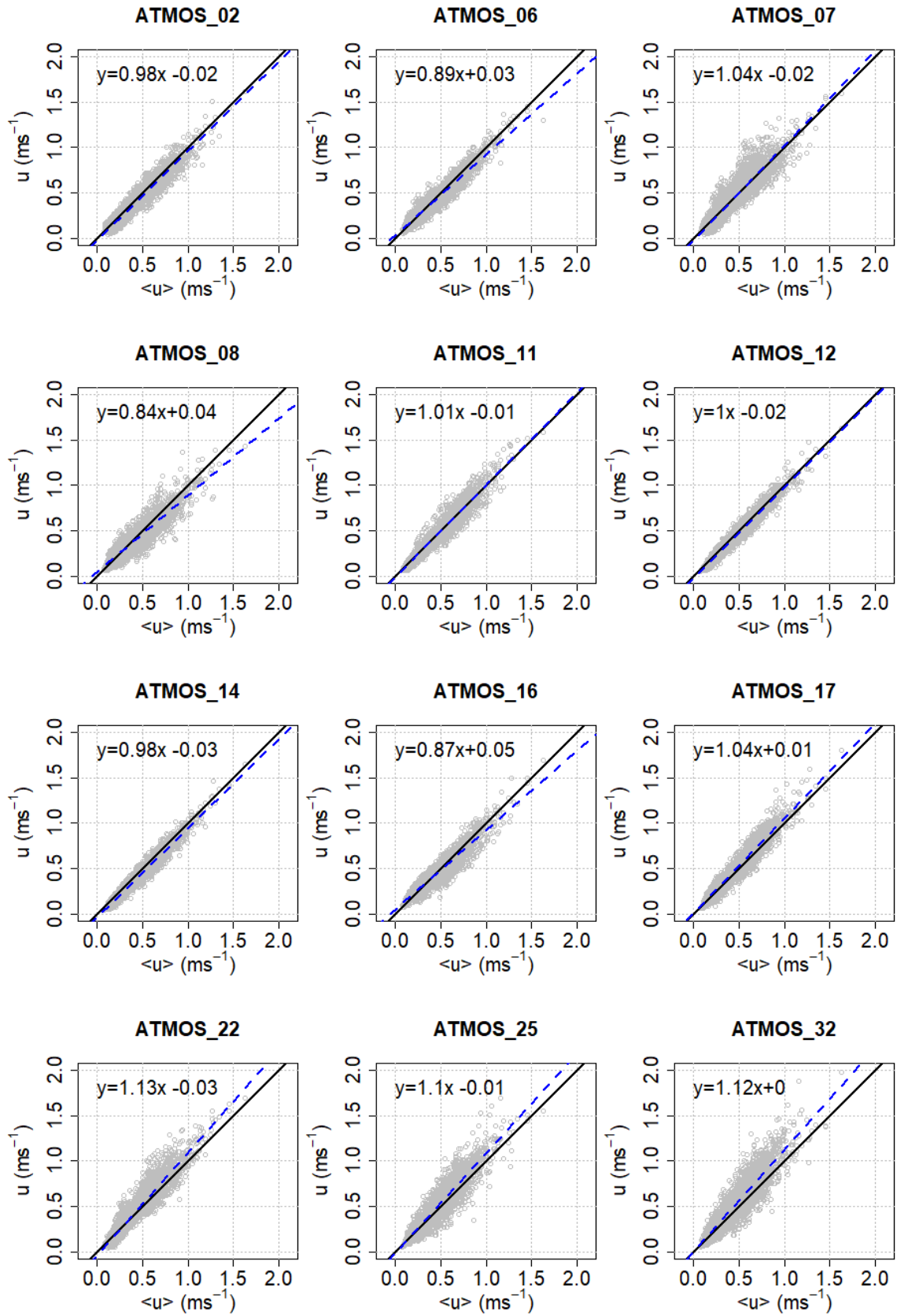


Figure B.8.: Instrument comparison of the micro weather stations regarding the wind speed u . Each station was compared to the mean value of all 12 stations $\langle u \rangle$. (data: 17d with 5min resolution $\rightarrow N = 4837$)

Heating and cooling rates (city-wide approach)

Table B.2.: Maximal heating and cooling rates of each site during the mean diurnal course of *extreme days*

site	time of max. heating	max. heating rate (K/h)	time of max. cooling	max. cooling rate (K/h)
Altstadt	9:25	3.5	17:35	-3.0
Birken	8:35	3.0	18:05	-2.7
Hofgarten	9:35	2.7	18:25	-1.9
Kämmerei	8:55	2.3	18:35	-1.6
Karstadt	9:05	2.6	18:25	-2.7
Markt	8:55	2.7	18:25	-2.5
Mistel	9:35	3.6	18:05	-3.3
Röhrensee	9:15	3.2	17:35	-3.5
Spinnerei	9:15	2.6	18:20	-2.9
St. Georgen	9:15	2.9	18:35	-1.7
Wilhelminaue	8:15	3.0	18:05	-3.2
EBG	9:05	3.6	17:25	-3.9

Comparison of the wind regime at the different measuring sites

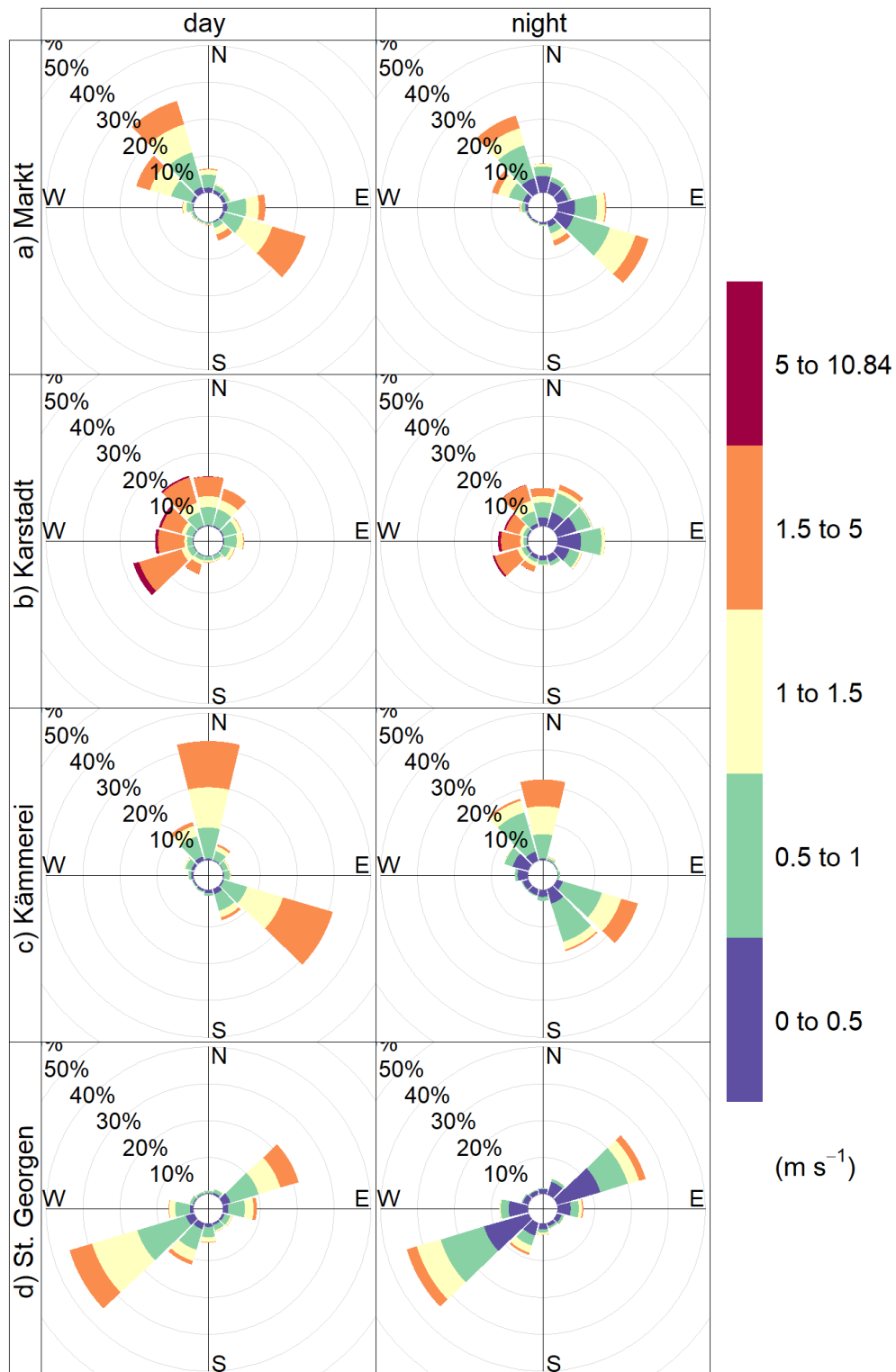


Figure B.9.: Comparison of the wind regime at the sites Markt (a), Karstadt (b), Kämmerei (c), St. Georgen (d); (data: 211 days with 5 min resolution)

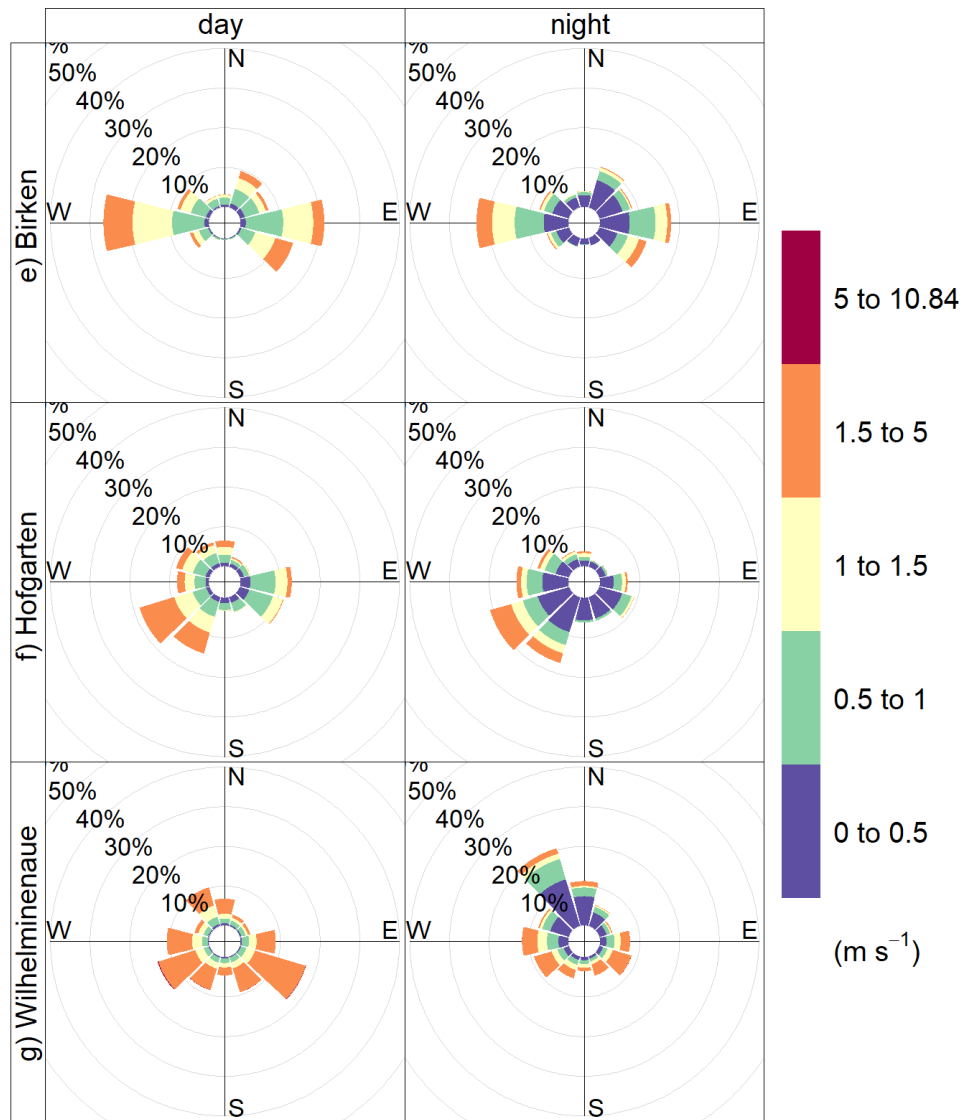


Figure B.10.: Comparison of the wind regime at the sites Birken (e), Hofgarten (f), and Wilhelminenaue (g); (data: 211 days with 5 min resolution)

Declaration of authorship

Hereby, I declare that I have authored the master thesis titled

“Urban Climate – just warm streets and cool parks?”

Investigating the variabilities of heat at street-canyon and city-wide scale in Bayreuth”

independently based on my own work. All direct or indirect sources used are acknowledged as references. This thesis has not been published or previously submitted to any other examination board.

Date

Isabel Spies